Air quality impacts of COVID-19 lockdown measures detected from space using high spatial resolution observations of multiple trace gases from Sentinel-5P/TROPOMI

Pieternel F. Levelt[1,2], Deborah C. Stein Zweers[1], Ilse Aben[3], Maite Bauwens[4], Tobias Borsdorff[3], Isabelle De Smedt[4], Henk J. Eskes[1], Christophe Lerot[4], Diego G. Loyola[5], Fabian Romahn[5], Trissevgeni Stavrakou[4], Nicolas Theys[4], Michel Van Roozendael[4], J. Pepijn Veefkind[1,2], Tijl Verhoelst[4]

[1]Royal Netherlands Meteorological Institute (KNMI), De Bilt, 3731GA, The Netherlands
[2]University of Technology Delft (TU Delft), Delft, 2628 CN, the Netherlands
[3]Netherlands Institute for Space Research (SRON), Utrecht, 3584 CA, The Netherlands
[4]Royal Belgian Institute for Space Aeronomy (BIRA-IASB), Brussels, 1180, Belgium
[5]German Aerospace Centre (DLR), Oberpfaffenhofen, Wessling, 82234, Germany

Correspondence to: Deborah C. Stein Zweers (stein@knmi.nl)

Abstract. The aim of this paper is ~~two-fold: to provide guidance on how to best interpret TROPOMI trace gas retrievals and~~ to highlight how TROPOMI trace gas data can be~~st be~~ used and interpreted to understand event-based impacts on air quality from regional to city-scales around the globe. For this study, we present the observed changes in the atmospheric column amounts of five trace gases (NO_2, SO_2, CO, HCHO and CHOCHO) detected by the Sentinel-5P TROPOMI instrument, driven by reductions of anthropogenic emissions due to COVID-19 lockdown measures in 2020. We report clear COVID-19-related decreases in TROPOMI NO_2 ~~concentrations~~ column amounts on all continents. For megacities, reductions in column amounts of tropospheric NO_2 range between 14% and 63%. For China and India supported by NO_2 observations, where the primary source of anthropogenic SO_2 is coal-fired power generation, we were able to detect sector-specific emission changes using the SO_2 data. For HCHO and CHOCHO, we consistently observe anthropogenic changes in two-week averaged column amounts over China and India during the early phases of the lockdown periods. That these variations over such a short time scale are detectable from space, is due to the high resolution and improved sensitivity of the TROPOMI instrument. For CO, we observe a small reduction over China which is in concert with the other trace gas reductions observed during lockdown, however large, interannual differences prevent firm conclusions from being drawn. The joint analysis of COVID-19 lockdown-driven reductions in satellite observed trace gas column amounts, using the latest operational and scientific retrieval techniques for five species concomitantly is unprecedented. However, the meteorologically and seasonally driven variability of the five trace gases does not allow for drawing fully quantitative conclusions on the reduction of anthropogenic emissions based on TROPOMI observations alone. We anticipate that in future, the combined use of inverse modelling techniques with the high spatial resolution data from S5P/TROPOMI for all observed trace gases presented here, will yield a significantly improved sector-specific, space-based analysis of the impact of COVID-19 lockdown measures as compared to other existing satellite observations. Such analyses will further enhance the scientific impact and societal relevance of the TROPOMI mission.

Key words: Air quality, Trace gases, Sentinel-5P, TROPOMI, COVID-19, emissions

1   Introduction

In an effort to limit the transmission of the SARS-CoV-2 virus responsible for the Coronavirus disease 2019 (hereafter referred as COVID-19), drastic lockdown measures were implemented around the globe in the first half of 2020. These policies led to dramatic reductions in human activity, especially in the transport and industrial sectors, resulting in large decreases in the concentration of air pollutants (Bauwens et al., 2020; Shi and Brasseur, 2020; Forster et al., 2020; Diamond and Wood, 2020; Kroll et al., 2020; Le Quéré et al., 2020; Guevara et al., 2021; Gkatzelis et al., 2021). These changes were observed over China as early as February 2020 (Bauwens et al., 2020; Liu et al., 2020; Zhang, Z. et al., 2020; Zhao, N. et al., 2020) and were detected later in many other countries as similar lockdown measures were adopted (Bauwens et al., 2020; Broomandi et al., 2020; Collivignarelli et al., 2020; Lee et al., 2020; Gkatzelis et al., 2021; Koukouli et al., 2021).

The TROPOspheric Monitoring Instrument (TROPOMI; Veefkind et al., 2012; Ludewig et al., 2020) on board the European Copernicus Sentinel-5 Precursor (S5P) satellite, launched on 13 October 2017, is specifically designed for tropospheric monitoring on the global scale and has a daily revisit time. Compared to its predecessor OMI, TROPOMI's highest spatial resolution (3.5 x 5.5 km^2) is about 16 times better and its signal-to-noise ratio per ground pixel is substantially higher. This results in a ~~spectacular~~ large improvement in measurement sensitivity for relevant air quality products, including NO_2, SO_2, HCHO, and CHOCHO, thus enabling the study of rapid emission changes for even smaller sources as compared to previous instruments. For CO measurements, the daily global coverage of TROPOMI at a resolution of 7 x 5.5 km^2 represents a huge improvement to its predecessor SCIAMACHY (Bovensmann et al., 1999; Borsdorff et al., 2016; Borsdorff et al., 2017) with a spatial resolution of 120 x 30 km^2.

The observations from TROPOMI thus provide a unique opportunity to observe the magnitude and timing of the changes in tropospheric trace gas constituents, resulting from unprecedented COVID-19 lockdown measures. The initial TROPOMI observations of dramatic reductions in NO_2 ~~concentrations~~ column amount over regions with strictly enforced lockdowns, over China in particular, triggered a high level of interest worldwide, and initiated a large number of studies, mainly aimed at regional scales and largely focused on NO_2. However, the unparalleled capacity of TROPOMI to provide relevant information on COVID-19 driven emission reductions based on multiple species measurements has not been exploited yet. The objective of this work is to investigate the COVID-19 driven changes in the ~~concentration~~ column amounts of five trace gases (NO_2, SO_2, CO, HCHO, and CHOCHO) from the global level down to individual cities using state-of-the-art TROPOMI operational and scientific data products. More specifically, we aim to

1. ~~Expand~~ Summarize the analysis of tropospheric NO_2 at city-scale for ~~to~~ all continents.

A large body of studies investigated the impact of the COVID-19 lockdowns on NO_2 concentrations (e.g. Bauwens et al., 2020; Baldasano, 2020; Huang et al., 2020), at regional and continental scale. Here, we analyze the time series of NO_2 measurements from a single satellite instrument for globally distributed locations on regional to city scales. In doing so, we further demonstrate the unique capabilities of how the TROPOMI instrument can be used to consistently track changes in air quality and anthropogenic emissions across the globe.

73

    2. Explore the high spatial resolution and simultaneous TROPOMI observations of NO$_2$, SO$_2$, CO, HCHO, and CHOCHO.

While all of these gases have significant anthropogenic sources, they differ in their relative contribution to the energy, industry, and transport sector emissions, and each sector exhibits a different response to COVID-19 lockdown measures. Therefore, the combination of several TROPOMI trace gas products contains additional information on sector-specific emissions and COVID-19 lockdown-induced changes in atmospheric composition. We show that meaningful trends and source detection can be obtained by using the ~~unprecedentedly~~ high spatial resolution of TROPOMI data and by averaging that data over relatively short time periods. Although this is in large part the result of the improved sensitivity of the instrument, we also introduce new developments in trace gas retrieval techniques and ad-hoc corrections to enhance the sensitivity of the TROPOMI datasets to even smaller emissions and smaller changes in emissions. In order to achieve these goals, we discuss the strengths and limitations of each of the retrievals for tracking global to city-scale changes.

In the next section, the TROPOMI data will first be described in general terms, followed by a description per species to address the retrieval methods, as well as a description of how we handle each data product in this study. The goal of this methods and data section is not only to explain how this study was conducted but also to provide guidance to data users on how to best interpret and analyze TROPOMI trace gas data not only for lockdown-driven emission changes but also for other event-driven changes. This will be followed by a context-setting section ~~describing~~ reviewing the global and regional impacts of COVID-19 lockdown measures and city-scale effects ~~on~~ for all continents, using TROPOMI NO$_2$ data. The next two sections will describe the effect of the lockdown measures on a regional scale by examining NO$_2$, SO$_2$, CO, HCHO, and CHOCHO for China and India. The last section will feature an outlook of future applications for this type of analysis followed by conclusions.

2   Methods and Data

In this work, our analysis is primarily based on TROPOMI data for regional lockdown periods in 2020 as compared to the same periods in 2019 and will be presented in the broader context of the TROPOMI operational data record, which started on 30 April 2018. We make use of observations from the TROPOMI instrument on board S5P which is a push-broom imaging spectrometer (Veefkind et al., 2012) measuring in the ultraviolet (UV), visible (VIS), near-infrared (NIR), and shortwave infrared (SWIR) spectral bands selected to measure the absorption by a large number of trace atmospheric constituents as well as by clouds and aerosols~~cover absorption regions for clouds and a large number of trace atmospheric constituents~~. Using the spectral radiance measurements from TROPOMI, atmospheric ~~concentrations~~ column amounts of different gases are retrieved as well as cloud and aerosol properties. For this work, we use the following TROPOMI data products: NO$_2$, SO$_2$, CO, HCHO and CHOCHO as summarized in Table 1. We did not include the following TROPOMI data products: tropospheric ozone columns, due to the tropics-only spatial coverage; methane, due to an even longer atmospheric lifetime than CO where its sources were not as impacted by lockdown measures; and aerosol index, designed to highlight long-range transported and/or elevated plumes of smoke, dust, and/or ash and which is not a quantitative measure of aerosol amount nor sensitive to near-surface emissions.

109   The S5P satellite flies in a Sun-synchronous orbit, with a local overpass time of 13:30. TROPOMI has a 2600 km

110   wide swath, providing near-daily global coverage. The spatial sampling of TROPOMI varies over the spectral bands.

111   The nadir sampling at the start of the operational period on 30 April 2018 was approximately 3.5 x 7 km^2 (across- x

112   along-track) for the ultraviolet and visible bands, and 7 x 7 km^2 in the shortwave infrared band. On 6 August 2019,

113   after implementation of a modified co-adding scheme, the sampling for these bands was improved to 3.5 x 5.5 km^2

114   and 7 x 5.5 km^2, respectively.

115   TROPOMI observations are being widely used within and beyond the scientific community and so it is crucial to

116   provide information on how these observations can best be used, interpreted, and analyzed. The COVID-19 lockdown

117   periods provide a unique use-case for the TROPOMI lead algorithm developers to highlight important differences in

118   the individual atmospheric lifetime and detectability of each trace gas and show how these characteristics are key to

119   the interpretation of the concomitant observations. It is not sufficient, for example, to illustrate lockdown-driven

120   changes in emissions simply by selecting a single day or week of TROPOMI column data for a given region as

121   measured during a lockdown period to the same day or week from year(s) prior (Braaten et al., 2020). We go further

122   to address the importance of delineating meteorological and seasonal variability from lockdown-driven changes in

123   emissions.

124   Therefore, we start this methods and data section with a general overview of considerations for the data user to take

125   into account for analyses aimed at the quantification of changes in the emission of these trace gases. Next, in dedicated

126   subsections, we provide a summary of the most relevant documentation and retrieval methods employed for each trace

127   gas (see Table A1). Even though each retrieval is based on the analysis of the amount of trace gas specific absorption

128   in measured radiance spectra, methods differ significantly per species.

129   **2.1   Understanding and Interpreting TROPOMI trace gas retrievals**

130   For this paper we will focus on TROPOMI trace gas retrievals for NO_2, SO_2, CO, HCHO, and CHOCHO (See Table

131   1). To understand and interpret the TROPOMI measurements of these trace gas species and how they vary with respect

132   to COVID-19 lockdown measures, it is necessary to consider their sources, variability through the atmospheric

133   column, and their atmospheric lifetimes. Although the mechanisms for the emission of each gas are different, there

134   are several common anthropogenic emission sources, most notably from transportation and industry, as listed in Table

135   1 which were significantly impacted by lockdown measures.

136

137 **Table 1: Summary of the retrieval spectral range, atmospheric lifetime, and ~~primary~~ main emission sources, for each trace**

138 **gas addressed in this study.**

Trace Gas Data Product Type (retrieval reference)	Spectral Range	Typical lifetime	~~Primary~~ Main emission sources
NO_2 Operational (van Geffen et al., 2019)	405-465 nm	2 to 12 hours	- Transportation - Industry - Power generation - Biomass burning

SO$_2$ Prototype (Theys et al., 2021)	310.5-326 nm	6 hours to several days	- Power generation - Industry - Transportation - Volcanoes[1]
CO Operational (Landgraf et al., 2016)	2324–2338 nm	Weeks to a month	- Transportation - Residential cooking and heating - Industry ~~Power generation~~ ~~- Industry~~ ~~- Transportation~~ ~~- Residential cooking and heating~~ - Biomass burning - Oxidation of biogenic hydrocarbons - Methane Oxidation - Power generation
HCHO Operational (De Smedt et al., 2018)	328.5-359 nm	Several hours (lifetime of NMVOC precursors up to several days)	Primary and secondary product (NMVOC precursors) from: - Biogenic emissions - Biomass burning - ~~Industry~~Transportation - ~~Transportation~~Industry
CHOCHO Prototype (Lerot et al., ~~2010,~~ 2020)	435-460 nm	Several hours (lifetime of NMVOC precursors up to several days)~~2 to 3 hours~~	Primary and secondary product (NMVOC precursors) from: - Biogenic emissions - Biomass burning - Transportation - Industry

139   [1]Volcanic emissions are not significant for this work.

140

141   A brief evaluation of how the sources of these trace gases were or were not affected by lockdown-driven changes

142   lends insight into expected changes. In general, primary production trace gases, like NO$_2$ and SO$_2$ with relatively short

143   atmospheric lifetimes exhibit emission changes most clearly and rapidly. Although NO$_2$ and SO$_2$ are both important

144   primary production anthropogenic pollutants, their sectoral sources are different. For instance, the impact of lockdown

145   on the transportation sector is expected to have a bigger impact on NO$_2$ than SO$_2$, since this sector is responsible for

146   about 30% of the global NOx emissions and only 1% of the global SO$_2$ emissions, according to the CAMS-ANT

147   inventory (Granier et al., 2019). On the other hand, SO$_2$ emissions are more likely to be impacted by possible changes

148   in power generation, since this sector accounts for 52% of the global SO$_2$ emissions and only 30% of the global NOx

149   emission (Granier et al., 2019).

150   For CO, secondary production by methane oxidation and the oxidation of (biogenic) hydrocarbons accounts for at

151   least 60% of the total atmospheric CO, followed by contributions from biomass burning and fossil fuel use (Müller et

152   al., 2018; Holloway et al., 2000). Anthropogenic CO emissions originate from the industry, transportation, and

153 residential sectors and account for about 30% of the global emissions (Granier et al., 2019). However, it is noted that
154 the relative contribution of these sources varies per global region (Granier et al., 2019 (Janssens-Maenhout et al.,
155 2015). Although local impacts of lockdown are likely for locations with strong anthropogenic CO emissions, overall
156 a much smaller lockdown-driven impact is expected for CO based on its longer atmospheric lifetime and smaller
157 contributions from lockdown affected sources (Clark et al., 2021).

158   Both HCHO and CHOCHO are short-lived indicators of non-methane volatile organic compound (NMVOC)
159 emissions resulting from biogenic processes, large biomass burning events, and anthropogenic activities (Millet et al.,
160 2008; Fu et al., 2008; Stavrakou et al., 2009; Bauwens et al., 2016; Chan Miller et al., 2016). They are mostly produced
161 as secondary products from oxidation of other NMVOCs but are also directly emitted from combustion and industrial
162 processes, although to a lesser extent. In general, the relative production of CHOCHO from such combustion processes
163 and from the oxidation of aromatics, originating mostly from the industrial sector, is higher than for HCHO. Thus, the
164 CHOCHO response to changes in anthropogenic emissions is expected to be stronger (Chan Miller et al., 2016; Cao
165 et al., 2018).

166   It is important to note that the retrievals provide information on the tropospheric or total column amount of these
167 gases, because the spectra contain limited information on their vertical distribution in the atmosphere. TROPOMI
168 observations thus provide a two-dimensional representation of the three-dimensional atmosphere. The vertical profiles
169 of each trace gas vary significantly depending on the injection height of the emissions and atmospheric lifetime (see
170 Table 1). For example, NOx emissions at the surface result in NO_2 vertical profiles that peak in the near-surface layer
171 (lowest 1-2 km of the troposphere), due to the short lifetime of NO_2. Similarly, SO_2 has a vertical profile which
172 generally peaks in the lower troposphere. CO on the other hand, has a lifetime of weeks to a month (depending on the
173 reaction with the hydroxyl radical) and can be transported over great distances, both horizontally and vertically.
174 Therefore, CO even though it is often co-emitted with NO_2, has a significantly higher background concentration
175 throughout the troposphere as compared to NO_2. HCHO and CHOCHO have lifetimes of a few hours but are generally
176 formed in the atmosphere via secondary production processes, which leads to an intermediate profile shape as
177 compared to NO_2 and CO.

178   In addition to vertical profiles that vary per trace gas species, the vertical sensitivity of the TROPOMI measurements
179 also varies per species. For the trace gases retrieved in the UV and VIS ranges, the sensitivity decreases towards the
180 surface so that the accuracy of the retrieved column depends on a well-characterized a priori knowledge of the vertical
181 distribution. Due to scattering, the near-surface sensitivity is lower in the UV (SO_2, HCHO) than in the VIS (NO_2 and
182 CHOCHO). In the SWIR range, the vertical sensitivity is more constant. As part of the retrieval process, a priori
183 vertical profiles of each trace gas are scaled to match the measured tropospheric column. An uncertainty in the
184 retrieved column amount or vertical column density (VCD) is associated with inherent differences between the true
185 and a priori vertical profiles. However, the averaging kernels, which are reported in the data products, can be used to
186 replace the a priori profiles with custom profiles (e.g. Eskes and Boersma, 2003; Eskes et al., 2020) thereby reducing
187 the corresponding uncertainty. In this study, we mostly focus on relative changes in VCDs and use standard a priori
188 profiles for each data product. Therefore, the uncertainty related to the vertical profile is rather small (as detailed in
189 Sect. 2.2 through 2.6). Another contribution to this error is the use of partly cloudy scenes by each retrieval which

190 increases the amount of data available but does change the vertical sensitivity. The cloud fraction threshold for each

191 trace gas is described in Sect. 2.2 through 2.6. In future studies, the averaging kernels could be used for inversion

192 modelling of emissions. As explained in Eskes and Boersma 2003, relative comparisons between the observations and

193 the model used in the inverse modelling system, and therefore the resulting emissions, no longer depend on the

194 retrieval a-priori profile shape when the kernel is applied to the model.In future studies, the averaging kernels could

195 be used for inversion modelling of emissions thus eliminating this error completely.

196 TROPOMI observes atmospheric concentrations of trace gases averaged over a vertical column, which is not the

197 same as a direct measurement of the (near-surface) emission. The column averaged amount of a given trace gas

198 measured at a certain location depends not only on emission and deposition, but also on atmospheric transport and

199 (photo)chemical reactions. TROPOMI observes atmospheric concentrations of trace gases integrated over a vertical

200 column, which is not the same as a direct measurement of the (near-surface) emission. The amount of a given trace

201 gas integrated over a vertical column at a certain location depends not only on emission and deposition, but also on

202 atmospheric transport and (photo)chemical reactions. Note that the background concentration is higher for trace gases

203 with a longer atmospheric lifetime. In turn, enhanced background concentrations will increase the relative importance

204 of atmospheric transport versus local emissions. Local NO_2 emissions have a relatively large impact on the measured

205 column amounts, while for CO the contribution of remote sources can in some cases be superimposed on local

206 emissions thus making the interpretation more difficult. To attribute a change in concentration to a corresponding

207 change in local emissions, the effects of meteorology and chemical lifetime must be accounted for as well.

208 While emissions can be estimated from satellite observations using data-driven methods (Beirle et al., 2019, Beirle

209 et al., 2021; Fioletov et al., 2016; Goldberg et al., 2019) or using complex inverse modelling techniques (e.g. Millet

210 et al., 2008; Stavrakou et al., 2009; Bauwens et al., 2016; Ding et al., 2020; Miyazaki et al., 2020; Borsdorff et al.,

211 2019; Borsdorff et al., 2020), here we use a more qualitative approach to probe emission changes. First we compare

212 the concentrations column amounts in 2020 with those from the same period from earlier years and then carry out

213 additional analysis to separate the lockdown-driven variability from seasonal and meteorological variability taking

214 into account local information about lockdown and anticipated impacts from different source sectors.taking in account

215 emission changes driven by mechanisms.

2.2   Nitrogen dioxide (NO_2)

217 The tropospheric column of nitrogen dioxide (NO_2) is a TROPOMI operational data product (Veefkind et al., 2012;

218 doi.org/10.5270/S5P-s4ljg54). Product versions are listed in the Product Readme File (PRF, Eskes and Eichmann,

219 2019a). The retrieval method is described in detail in the NO_2 Algorithm Theoretical Basis Document (ATBD, van

220 Geffen et al., 2019). The data product and data usage are described in in the NO_2 Product User Manual (PUM, Eskes

221 et al., 2020). The dataset used for most of NO_2 analyses cover the period from 1 January 2018 to 30 May 2020. For

222 Europe, the dataset was extended through 31 August 2020.

223 The retrieval algorithm derives NO_2 information from spectral range 405-465 nm and is largely based on the OMI

224 NO_2 retrieval developments implemented during the EU QA4ECV project (Boersma et al., 2018). The retrieval

225 consists of three steps. The first step is based on the DOAS approach, in which the total slant column of NO_2 is

226 retrieved from the TROPOMI spectra, as discussed in van Geffen et al. (2020). The second step is the estimation of
227 the 3-D stratospheric distribution of NO_2 based on an assimilation of the TROPOMI slant column data of previous
228 days using the chemistry-transport model TM5-MP (Williams et al., 2017) run at 1° x 1°. This assimilation is set up
229 to predominantly make use of measurements over clean areas (e.g. ocean and remote land regions) with limited
230 tropospheric NO_2. The third step is the conversion of the tropospheric slant column (total minus stratosphere) into a
231 tropospheric vertical column by combining radiative transfer calculations with a priori profile shapes from the TM5-
232 MP model. The data product is very comprehensive and provides all the input (such as surface and cloud information)
233 and intermediate products.

234   The tropospheric column is delivered with corresponding averaging kernels and a detailed error estimate. The
235 random error on the slant column is discussed in van Geffen et al. (2020), and is on the order of 0.56×10^{15} molec cm⁻
236 ² for individual measurements after 6 August 2019 (for pixel size 3.5 x 5.5 km²). This translates to only small random
237 errors in the total columns on the order of 0.2×10^{15} molec cm⁻². Uncertainties in the estimate of the local stratospheric
238 column amount is of the same order of magnitude. The uncertainty related to the computation of the air mass factor
239 (AMF) is much more significant for tropospheric columns over polluted areas. The AMF uncertainties are driven by
240 the treatment of surface albedo, clouds, aerosols, and profile shape. Such errors are multiplicative, and are of the order
241 of 20-60% depending on the geographical location, time of day, and season (van Geffen et al., 2021). These
242 uncertainties are modelled for individual observations and are provided in the data product.

243   As for all operational TROPOMI data products, a quality assurance value (qa_value) is provided to filter the data
244 and remove lower quality data where, the recommended threshold value depends on the application (see also Appendix
245 A, Table A1). For direct visualization or gridding applications a qa_value greater than 0.75 is recommended. For
246 comparisons with models and data assimilation through the use of the averaging kernels, a relaxed qa_value of greater
247 than 0.5 may be used. In this study we use NO_2 retrievals with a qa_value greater than 0.75. Application of this
248 qa_value threshold corresponds to data with mostly clear-sky conditions (cloud radiance fractions < 0.5) and implies
249 that the data is filtered to remove retrievals which do not meet certain quality criteria as described van Geffen et al.
250 (2019).

251   Several recent papers discuss the validation of the NO_2 product against independent observations (Verhoelst et al.,
252 2021; Tack et al., 2021; Judd et al., 2020; Dimitropoulou et al., 2020; Ialongo et al., 2020). The main findings can be
253 summarized as follows: the stratospheric and slant columns are in good overall agreement with other satellite
254 measurements (van Geffen et al., 2020) and with ground-based observations (Verhoelst et al., 2021). However, the
255 tropospheric column presents a negative bias of the order of 30% with respect to ground-based remote sensing
256 reference observations (Verhoelst et al., 2021; Dimitropoulou et al., 2020), as well as with imaging data from airborne
257 measurements (Judd et al., 2020; Tack et al., 2021). Although the origin of this bias remains unclear and may be due
258 to several causes, validation results indicate that it scales linearly with the retrieved tropospheric column amount
259 (Verhoelst et al., 2021; see Fig. C1). As a result, (COVID-related) relative changes in the NO_2 column, e.g., (2020-
260 2019)/2019, should be largely insensitive to this bias.

2.3 Sulphur dioxide (SO$_2$)

Initial analyses were performed using the TROPOMI operational data product for SO$_2$ (Theys et al., 2017). However, biases present in those data (Fioletov et al., 2020) hamper the detection of the type of small changes in SO$_2$, typically on the order of -0.1 DU, that are under investigation in this work. Therefore, an alternative retrieval scheme was applied, the so-called COvariance-Based Retrieval Algorithm (COBRA; Theys et al., 2021). In brief, the approach considers a set of SO$_2$-free spectra in the wavelength range 310.5-326.0 nm (from TROPOMI band 3) to represent the radiance background variability, in the form of a covariance matrix. The latter is updated for each orbit, TROPOMI row, and per latitude band. The covariance matrix is used to determine the SO$_2$ slant columns from individual spectral measurements using an optimally weighted single parameter retrieval (see Walker et al., 2011). We note that COBRA does not recalculate air mass factors (AMF). These are simply extracted from the operational product to convert SO$_2$ slant columns into vertical columns (VCDs). Compared to the operational DOAS results, COBRA significantly improves the SO$_2$ VCDs, both in terms of precision and accuracy. Because the approach empirically accounts for all sources of systematic variability in the measured signal, large-scale biases typically observed with the DOAS approach are efficiently removed leading to a large gain in sensitivity (see Fig. C2).

In this study, we use SO$_2$ retrievals under clear-sky conditions (cloud fractions less than 30%) with solar zenith angles lower than 60°, and we eliminate 25 swath edge pixels from each side of the orbit swath (450 pixels wide). The random error in the SO$_2$ vertical columns is rather small in the range of 0.5-1.0 DU, and can be largely reduced by data averaging. Errors due to spectral interferences are estimated to be very low, about 0.05 DU (Theys et al., 2021). Remaining systematic uncertainties are mostly from the auxiliary data used in the AMF calculation, and are in the 30-50% range. The dataset used for this analysis covers the period from May 2018 to June 2020.

2.4 Carbon monoxide (CO)

The total column of carbon monoxide (CO) is a TROPOMI operational data product obtained using TROPOMI 2.3 micron measurements (Veefkind et al., 2012; doi.org/10.5270/S5P-1hkp7rp). Product versions are listed in the Product Readme File (Landgraf et al., 2020). The data product and data usage are described in in the CO Product User Manual (Apituley et al., 2018). This CO retrieval uses the Shortwave Infrared CO retrieval (SICOR) algorithm method and is described in detail in the CO Algorithm Theoretical Basis Document (Landgraf et al., 2018). The algorithm software is based on a scattering forward model and retrieves trace gas columns simultaneously with effective cloud parameters (cloud height, cloud optical thickness) from the SWIR channel to account for cloud contaminated measurements (Landgraf et al., 2016, 2018). The inversion deploys a profile scaling approach by which a vertical CO reference profile is scaled to obtain agreement between the forward simulation and the spectral measurement (Borsdorff et al., 2014). The reference profile is based on a monthly averaged simulation from the global chemical transport model TM5 and thus varies spatially and temporally (Krol et al., 2005). The vertical sensitivity of the retrieval for clear-sky conditions is good throughout the atmosphere while measurements for cloudy conditions have reduced sensitivity under the cloud (Borsdorff et al., 2018).

In this study, we use the CO retrieval for measurements under clear-sky and cloudy atmospheric conditions (cloud altitude less than 5000m). This corresponds to filtering the dataset by using the quality assurance values (qa_value

297 greater than 0.5) that are supplied with the data product. CO retrievals under low cloud conditions perform well for
298 unpolluted scenes however can lead to e.g. lower CO values when pollution hot spots are present below the cloud due
299 to optical shielding and scattering (Borsdorff et al., 2018). Consequently, retrievals under cloudy conditions must be
300 considered with care, however they are essential to improve the data coverage especially over the oceans where clear-
301 sky measurements are hampered by the low reflectivity of water in the SWIR spectral range.

302   The CO retrieval skill lies well within the requirements of the TROPOMI mission (Veefkind et al., 2012) on accuracy
303 (< 15%) and precision (< 10%). This was shown by validation with ground-based FTIR measurements operated by
304 the Total Carbon Column Observing Network (TCCON). TROPOMI CO is biased high compared to TCCON by
305 about 6 ppb with a station to station variability of about 4 ppb (Borsdorff et al., 2018; Lambert et al., 2020). The
306 dataset used for this analysis covers the period from 1 January 2018 to 30 May 2020.

307 **2.5   Formaldehyde (HCHO)**

308 The tropospheric column of formaldehyde (HCHO) is a TROPOMI operational data product (Veefkind et al., 2012;
309 doi:10.5270/S5P-tjlxfd2). Product versions are listed in the HCHO Product Readme File (De Smedt et al., 2020a).
310 The data product and data usage are described in in the HCHO Product User Manual (PUM, Romahn et al., 2020).
311 The TROPOMI HCHO retrieval algorithm has been fully described in De Smedt et al. (2018) and in the HCHO ATBD
312 (De Smedt et al., 2020b). It is based on the DOAS method, and is directly inherited from the OMI QA4ECV product
313 (https://doi.org/10.18758/71021031). The fit of the slant columns is performed in the spectral interval of 328.5-359.0
314 nm. Reference spectra are updated daily using an average of Earth radiances selected in the Equatorial Pacific region.
315 The conversion from total slant to tropospheric vertical columns is performed using a look-up table of vertically
316 resolved air mass factors calculated at 340 nm. A priori vertical profiles are provided by the TM5-MP daily forecast
317 with a spatial resolution of 1 x 1 degree (Williams et al., 2017). Cloud properties are taken from the S5P operational
318 product Cloud as Reflecting Boundary (CRB; Loyola et al., 2018). In order to correct for any remaining offset and
319 striping due to instrumental artefacts or unknown misfits in the spectral retrieval, a background correction is applied
320 based on HCHO slant columns selected in the emission-free Pacific Ocean. The background HCHO vertical column,
321 due to the methane oxidation, is added using data from the TM5 model in the reference region. We use the quality
322 assurance values (qa_value greater than 0.5) to filter out observations presenting a solar zenith angle larger than 70°
323 or cloud fractions larger than 0.4.

324   The HCHO retrieval fulfils the requirements of the TROPOMI mission (Veefkind et al., 2012) on accuracy (40-
325 80%) and precision ($12x10^{15}$ molec cm^{-2}). The precision of a single observation is estimated to be $5x10^{15}$ molec cm^{-2}
326 in remote locations. The dispersion is naturally larger over polluted sites (from $7-10x10^{15}$ molec cm^{-2}). Validation
327 using a global network of FTIR measurements indicates that TROPOMI HCHO columns present a negative bias over
328 high emission sites (-30% for HCHO columns larger than $7.5x10^{15}$ molec cm^{-2}) and a positive bias for clean sites
329 (+20% for HCHO columns lower than $2.5x10^{15}$ molec cm^{-2}) (Lambert et al., 2020; Vigouroux et al., 2020).

330   To characterize the HCHO interannual and seasonal variability, we have used the QA4ECV OMI dataset to construct
331 a climatology based on recent years (2010-2018). This is justified the good agreement between OMI and TROPOMI

332 HCHO columns which is better than 10% for most regions (Lambert et al., 2020). For our analysis, we use two-week
333 averaged columns. This reduces the random uncertainty to about 10%.

334   One of the main drivers of the observed HCHO variability is temperature, which has a direct impact on NMVOC
335 emissions and on the chemical production of HCHO (Stavrakou et al., 2018). It results in a strong correlation between
336 HCHO columns and surface temperatures. For this paper, we correct the HCHO ~~concentrations~~ column amounts for
337 this meteorological impact prior to using the data in the analyses. We introduce a temperature correction method (Zhu
338 et al., 2017) based on data from OMI for 2005-2020, and from TROPOMI for 2018-2020. In brief, this correction
339 entails fitting a second-order polynomial through daily HCHO columns reported as a function of the temperature. This
340 ~~novel analysis~~temperature correction is performed for each region and on the OMI and TROPOMI time series
341 separately. On this basis, the temperature-induced variations in HCHO are removed from the time series using local
342 daily temperatures specified by ERA5-Land 2m meteorological datasets (Muñoz Sabater, 2019a; See Fig. C3). This
343 correction is designed to minimize the impact of temperature fluctuations on the HCHO anomalies. Finally, a
344 polynomial obtained using a climatology of surface temperatures is added to the differential HCHO columns, in order
345 to reintroduce the natural seasonal cycle, assuming the same temperature every year. These temperature-corrected
346 HCHO columns are used throughout this paper. Note that the difference with uncorrected HCHO columns is generally
347 small (less than 10%), but can be significant when looking for small effects such as those induced by COVID-19
348 related emission changes. The dataset used for this analysis covers the period from May 2018 to June 2020.

2.6   Glyoxal (CHOCHO)

350 Glyoxal (CHOCHO) is not one of the TROPOMI operation~~als~~al data products. For this study we used the prototype
351 data product developed as part of the ESA S5p+I GLYRETRO project, which relies on scientific developments
352 performed using the GOME-2 and OMI instruments (Lerot et al., 2010). The algorithm is described in detail in the
353 GLYRETRO ATBD (Lerot et al., 2020). In brief, the retrieval approach consists of a DOAS-type spectral fit for the
354 observed optical depth with reference absorption cross-sections for glyoxal and other absorbing species (NO_2, O_3, O_2-
355 O_2, liquid water and water vapor, and the Ring effect) in the spectral interval of 435-460 nm to derive glyoxal slant
356 column densities. The latter are converted into tropospheric columns using calculated air mass factors, after application
357 of a background correction procedure aimed at reducing possible remaining (row-dependent) systematic biases. Air
358 mass factors are calculated following the formulation of Palmer et al. (2001), which combines altitude-dependent air
359 mass factors (or Box-AMFs) with a priori glyoxal concentration profiles. The Box-AMFs represent the instrumental
360 sensitivity to changes in concentration at any altitude and are precomputed using the radiative transfer model
361 VLIDORT v2.7 (Spurr and Christi, 2019), while the a priori profiles are provided by the MAGRITTE chemistry-
362 transport model (Müller et al., 2018, 2019). ~~Air mass factors are calculated following the formulation of Palmer et al.~~
363 ~~(2001), which combines box air mass factors precomputed with the radiative transfer model VLIDORT v2.7 (Spurr~~
364 ~~and Christi, 2019) and a priori glyoxal concentration profiles provided by the MAGRITTE chemistry-transport model~~
365 ~~(Müller et al., 2018, 2019).~~
366   The glyoxal optical depth is very small ($< 5 \times 10^{-4}$), which makes its retrieval very sensitive to instrumental noise and
367 to interferences with spectral signatures of species absorbing more significantly in the same spectral region. The first

368 factor introduces large random errors, in the range $6\text{-}10\text{x}10^{14}$ molec cm^{-2}, which can however be reduced by spatial-

369 temporal averaging, that is, using multiple observations averaged time and/or space. Systematic uncertainties are

370 dominated by spectral interferences, but also by uncertainties associated with the auxiliary data used as an input for

371 the AMF calculation. These uncertainties are estimated to be $2\text{-}3\text{x}10^{14}$ molec cm^{-2} (~50% for source regions). To limit

372 uncertainties related to cloud contamination, glyoxal observations are only provided for scenes with effective cloud

373 fractions smaller than 20% (taken from the operational NO_2 product). As with HCHO, to account for seasonal and

374 interannual variability, a climatology of OMI CHOCHO columns was built to further delineate sources of variability

375 for glyoxal column amounts.

376 Validation of satellite glyoxal column observations is generally limited, mostly due to the scarcity of independent

377 ground-based data. However, a preliminary validation based on a few MAX-DOAS stations in Asia and Europe,

378 indicates that the satellite and ground instruments measure consistent glyoxal tropospheric column amounts with mean

379 differences generally less than $2\text{x}10^{14}$ molec cm^{-2}, except in particular conditions such as low sun elevation or for

380 stations that are frequently covered by clouds (Alvarado et al., 2020). The dataset used for this analysis covers the

381 period from May 2018 to June 2020.

382 **3   Global Observations of Nitrogen Dioxide**

383 Numerous papers have shown that TROPOMI measurements of tropospheric NO_2 column amount are well-suited for

384 detecting emission from a variety of anthropogenic sources including traffic, power plants, and industry (van der A et

385 al., 2020; Goldberg et al., 2019). The atmospheric lifetime of NO_2 and its vertical profile shape dictate that the high

386 spatial resolution measurements from TROPOMI can readily capture rapid week-to-week changes in near-surface

387 emissions from COVID-19 impacted cities and point sources (Sekiya et al., 2021; Fioletov et al., 2021; Stavrakou et

388 al., 2021; Gkatzelis et al., 2021). To give context and overview, the global distribution of tropospheric NO_2 based on

389 an annual average for 2019 with an oversampling resolution of approximately $0.02°$ x $0.02°$ is illustrated in ~~Figure 1.~~

390 The high resolution of these measurements enables further zooming to the regional, suburban, and city scale providing

391 detailed information about spatial distributions. Three further zoom-in cases for central Chile and its capital Santiago,

392 for Paris, and for New Delhi are shown in ~~A regional zoom-in over central South America reveals high NO_2 levels~~

393 ~~over the megacities of Rio de Janeiro, São Paulo, Buenos Aires, and Santiago. A further zoom-in to central Chile and~~

394 ~~its capital Santiago is shown in Figure 1.,~~ These cases focus~~ing~~ on a shorter period~~s~~ coinciding with region-specific

395 COVID-19 lockdowns (see Appendix B). Observed column amounts of NO_2 are compared to similar periods in 2019,

396 which are chosen to be longer than the 2020 period in order to reduce the effects of natural variability. Strong

397 reductions in the NO_2 tropospheric column amounts are observed during lockdown periods (Bauwens et al., 2020;

398 Barré et al., 2021; Griffin et al., 2020; Qu et al., 2021). Interestingly, further zoom in shows that the relative reduction

399 is not uniform over a city, reflecting differences in the mix of source contributions for different quarters of a given

400 city. ~~from 23 March to 10 April 2020, which coincides with a region-specific COVID-19 lockdown (Figure 2k), as~~

401 ~~compared to the mean tropospheric NO_2 column for March-April 2019. Note that the period in 2019 is chosen to be~~

402 ~~longer than 2020 in order to reduce the effects of natural variability, but the period is centered at the beginning of~~

403 ~~April to avoid the influence of the seasonal NO_2 cycle. A strong reduction in the NO_2 tropospheric concentration of~~

about 40% is observed over Santiago during this period, and a 28% reduction is observed between 23 March and 15 May corresponding to the period when restrictions were eased (Figure 2k). Interestingly, a further zoom shows that the relative reduction is not uniform over the city, reflecting differences in the mix of source contributions for the different quarters of the city.

411
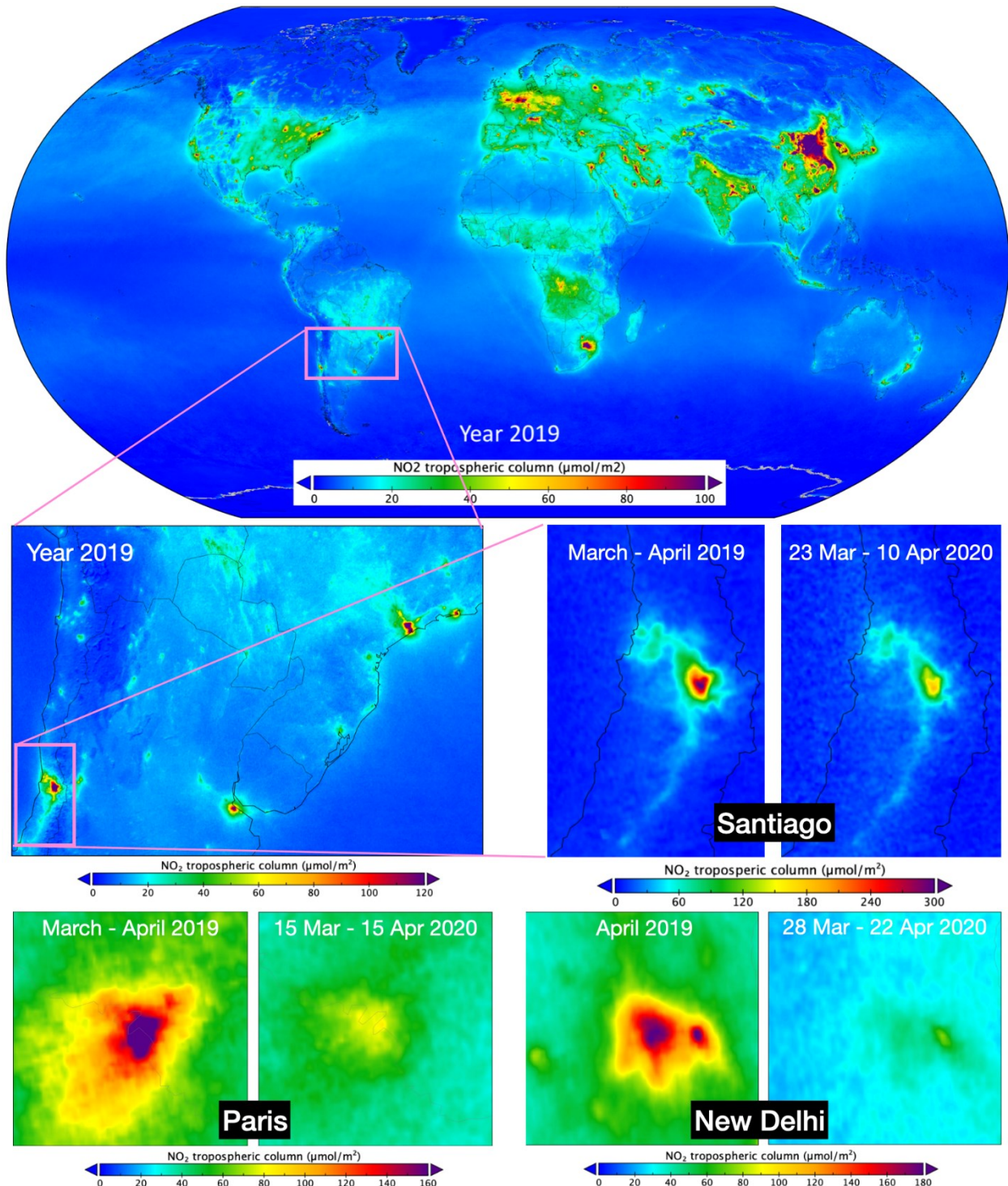
Figure 1: Global distribution of NO₂ based on the annual average of tropospheric column amounts of NO₂ measured by TROPOMI for 2019 (top panel) shown in units of micromole per m². Using the same data, several zoom-in plots are shown in the middle and bottom panels: regional zoom-in for central South America (middle left) and a city-scale zoom-in over Santiago, Chile (middle right panels, comparing 23 March to 10 April 2020 with March-April 2019), over Paris (lower left, comparing 15 March to 15 April 2020 with March-April 2019) and over New Delhi (lower right, comparing 28 March to 22 April 2020 with April 2019). Note the different color scales in the three subpanels. The domain size of the panels is 1.5 x 1.0 degree for Paris, and 1.1 x 1.0 degree for New Delhi.

419

420

421   The lockdown periods and the measures taken to mitigate the spread of COVID-19 were rolled out on country- and

422   often city-specific basis. Figure 2 illustrates the temporal evolution of NO_2 tropospheric column amounts from January

423   to May over large cities across different continents. The observed reductions in China and India are discussed in more

424   detail in Sections 4 and 5. Detailed information about the lockdown measures adopted for those cities is given in Table

425   B2. Appendix B provides a detailed description of the observed reductions during the specific lockdowns for

426   individual (mega)cities shown in Figure 2 and Figure 3. The TROPOMI observations indicate substantial decreases

427   in NO_2 during the lockdowns in all studied cities, but the reductions vary significantly from one city to another. Two

428   more examples of lockdown related NO_2 column reductions in major cities are shown for Paris and New Delhi in

429   Figure 1 with time windows selected to reflect region specific lockdown periods. In Paris, the NO_2 levels for the

430   period 15 March to 15 April 2020 are about a factor of two lower than in March-April 2019 (see also Figure 4). For

431   New Delhi the reduction is even more striking in comparison to April 2019 (about a factor of 3, Figure 2c). Both Paris

432   and New Delhi also show significant reductions in background values around the cities. Background locations are

433   subject to a variety of wind directions and sometimes downwind of city plumes thus influencing background

434   concentrations. Such plumes are typically on the order of 100 km long, and, given the atmospheric residence time of

435   NO_2 (2-12 hours), these plumes can fill the small domains around Paris and New Delhi shown in Figure 1.

436

437
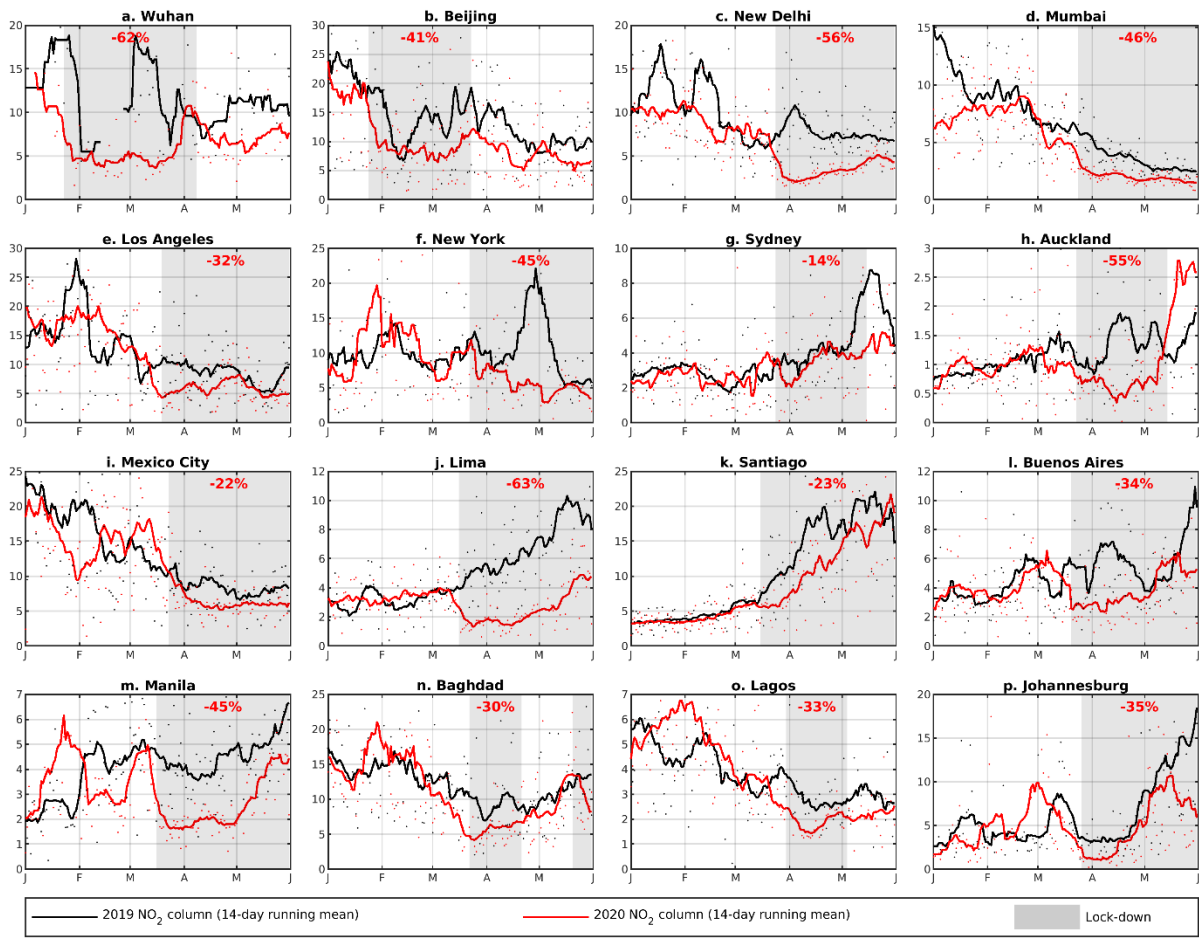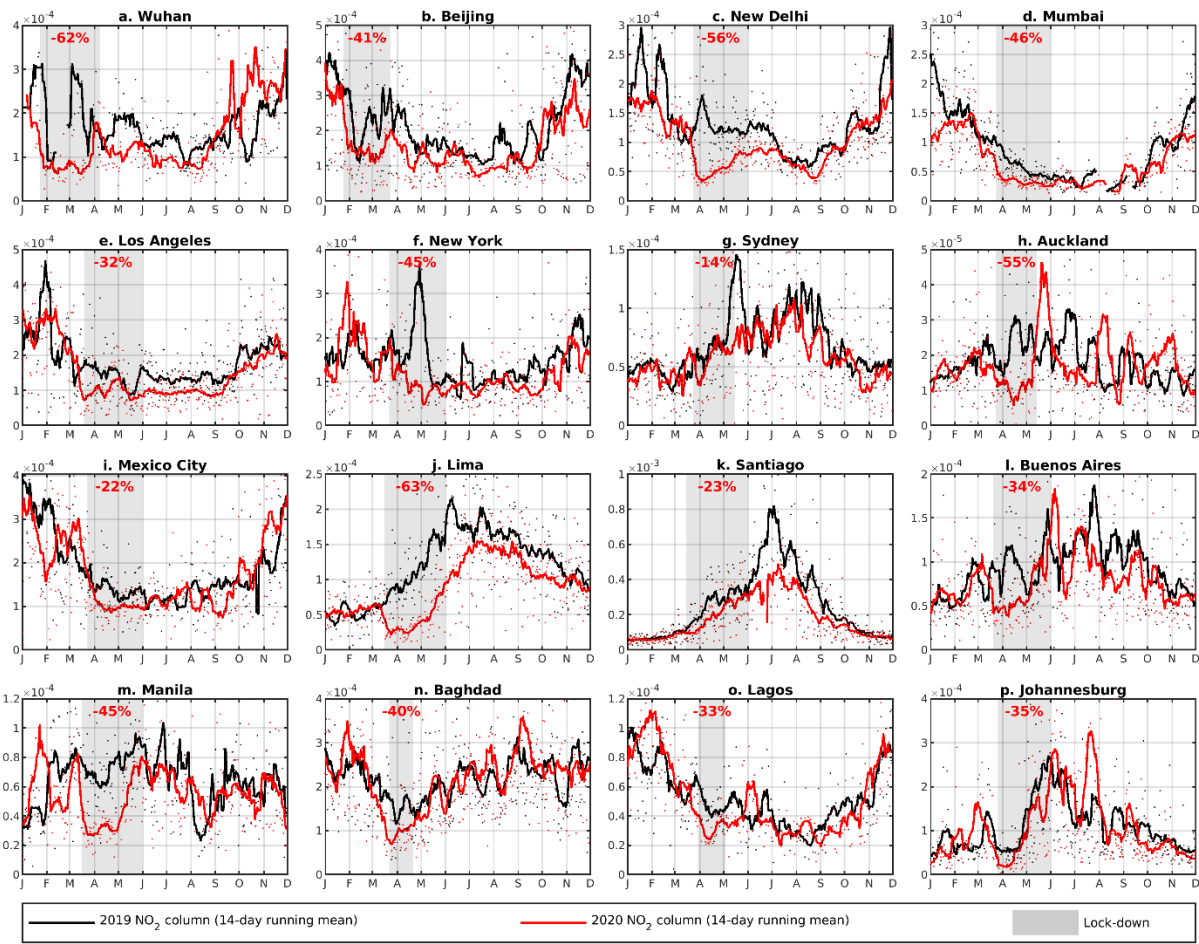
Figure 2: Time series of TROPOMI NO₂ column amounts (in ~~10¹⁵ molce~~mol cm⁻²) for selected cities for the period 1 January to ~~11 June~~December in 2019 (black dots) and 2020 (red dots). TROPOMI observations are averaged over a 25 x 25km² box around the city center. The lines indicate the two-week running mean for 2019 (black) and 2020 (red). The grey zones indicate the official lockdown period for each city. The reduction of the average NO₂ column during the lockdown period relative to the same period in 2019 is given inset. Details about the lockdown dates are summarized in Table ~~B~~C2.

The lockdown periods and the measures taken to mitigate the spread of the COVID-19 were rolled out on a country- and often city-specific basis. Figure 2 ~~Figure 2~~and Figure 3 illustrate~~s~~ the temporal evolution of NO₂ tropospheric columns from January to May over large cities for different continents. The observed reductions in China and India are discussed in more detail in Sect. 4 and 5. Detailed information about the lockdown measures adopted for those cities is given in Table B~~C~~2. The TROPOMI observations indicate substantial decreases in NO₂ during the lockdowns in all studied cities, but the reductions vary significantly from one city to another.

~~In Wuhan, the first city to issue quarantines and lockdown measures, the observed NO₂ column drastically declined (-60%) between 23 January and 8 April 2020 compared to the same period in 2019 (Table C2). This decrease is in good agreement with estimated reductions for the period 11 February to 2 March 2020 based on TROPOMI NO₂ (-43%, Bauwens et al., 2020) and in situ NO₂ observations in Wuhan (-55%, Shi and Brasseur, 2020). However, it should be noted that there was strong day-to-day variability in the NO₂ column amount due to meteorological factors,~~

as well as missing data over Wuhan in February 2019 due to clouds. Model calculations by Liu et al. (2020) indicate that meteorological variability could have led to increased NO_2 columns in 2020 compared to 2019, suggesting that the observed NO_2 reductions underestimate the impact of emission reductions due to COVID-19. The partial lifting of the restrictions on 8 April led to a progressive increase in NO_2 levels, yet remained lower than in 2019, likely because the population was still advised to stay at home and schools remained closed. A similar response in NO_2 levels was observed in Beijing. The decreases were less pronounced (-40%) and are in excellent agreement with the reported decrease based on in situ NO_2 measurements (-40%, Shi and Brasseur, 2020). The weaker response could be due to the less drastic measures adopted in Beijing, because locally sustained COVID-19 cases were lower than in the Hubei province (Leung et al., 2020). Strong NO_2 reductions were observed for other Chinese cities, like Nanjing, Qingdao, and Zhengzhou, based on TROPOMI NO_2 observations (Bauwens et al., 2020).

India enforced strict restrictions of human activities on 24 March 2020 to tackle the spread of COVID-19. In New Delhi and Mumbai, the onset of the lockdown induced a sharp decline in the observed NO_2 columns (by a factor of 2). The columns remained low during the entire lockdown period (-56% and -46%, respectively) (see Table 2 for timing of lockdown phases). This is very much in line with the decreases reported in New Delhi based on NO_2 data from monitoring stations, -53% (Mahato et al., 2020) and -48% (Jain and Sharma, 2020).

As compared to other cities, a very strong NO_2 decrease was observed in Lima (-63%), where strict regulations to stay indoors were enforced (Collyns, 2020). A drastic drop in NO_2 compared to the 2019 levels marked the start of the lockdown, and the levels remained very low throughout the entire lockdown period. The gradual increase of NO_2 columns in Lima and other Southern Hemispheric cities from January to May (Figure 2) reflects the natural seasonal variation when levels peak during the Southern Hemispheric winter, as temperatures decrease and NO_2 lifetime increases.

In Buenos Aires, the observed reduction was not as strong compared to Lima for the entire lockdown period (-34%, Table C2), but was particularly marked during the first month of the lockdown (20 March through 20 April 2020), due to a compulsory quarantine period and strict limitation of activities for many sectors. Although partial lifting of measures was issued after 10 April for many provinces in Argentina, the measures in the Buenos Aires agglomeration were maintained due to the elevated number of cases (Raszewski and Garrison, 2020). More moderate reductions are found for Mexico City (-22%) and Santiago (-23%) during the lockdown in comparison to the same period in 2019, that could be attributed to less strict adherence to and enforcement of lockdown measures (Uchoa, 2020; Pasley, 2020).

Strong reductions were observed over the entire lockdown period in the heavily hit cities in southwest Europe, Los Angeles, and New York, with reductions ranging between -32% and -54% (Bauwens et al., 2020). It should be noted however, that in these regions, the start of the lockdown period is generally less marked partly because the lockdowns were not as strictly enforced in Europe and the U.S. as in China and India. Moreover, the observed TROPOMI data displays a strong variability attributable to meteorology, e.g. over Paris, New York and Los Angeles in 2019.

In Sydney, the reduction was moderate (-14%) and delayed with respect to the onset of the measures (Figure 2). This could be related to observations of less strict compliance in the early period of lockdown measures (New South Wales Public Health, 2020). A rapid and strong decrease was observed for NO_2 column amount as a result of lockdown measures in Auckland, New Zealand (-55%). Similarly, the lockdown measures in New Zealand were implemented

493 swiftly with high levels of compliance (Matthews, 2020). The end of the lockdown coincided with a strong increase

494 in NO$_2$ pollution, from 1.8×10^{15} molec cm^{-2} to 3×10^{15} molec cm^{-2} in the last three weeks of May.

495 In Africa, Nigeria is among the countries most affected by COVID-19 and reported the first confirmed case in sub-

496 Saharan Africa (Odunsi, 2020; Adigun and Anna, 2020). A two-week lockdown period was put in place for Lagos

497 starting 30 March. The NO$_2$ column amount decreased by 33% during the lockdown (Figure 2) with respect to the

498 same period of 2019 and remained lower even after the lifting of restrictions on 4 May (Table C2). An NO$_2$ column

499 decrease of similar magnitude (-35%) was observed in Johannesburg, where a national lockdown was issued on 26

500 March 2020, with a gradual easing of restrictions starting 1 May. In Sub-Saharan Africa, the emission reductions in

501 April were significant for larger populous and industrialized areas, whereas no noticeable drop was found in less

502 developed regions (Masaki et al., 2020).

503 Finally, the Iraqi capital of Baghdad faced an initial lockdown from 22 March through 21 April. A second partial

504 lockdown was issued starting 20 May in response to a sharp increase in COVID-19 cases due to the temporary

505 relaxation of restrictions to allow the celebration of Ramadan in late April (Table C2). The NO$_2$ column responded

506 quickly (Figure 2n) as confirmed by the rapid decrease once curfew measures were issues in late May.

507 Figure 3 and Figure 4 illustrate the tropospheric concentration of NO$_2$ over Europe, focusing on Milan, Madrid,

508 Paris and Berlin (Figure 3), extending the analysis to include summer months. In France, Spain and Italy we detect

509 strong reductions of NO$_2$, which can be largely attributed to the lockdown measures. In Berlin, the measured

510 differences are smaller, and a more detailed analysis of the meteorological variability is needed to quantify the impact

511 of the lockdown (see Figure 3). The extended time series shows a recovery of the NO$_2$ pollution levels to pre-COVID-

512 19 values. However, the recovery is not complete, suggesting that remaining restrictions, new stay-at-home life and

513 working practices, together with a downturn in industrial and service-based activities have contributed to a longer

514 lasting impact.

515

516

517

518

519
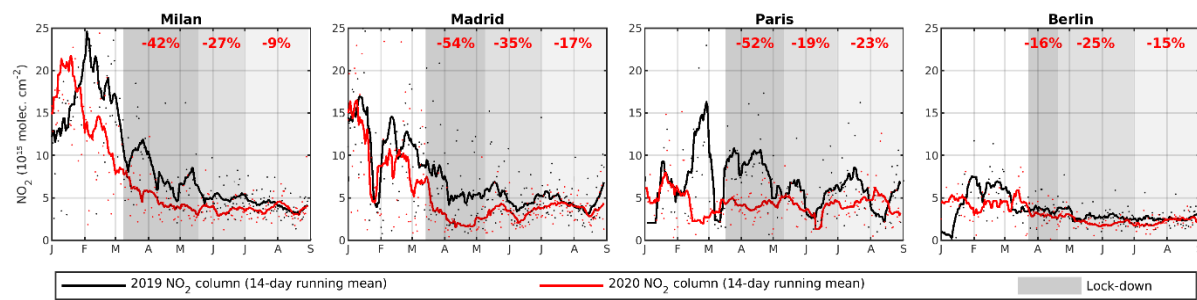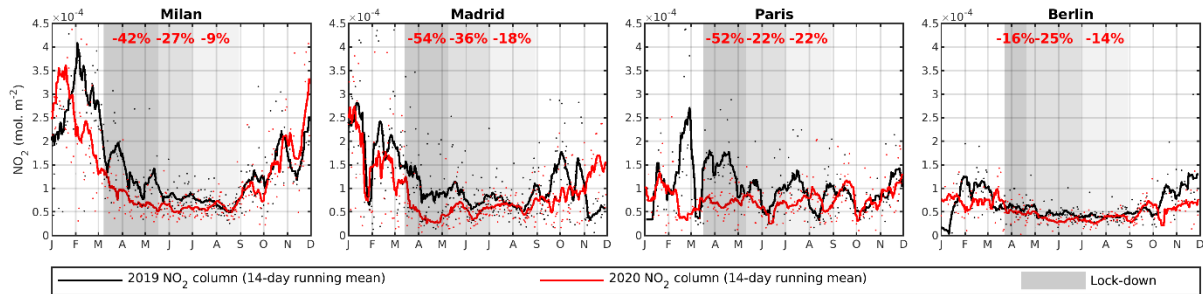
Figure 3: Same as Figure 2, ~~Figure 2,~~ for the European cities Milan, Madrid, Paris, and Berlin, for ~~an extended~~the same period of 1 January to ~~11 September~~December in units of mol m^{-2}. Additional shading indicates the lockdown period (dark grey), a transition period (grey), and the period with relaxed regulations (light grey).

524

525
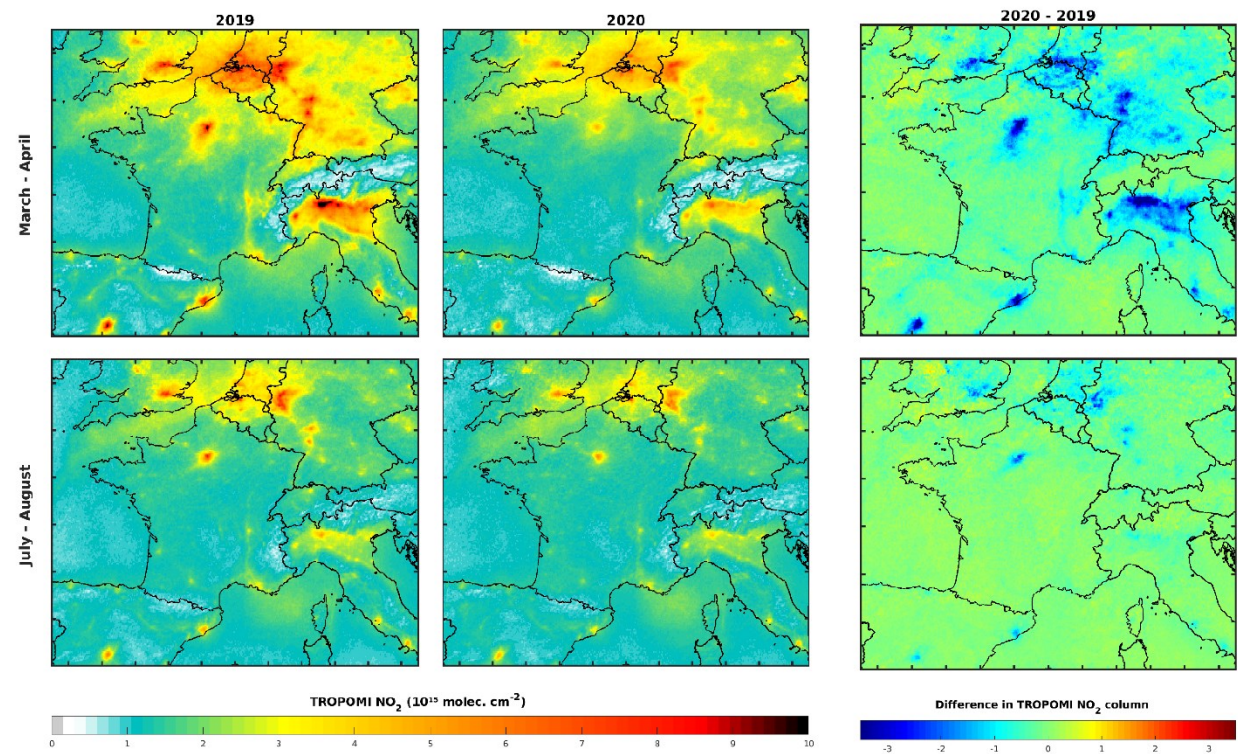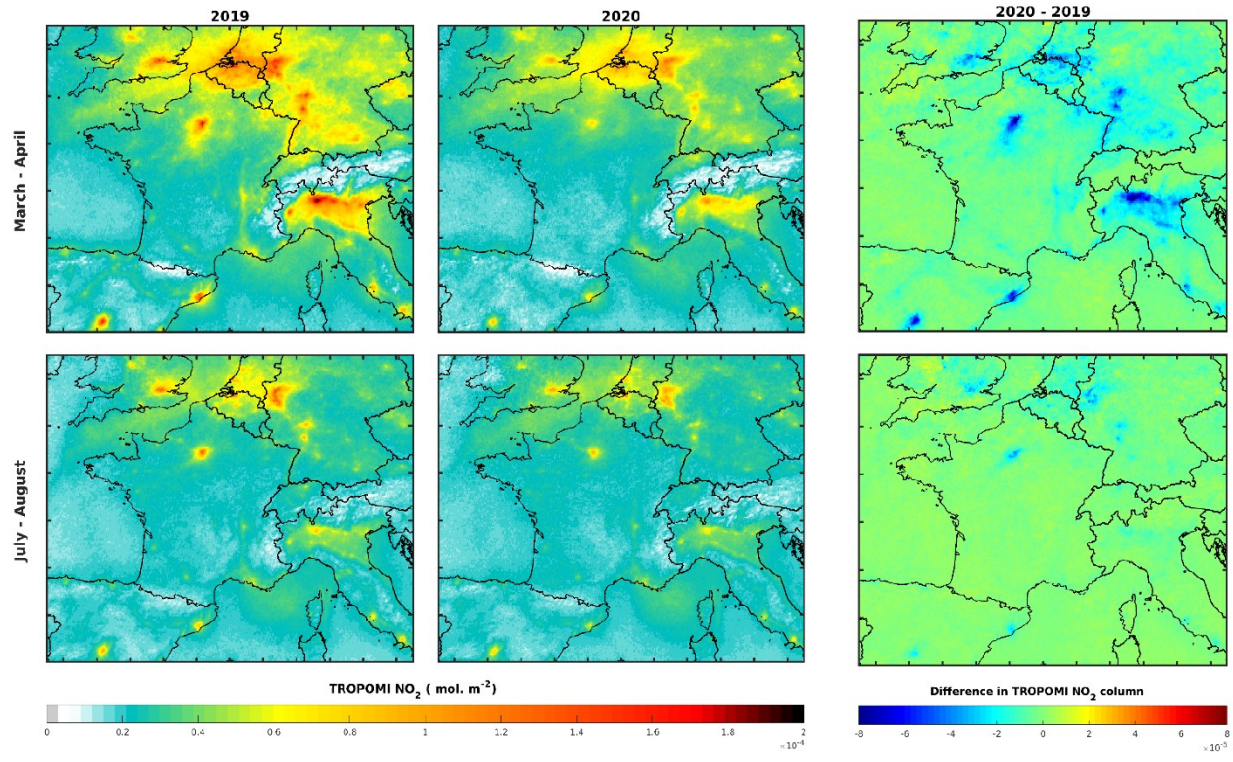
Figure 4: TROPOMI NO₂ tropospheric columns over Europe in the lockdown months March-April (top) and the post-lockdown months July-August (bottom), comparing 2019 (left) with 2020 (middle) in units of mol m⁻². The difference is shown in the right panel.

529

~~Relative concentration changes between 2019 and 2020, as mentioned previously, should not be fully attributed to COVID-19 lockdown measures and the subsequent reduction of emissions. Daily changes in the weather have a strong influence on the NO₂ concentrations, even when the data is averaged over a month. In order to estimate the impact of meteorological variability on TROPOMI based NO₂ observations, simulations were performed with the LOTOS-EUROS chemistry-transport model over Europe at a resolution of 0.1° x 0.1°. Using the same emissions for 2019 and 2020, the simulations show that meteorological variability is responsible for changes in the monthly-mean, city-averaged NO₂ columns with a 1-sigma standard deviation of about 13%. This variability is clearly illustrated in e.g. the individual daily observations in Figure 2. The drastic changes in the range of 30-60% observed in the TROPOMI data and shown in Figure 1 through Figure 4 clearly fall outside this range and cannot be attributed to weather alone.~~

Relative concentration changes between 2019 and 2020 (as shown in Figure 4), as mentioned previously, should not be fully attributed to COVID-19 lockdown measures and the subsequent reduction of emissions. Daily changes in the weather have a strong influence on the NO₂ concentrations, even when the data is averaged over a month. In order to estimate the impact of meteorological variability on TROPOMI-based NO₂ observations, simulations were performed with the LOTOS-EUROS chemistry-transport model over Europe at a resolution of 0.1° x 0.1°. Using the same emissions for 2019 and 2020, the simulations show that meteorological variability is responsible for changes in the monthly-mean, city-averaged NO₂ columns with a 1-sigma standard deviation of about 13%. This variability is clearly illustrated in e.g. the individual daily observations in Figure 2. The drastic changes in the range of 30-60% observed

547   in the TROPOMI data and shown in Figure 1 through Figure 4 clearly fall outside this range and cannot be attributed

548   to weather alone.

549   A second complication is the presence of clouds. Months with persistent local cloud cover will therefore have a

550   reduced number of tropospheric column observations and will exhibit more natural variability. For quantitative

551   estimates of the COVID-19 measures, these factors should be carefully taken into account. This can be done through

552   (i) daily-based analysis of the NO_2 plumes from cities using wind speed fields from meteorological models and

553   subsequent emission derivation (Lorente et al., 2019; Goldberg et al., 2019); (ii) combining NO_2 observations with

554   analyzed wind fields (Beirle et al., 2019, 2021); (iii) regression models to estimate the impact of natural variability

555   and emission trends in the observations (Diamond and Wood, 2020); (iv) chemistry-transport modelling (Chang et

556   al., 2020; Liu et al., 2020; Barré et al., 2021); and (v) inverse modelling and data assimilation approaches (Ding et

557   al., 2020; Miyazaki et al., 2020).

4   Regional Observations for China

559   China was the first country to impose measures to limit the spread of the SARS-CoV-2 virus. Although no national

560   lockdown was declared, strict local lockdown measures were implemented in many cities and provinces. In Wuhan,

561   the epicenter of the virus outbreak, the lockdown period lasted from 23 January 2020 until 8 April 2020, while in other

562   regions, it generally started in early February with measures being eased and lifted through March. In addition to the

563   lockdown measures, the yearly Chinese New Year holidays also affected the amount of anthropogenic emissions (Tan

564   et al., 2009), and so needs to be considered for proper interpretation of the observations. The timing of the holiday

565   period differs from year to year and took place from 24 January to 2 February in 2020, and in the periods 4-10 February

566   and 15-21 February for 2019 and 2018, respectively.

567   The impact of the COVID-19 crisis on air quality in China has already been investigated in several studies. Bauwens

568   et al. (2020) reported that tropospheric NO_2 column amounts observed by TROPOMI during the lockdown dropped

569   by 40-50% in the most impacted cities compared to the same period in 2019 (see Sect. 3). Accordingly, top-down

570   estimated NOx emissions exhibited sharp reductions of up to 50% during the strict lockdown period in late January

571   through early February (Ding et al., 2020; Liu et al., 2020; Zhang, R. et al., 2020).

572   In situ data indicate significant reductions of ground concentrations for NO_2, but also for PM, SO_2, and CO (Shi and

573   Brasseur, 2020; Wang et al., 2020; Zhang, Z. et al., 2020; Zhao, Y. et al., 2020). On the other hand, those studies

574   consistently reported increases of ozone concentrations. With the support of models, Zhao, Y. et al. (2020) have shown

575   that the observed decreases in NO_2 concentration were mostly caused by emissions reductions. They also show that

576   the contribution of meteorological changes to the observed concentration reductions of other species depends on the

577   exact location. Based on OMI observations, Zhang, Z. et al. (2020) observed reductions in East Asia of about 33%

578   and 41% for NO_2 and SO_2, respectively.

579   City-scale impacts of lockdown on NO_2 tropospheric column amounts for Wuhan and Beijing are presented in Sect.

580   3. Here, we investigate whether a lockdown signature can be detected from space at the regional scale for other key

581   pollutants by focusing on TROPOMI tropospheric column measurement of SO_2, CO, HCHO, and CHOCHO. We also

582   compare the identified changes with the marked changes in NO_2 concentration. Figure 5 compares monthly mean

tropospheric columns of those different species for February 2019 and 2020. The NO_2 and SO_2 tropospheric column amounts are clearly lower in February 2020 compared to 2019. A small general reduction is also visible in the CO, HCHO and glyoxal column amounts. As discussed before, many factors other than the lockdown measures may explain changes in pollutant concentrations, such as the meteorology or emission reduction related to the timing of holidays. Another difficulty to compare different years is the data sampling. In February 2019, large parts of Southern China were covered by clouds, preventing space-based observation of the lowermost atmospheric layers. This is clearly illustrated in the upper panel of Figure 5 showing CHOCHO ~~concentrations~~column amounts, where data is missing over large regions since this product uses the most stringent cloud filtering as compared to the other trace gases. Therefore, the following detailed discussion only focuses on the northern part of China (black box in Figure 5 top left panel), even though the lockdown measures were stricter in the region of Wuhan.
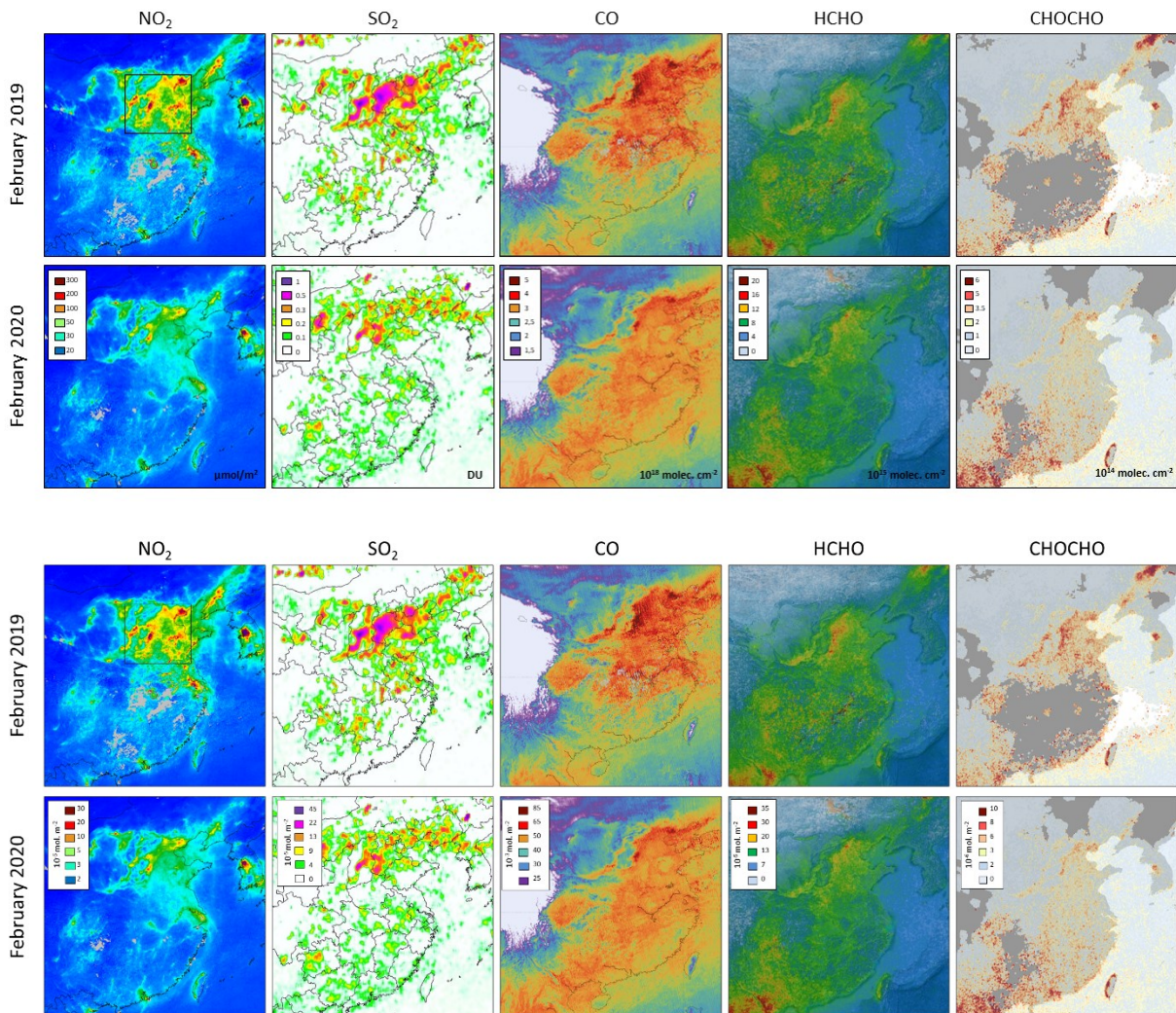
Figure 5: Tropospheric and total columns for various trace gases over China as observed by TROPOMI over China in February 2019 (upper panels) and 2020 (lower panels) in units of mol m^{-2}. The black box indicates the geographical region

599 **used in the time series analysis (Figure 6). Note: the grey-shaded regions in NO$_2$ and CHOCHO panels (far left and far**
600 **right, respectively) indicate areas with little or no data available due to persistent local cloud cover.**

601

602   Figure 6 shows the seasonal cycles for tropospheric column amounts of TROPOMI NO$_2$, SO$_2$, CO, HCHO, and

603 CHOCHO for different years in northern China (region in black box highlighted in Figure 5) starting at the beginning

604 of the operational phase of the S5P/TROPOMI mission (30 April 2018). The different colored curves show two-week

605 medians of the daily mean tropospheric columns. In order to focus on the effect of COVID-19 lockdown measures for

606 HCHO and CHOCHO, the TROPOMI-based time series are compared with an OMI-based climatology for these

607 species using OMI data from 2010 to 2018, and shown by the black dashed curves. The associated uncertainties

608 represent the interannual variability as estimated from OMI. This type of climatological reference based on a longer

609 time series is not available for CO. Therefore, Figure 6 shows CO columns starting from 1 January 2018, which have

610 been added to extend the time series even though the data sampling was more limited in the early phase of the mission.

611 The light vertical boxes in January and February indicate the period of Chinese New Year holidays. Note that the 2020

612 holiday period was slightly extended as a first measure against the COVID-19 spread.

613

614

615

616
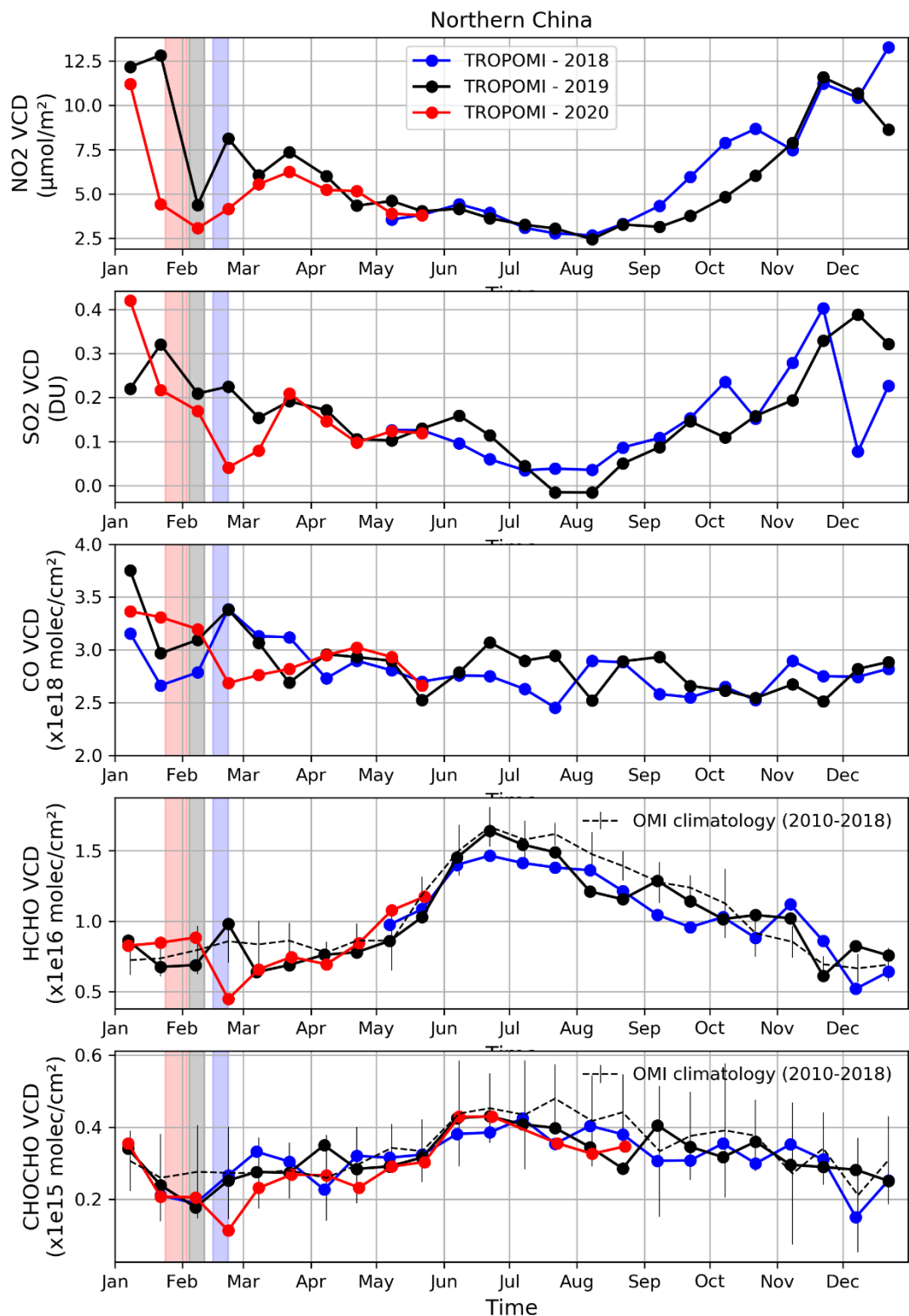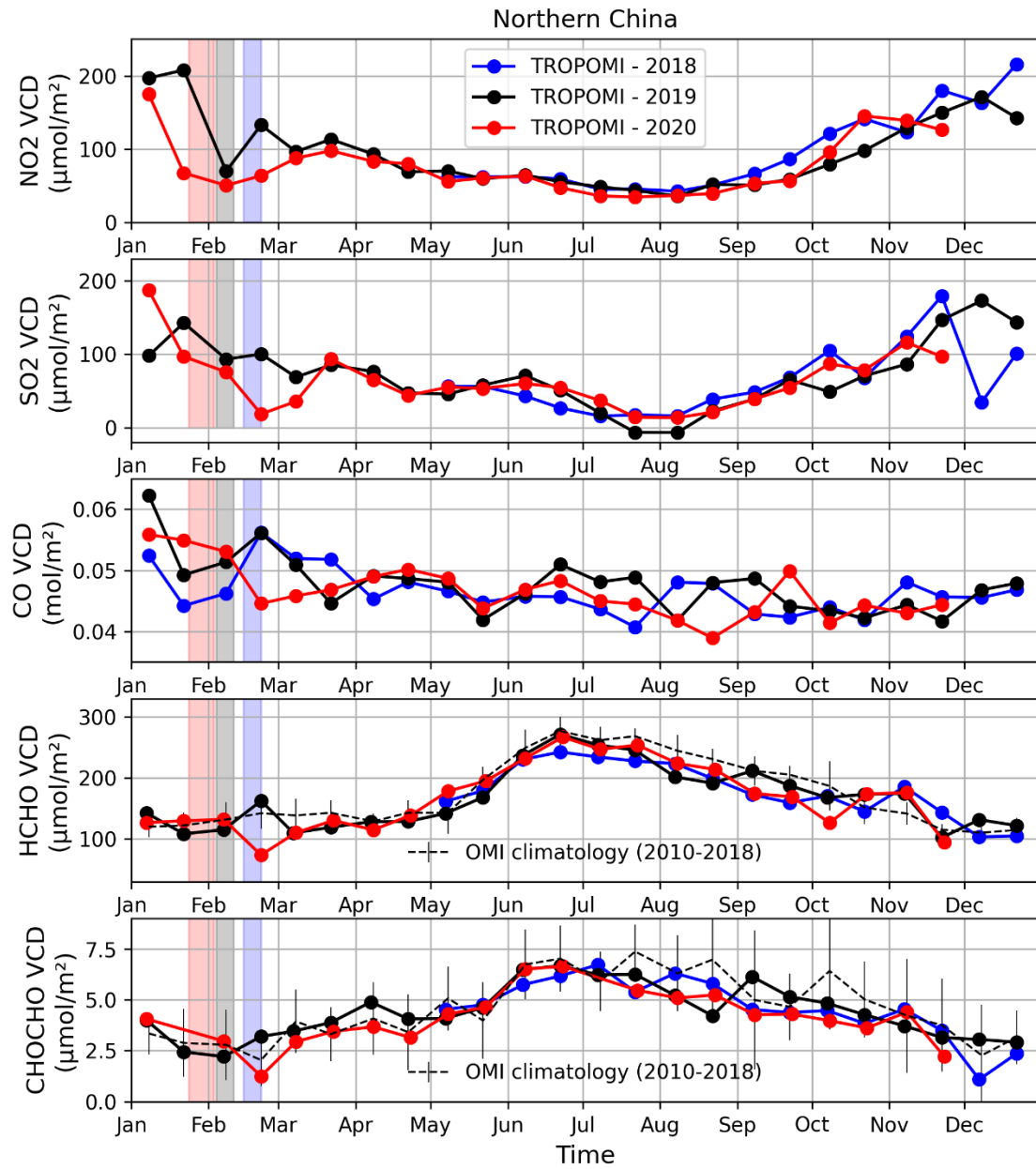
Figure 6: Two-week median tropospheric column ~~concentrations~~ amounts of NO₂, SO₂, CO, HCHO and CHOCHO (from top to bottom) for northern China (34°N-40°N; 110°E-120°E) in units of (micro)mol m⁻². The year 2020 is represented in red (2018 in blue, 2019 in black) and ~~The different curves represent different years~~ as indicated in the legend. The colored boxes ~~represent~~ correspond to the yearly Chinese New Year holidays for those same years. The dashed black lines in the HCHO and CHOCHO panels represent a climatological seasonality as obtained using the OMI data sets from 2010 to 2018 and the error bars represent the interannual variability (1-sigma standard deviation).

623

624   Superimposed on the overall seasonal cycle of NO₂ (maximum during wintertime caused by a longer atmospheric

625   lifetime), a clear reduction of the NO₂ columns is systematically observed which corresponds to the New Year

626   festivities. While a quick return to higher values is usually observed after that period (Tan et al., 2009), the NO₂

627   columns remained lower for several weeks in 2020 likely as a consequence of the reduced traffic and industrial

628   activities. For example, NO_2 column amounts at the end of February were about 45% lower than those of 2019. In

629   March 2020, NO_2 columns return progressively to a similar level as compared to other years.

630   SO_2 emissions in China mostly originate from fossil fuel burning of coal and oil (Wang et al., 2018). Although

631   Chinese SO_2 emissions have dropped significantly in the last decade (van der A et al., 2017; Zheng et al., 2018a),

632   enhanced SO_2 columns are still observed in some regions of northern China (Figure 5). As illustrated in Figure 6, SO_2

633   column amounts are larger during wintertime mostly due to its longer atmospheric lifetime (Lee et al., 2011). No clear

634   reduction could be related to the yearly holidays. However, in 2020 a sharp drop is observed starting in late January

635   through mid-March with a reduction of up to 77% as compared to 2019. By late-March/early-April values returned to

636   levels similar to previous years, which is consistent with the NO_2 lockdown signature.

637   In northern China the residential sector, consisting of mostly of emissions from heating and cooking, accounts for

638   nearly half of the anthropogenic CO emissions, while the rest is distributed between traffic, power generation, and

639   industry (Zheng et al., 2018b). Since the impact of lockdown measures is more limited for the residential sector as

640   compared to the transport or industrial sectors, the response of CO to the lockdown measures is expected to be less

641   distinct. Also, due to the longer atmospheric lifetime of CO (weeks to a month), the observed column amounts result

642   from the accumulation of the trace gas over source regions and from long-range transport from regional and global

643   sources. As such, meteorology significantly influences CO concentrations. The observed day-to-day variability is

644   indeed large, leading to more scatter in the two-week median time series shown in Figure 6. The CO columns observed

645   in late February/early March are lower than those observed in the last two years, which might be partly caused by the

646   lockdown measures. However, the high temporal and spatial natural variability of the CO column amount is of the

647   same magnitude as the possible COVID-19 lockdown signal, and the large, year-to-year interannual differences

648   prevent firm conclusions from being drawn. Dedicated model simulations or a longer time series of the TROPOMI

649   CO data may help to disentangle these effects in the future.

650   There are difficulties associated with the investigation of a possible lockdown signature in the satellite HCHO and

651   CHOCHO data sets. Large uncertainties are associated with both of these column retrievals owing to their low optical

652   depth. Moreover, HCHO and CHOCHO columns are dominated by biogenic emissions, which explains the observed

653   seasonal pattern of HCHO and CHOCHO column values with a maximum during summertime as illustrated in Figure

654   6. Variability in meteorology (temperature changes, winds, precipitation) may lead to changes in column amounts on

655   the same order of magnitude as the expected lockdown-related reduction in anthropogenic emission changes. The

656   interannual variability as inferred from the OMI data sets is estimated to be in the range of 1×10^{14} molec cm^{-2} (~30%)

657   and 1.2×10^{15} molec cm^{-2} (~12%) for CHOCHO and HCHO, respectively. Despite those issues, a clear minimum is

658   visible for both HCHO and CHOCHO in late February 2020, with columns significantly lower than 2019 and lower

659   than the OMI climatology (about -40% and -50% for HCHO and CHOCHO, respectively). The differences are also

660   larger than what can be explained by the typical interannual variability. This is in agreement with Sun et al. (2021),

661   who finds a significant HCHO decrease in the Northern China Plain. For glyoxal, a reduction of the column amounts

662   starts already in late January but similar reductions are observed in other years and might be related to a holiday effect

663   similar to that observed for NO_2.

It is interesting to note that local minima are observed simultaneously in late February 2020 for all species except NO$_2$, despite the data products being generated using independent retrieval algorithms. This gives confidence into the detected reductions and their anthropogenic origin. The small delay between the initial decrease in NO$_2$ ~~concentration~~ column amount and the observed decreases in the other trace gas~~es~~ ~~signals~~ is related to a combination of longer atmospheric lifetimes and production being dominated by secondary processes as compared to NO$_2$ (Stavrakou et al., 2021) and is also likely tied to the early timing of the Chinese New Year in 2020.

5   Regional Observations for India

India implemented strict national lockdown measures limiting activities across the country starting 24 March 2020 for a period of 21 days in order to tackle the spread of the SARS-CoV-2 virus amongst its 1.3 billion inhabitants. The initial stringent phase 1 restrictions were followed by careful region-based relaxations in three subsequent phases carried out through the end of May as shown in Table 2.

Table 2: Lockdown phases in India.

	Dates	Measures	Reference
Phase 1	24 Mar to 14 Apr	Nearly all services and factories suspended.	Singh et al. (2020)
Phase 2	15 Apr to 3 May	Extension of lockdown with relaxations, reopening of agricultural businesses and small shops at half capacity.	BBC News (2020)
Phase 3	4 May to 17 May	Country split in 3 zones: (i) lockdown zone, (ii) zone with movement with private and hired vehicles, and (iii) normal movement zone.	India today (2020)
Phase 4	17 May to 31 May	Additional relaxations, more authority given to local bodies.	The Economic Times, 2020

Figure 7 gives an overview of TROPOMI observations of NO$_2$, SO$_2$, CO, HCHO, and CHOCHO, over India for April 2020, thus covering most of phase 1 and 2 of the Indian lockdown, as compared to the same month in 2019. For NO$_2$ and SO$_2$ the ~~concentrations~~ column amounts are clearly lower across the country in 2020 as compared to 2019. Although less prominent, ~~concentrations~~ column amounts of CO, HCHO, and CHOCHO appear to be lower in April 2020 over the domain of the Indo-Gangetic Plain (IGP), which is one of the most densely populated areas of the world with roughly 900 million people.

686

688
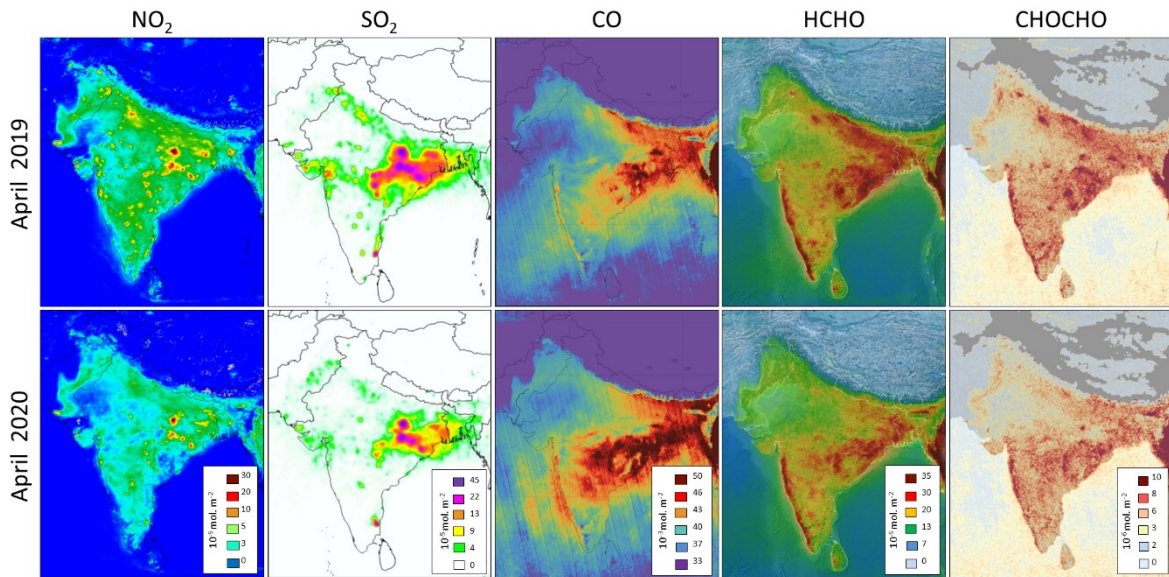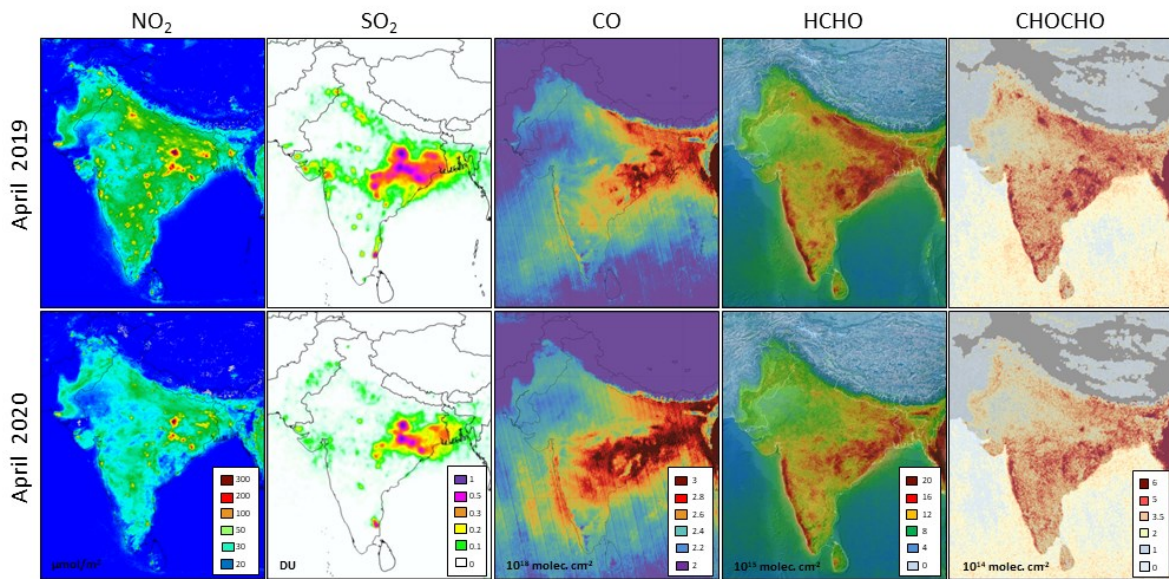
Figure 7: Tropospheric and total columns ~~Concentrations~~ maps for April 2019 (top row) and April 2020 (bottom row) for the various trace gas species measured by TROPOMI from left to right, NO_2, SO_2, CO, HCHO and CHOCHO, shown in units of mol m^{-2}.

692

The two main sources of NO_2 are road transport and power generation, each accounting for about 30% of total anthropogenic emissions in India (Granier et al., 2019). During phase 1 of the lockdown the Tom-Tom traffic index dropped by 80% (Aloi et al., 2020; Prabhjote, 2020) and energy consumption dropped by 25% compared to 2019 (Dattakiran, 2020; POSOCO, 2021) (Fig. D1). As such, we expect a strong reduction in NO_2 particularly in urban

697 areas due to large decreases in transport sector activities and we expect a weaker reduction near power plants due to

698 smaller decreases in energy demand.

699 Indeed, as indicated by the maps of NO_2 column ~~concentrations~~ amounts in Figure 7, a notable reduction in NO_2 can

700 be seen in April 2020 as compared to April 2019. A clear reduction is observed over major cities as well as over the

701 eastern part of India where most large power plants are located. Figure 8a shows the average NO_2 total column

702 ~~concentrations~~ amounts as measured by TROPOMI for 2018, 2019 and 2020, for the 40 largest cities in India selected

703 on the basis of the number of inhabitants (www.geonames.org) where NO_2 is averaged over a 15 x 15 km^2 area around

704 each city center. When both city centers and power plants are located within a 45 x 45 km^2 box, this box is excluded

705 from the averages to avoid potential outflow of one source to the other. A sharp reduction of 42% can be seen in the

706 amount of NO_2 over cities during the first phase of the lockdown period starting at the end of March, as compared to

707 the same period in 2019. This initial drop in NO_2 is then followed by a slow but gradual increase in line with the

708 successive relaxation phases (Table 2). Power generation is a major source for NO_2 in India, in particular from coal-

709 fired power plants. When examining the average amount of NO_2 over the 100 largest coal-fired power plants

710 (www.wri.org), we observe a significant drop in NO_2 during phase 1 of the lockdown period. This drop, observed

711 over coal-fired power plants of 23% as compared to 2019 (Figure 8b), is less pronounced than the observed drop in

712 NO_2 over cities (Figure 8a). The TROPOMI-observed reduction in NO_2 over coal-power plants is in line with the

713 initial 25% decrease in maximum electricity demand reported by National Load Dispatch Centre (NLDC) during phase

714 1 and tapering to an 8% decrease during phase 4 of the lockdown as compared to 2019 (Fig. D1, Dattakiran, 2020).

715

716
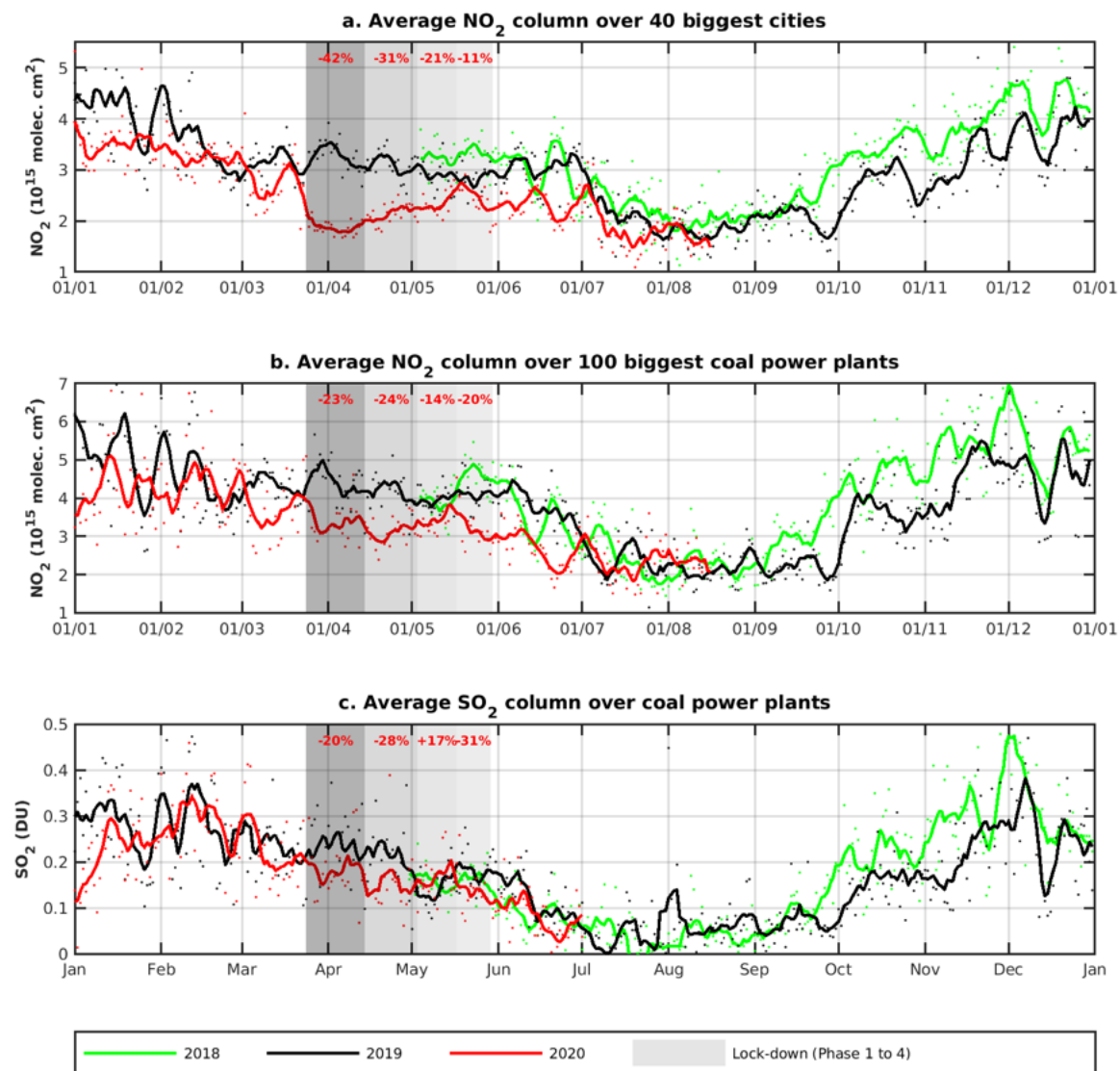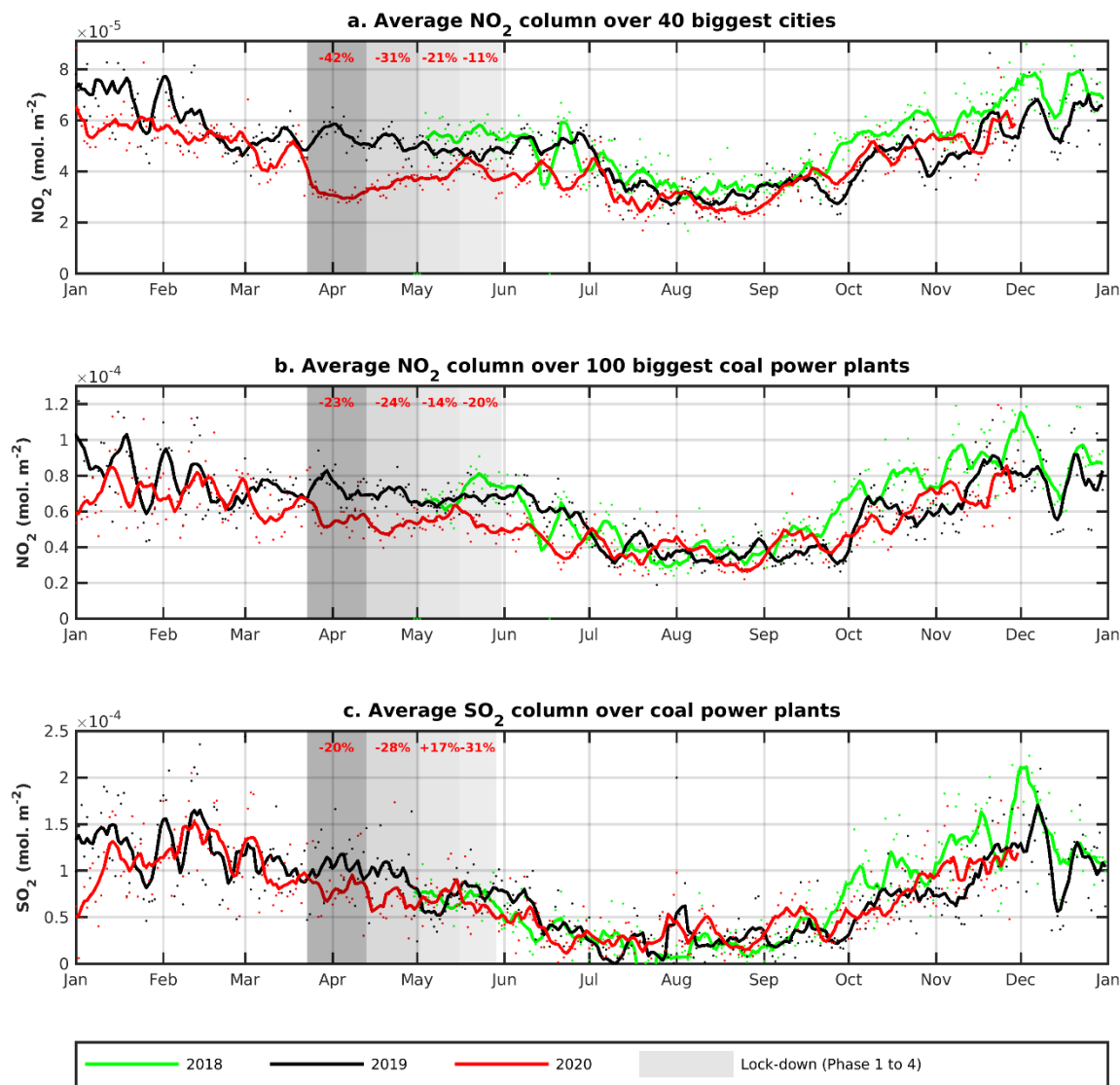
Figure 8: Average tropospheric NO₂ ~~concentrations~~ column amounts for May 2018 (green), 2019 (black) up until ~~June~~ December 2020 (red) over the 40 largest Indian cities (top); over the 100 largest power plants in India (middle); and average SO₂ concentrations over the 59 largest SO₂-emitting power plants in India (bottom). The four different phases of the lockdown period are denoted by the different grey shading. For each phase, the reductions in NO₂ (or SO₂) concentrations are given relative to the same period in 2019. The dots are the daily means, and the solid lines represent the 7-day running means.

According to the CAMS-GLOB-ANT emission inventory for 2019 the major sources for SO₂ in India are power generation (65%) and industry (25%) (Granier et al., 2019). Since India largely relies on coal for producing energy, it is the world's top emitter of anthropogenic SO₂ (Li et al., 2017). So, most of the SO₂ signal we see in TROPOMI data for this region (Figure 7) is from coal-fired power plants, where contributions from oil and gas plants in India comprise a much smaller part of the signal (Fioletov et al., 2016). From Figure 7, a reduction in SO₂ is visible over most areas, and is especially noticeable for the easternmost part of India, which is India's largest SO₂-emitting region with more than 20 coal-fired power plants.

732   We have investigated the SO_2 VCD amounts over the largest power plants, and adapted the selection method used
733   for NO_2 by considering a larger area of 50 x 50 km² around each power plant. This is justified by (1) the longer lifetime
734   of SO_2 compared to NO_2, (2) the lower contamination by other sources, and (3) the need to reduce the noise on the
735   SO_2 data to more clearly isolate the signal from the power plant. The results of the averaged SO_2 VCD time series are
736   presented in Figure 8c. It should be noted that, compared to NO_2, an additional selection of the power plants was
737   applied. Based on the SO_2 VCD map for April 2019 (Figure 7), only the power plants with mean SO_2 columns larger
738   than 0.15 DU were considered (59 power plants in total). Although the signal is relatively weak for SO_2, we find very
739   similar reductions in SO_2 as compared to NO_2. Especially during the first two phases of the lockdown, a reduction of
740   about 20% is found which is in line with the NO_2 observations and the reported reduction in energy demand. In May,
741   for the different years, the consistency between NO_2 and SO_2 VCDs is less straightforward and the reason for this is
742   not fully understood. It should however be noted that the NO_2 and SO_2 data products do not use the same cloud
743   products for filtering and this might be a reason for discrepancy. Moreover, the possibility of a systematic
744   contamination of the NO_2 signal over power plants by other sources cannot be ruled out completely. A noticeable
745   feature of Figure 8b and Figure 8c is the overall excellent correspondence between NO_2 and SO_2 VCD evolution (on
746   short-term/seasonal basis, and outside the lockdown periods) as well as from year to year. This further strengthens the
747   observed COVID-19 related drop in both trace gases, although it is clear that meteorology and chemistry likely play
748   a large role in the observed VCD variability. Also, ground-based studies in New Delhi find a more important reduction
749   in NO_2 compared to SO_2 (Mahato et al., 2020; Kumari and Toshniwal, 2020).
750   For HCHO, CHOCHO, and CO, various regions over India have been investigated to detect a possible signal
751   resulting from COVID-19 lockdown measures. We could only identify such a signal in the densely populated areas of
752   the Indo-Gangetic Plain and New Delhi. These areas, due to the high intensity of traffic and industrial activities, are
753   most likely to exhibit large impacts on atmospheric pollution levels due to COVID-19 lockdown measures.
754
755   Figure 9Figure 9 shows two-week averaged column values for HCHO, CHOCHO, and CO over the IGP and New
756   Delhi, based on TROPOMI data from January 2018 to June 2020. To support the interpretation of the observed
757   seasonal and interannual variations, Fig. D2 presents the corresponding temperature, precipitation amount, and fire
758   count. The temperature starts increasing in January and reaches a maximum in June. The period from July to
759   September corresponds to the monsoon season with heavy rains and lower temperatures, and therefore lower pollution
760   levels. Fire activity peaks around May with a second peak is observed in November for the IGP. The time series of
761   the HCHO, CHOCHO, and CO columns correlate with these seasonal events, although with a different amplitude. For
762   example, HCHO shows the strongest correlation with temperature (see Sect. 2.5), while CHOCHO mainly follows
763   fire emissions. The smaller amplitude in CO variations is caused by its longer lifetime.

765
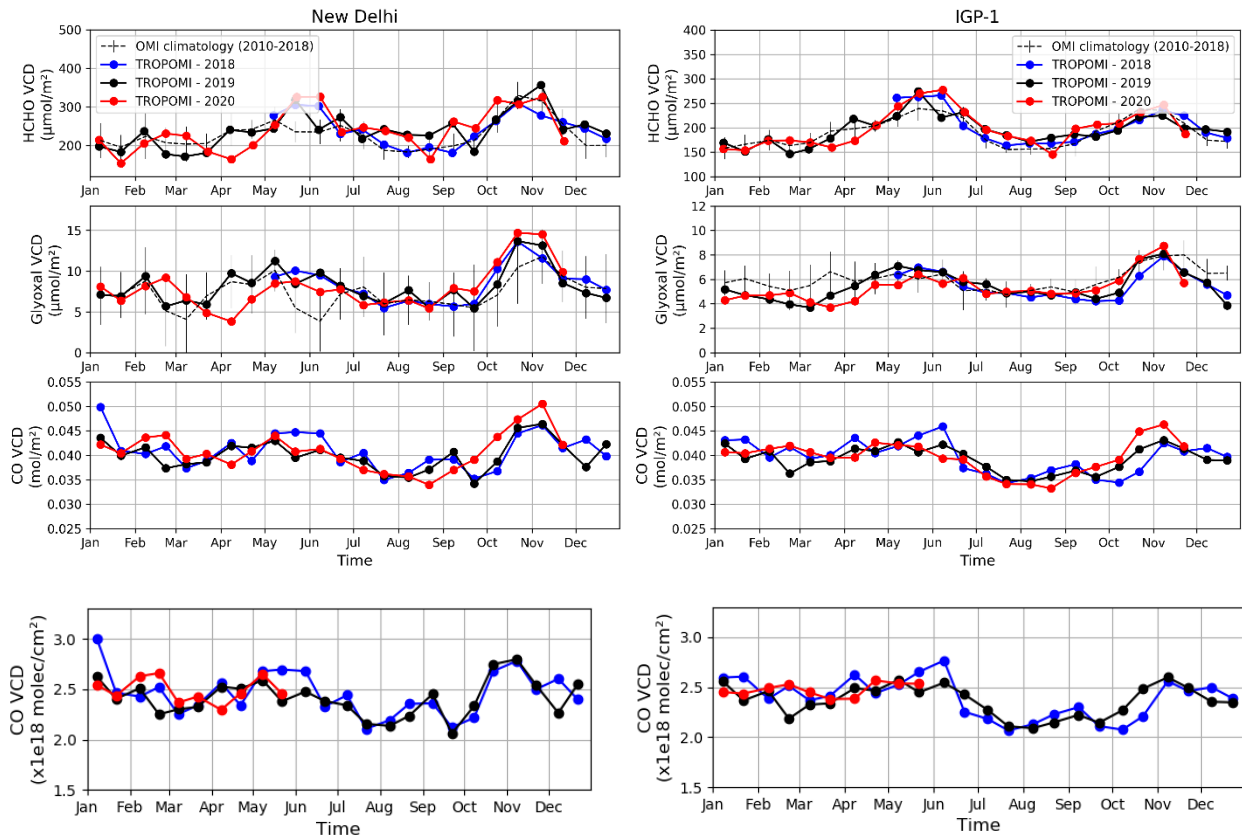
Figure 9: Time evolution of HCHO, CHOCHO, and CO over the densely populated Indo-Gangetic plain (right panel, defined by the region within this 4 coordinates: 29.5°N 72°E, 21.5°N 86°E, 24.5°N 88.5°E , 32.5°N 74.5°E), and over the megacity New Delhi (left panel, radius of 25 km, or 50 km for CHOCHO) as observed with TROPOMI. The year 2020 is represented in red (2018 in blue, 2019 in black). With the HCHO and CHOCHO time series, the OMI climatology is shown for comparison (dashed black line, 2010-2018), the error bars represent the interannual variability of the two-week averaged columns. The HCHO columns have been corrected in order to assume the same temperature every year (see Sect. 2).

A large part of the observed HCHO and CHOCHO columns for India are due to natural emissions which can vary significantly due to changes in meteorology, in particular temperature and precipitation. Hence a possible reduction of the anthropogenic VOC emissions due to the lockdown measures is expected to have a small contribution to the variability of the measured columns. During the most stringent phase 1 lockdown, a reduction in HCHO column concentrations amount is observed for the IGP and is even more pronounced over New Delhi (

Figure 9Figure 9 top panels; respectively -2 and -4x10^{15} molec cm^{-2} [-20% and -40%] compared to the OMI climatology for 2010-2018). In both cases, the anomaly is larger than the interannual variations observed during this period (about 1.5x10^{15} molec cm^{-2}), where changes in temperature or precipitation do not seem to explain the observed

784   column decrease during phase 1. The observed column decline is even more pronounced over New Delhi than over

785   the IGP, suggesting that the origin of the reduction is mostly anthropogenic.

786   The case for lockdown-driven reductions is further supported by the CHOCHO observations, which exhibit the

787   clearest COVID-19 signal during phase 1 of the lockdown (

788   Figure 9Figure 9). The reduction of CHOCHO during the lockdown period over the IGP is slightly larger than the

789   interannual variability of 1×10^{14} molec cm^{-2} (or -25%) as determined from the OMI CHOCHO climatology. Similar

790   to HCHO, the reduction in CHOCHO over New Delhi is twice as large (-50%) and well beyond the 1-sigma OMI

791   climatology range. Phase 2 is also characterized by lower CHOCHO column amounts in 2020 as compared to 2019,

792   but temperatures are also lower, unlike phase 1. Accounting for temperature-driven variability (Sect. 2.5) brings the

793   HCHO columns close to the mean HCHO seasonal levels. The somewhat more pronounced effect of the lockdown on

794   CHOCHO compared to HCHO in New Delhi is most likely due to the strong contribution of anthropogenic VOC

795   precursors to CHOCHO amounts (Chan Miller et al., 2016). Interestingly, fire counts show that there were fewer fires

796   in May 2020 compared to previous years (Fig. D2), most likely as a consequence of the lockdown measures, which

797   may also contribute to the lower glyoxal columns.

798   As it was the case for China, it is more difficult to identify a signal in CO column data driven by the COVID-19

799   lockdowns over India. An important reason for this is the much longer atmospheric residence time of CO that varies

800   depending on the OH concentration (Holloway et al., 2000). Moreover, according to bottom-up inventories, the major

801   anthropogenic CO source in India are due to the residential sector (42%), road transportation (21%), agricultural waste

802   burning (18%) and the industrial sector (16%) (Granier et al., 2019). Hence, during a lockdown we expect that the

803   main source of CO, residential, to be less affected. Figure 7 shows that the CO amounts in southern India are higher

804   in 2020 as compared to 2019. The enhanced CO values in 2019 and 2020 are detected above regions (e.g. Madhya

805   Pradesh, Odisha, and Chhattisgarh) where seasonal forest fires commonly occur in April/May (Chandra and Kumar

806   Bhardwaj, 2015, Srikanta et al. 2020). Thus, the enhancement of CO for the different years depends not only on the

807   fire activity but also on how the meteorological situation prevents or permits the accumulation of CO in the

808   atmosphere. To more fully address the reasons why CO is higher in 2020 than 2019, future studies could carry out

809   calculations using a chemical transport modelFigure 7 shows that the CO amounts in southern India are higher in 2020

810   compared to 2019. The reason could be the accumulation of CO originating from elsewhere prior to the lockdown

811   period. The long atmospheric residence time of CO complicates the identification of COVID-19 lockdown signals.

812   Also for CO we derived the full TROPOMI time series for the IGP and New Delhi as shown in

813   Figure 9Figure 9 (lower panel). The time series for New Delhi in mid-April shows somewhat lower CO values in 2020

814   compared to 2019, but the large natural variability of CO prevents clear identification of a COVID-19 lockdown driven

815   effect. In future, analysis of a longer TROPOMI CO time series or model experiments may help to quantify the

816   COVID-19 effects.

817

6   Conclusions

In this paper, we have analyzed the impact of COVID-19 lockdown measures on air quality around the globe, based on observations of several trace gases from the Sentinel-5P/TROPOMI instrument. TROPOMI provides daily, global observations of multiple trace gases, where the measured vertical column amounts are driven by emissions as well as atmospheric and chemical processes of transport, transformation, and deposition. We compared the 2020 TROPOMI data with similar periods from previous years and carried out additional analysis to disentangle changes in emissions due to COVID-19 lockdown measures from meteorological variability, seasonal variability, and from other non-lockdown emission drivers. We analyzed time series of NO_2 measurements from city to regional scales for several locations around the globe, showing the potential of TROPOMI to globally monitor local to regional impacts of COVID-19 lockdown measures on air quality and anthropogenic emissions. Furthermore, for the first time, we used a combination of five trace gases observed by TROPOMI, specifically NO_2, SO_2, CO, HCHO and CHOCHO, to assess the impact of COVID-19 related lockdown measures on trace gas concentrations.

From the global to city scale, we have illustrated consistent, sharp decreases in NO_2 ~~concentrations~~ column amount driven by the COVID-19-related lockdown measures. These findings are based on detailed analysis of the distribution of NO_2 using daily measurements from TROPOMI. For the city of Wuhan in China, the first city to issue a lockdown, NO_2 concentrations measured by TROPOMI were about 60% lower than the same period in February-March 2019. After China, lockdowns were issued across all continents and for the majority of countries from March through May 2020. For megacities all over the world, reductions in column amounts of tropospheric NO_2 range between 14% and 63%. The strength of the reduction depends on the type and efficiency of local measures carried out and on the relative contribution of traffic, industry, and power generation to NO_2 emissions for a given area. Owing to the unprecedented resolution of TROPOMI of about 5 km, reductions of different source contributions to NO_2 such as city traffic, highways (Liu et al., 2020), power plants (Miyazaki et al., 2020), industry, and shipping (Ding et al., 2020) can be estimated separately.

As demonstrated by time series analysis of the NO_2 observations, there is substantial variability even in two-week averages, which is attributable to meteorological variability. On average, we estimate the standard deviation of this variability to be about 13% (1-sigma standard deviation) for major cities in Europe, but locally the effect can sometimes be larger. The large and systematic reductions (30-60%) observed, however, cannot be explained by meteorological variability alone and are therefore attributed to the effect of the lockdown measures.

For SO_2, we observe significant column reductions in China and India over coal-fired power plants, which are the primary sources of anthropogenic SO_2 in these areas. Over northeastern China in late February 2020, large reductions of SO_2 vertical column amounts were observed, as a result of lockdown measures, with a decrease up to 77% as compared to the same time period in 2019, which cannot be explained by interannual variability alone. An analysis of SO_2 vertical column amounts over the largest SO_2-emitting power plants in India, reveals a reduction in SO_2 of about 25% during the first two phases of the lockdown, as compared to 2019. For India, the reductions in SO_2 were highly correlated with NO_2 reductions for the same power plants and with the national energy demand for that period.

853   The natural variability of HCHO and CHOCHO does not allow detection of a significant decrease due to the COVID-
854   19 measures in most regions of the world based on TROPOMI observations alone. Exceptions are northern China and
855   New Delhi, where observed reductions could be attributed to the lockdown measures. For northeastern China, a 50%
856   reduction in the CHOCHO ~~concentration~~ column amount is observed during the second half February, which is larger
857   than the typical observed interannual variability of 30%. For HCHO, after correcting for the effect of seasonal and
858   temperature variations, we observe a coincident 40% reduction. We analyzed column amounts of CO, CHOCHO, and
859   HCHO over the Indo-Gangetic Plain, which is the most densely populated region of India. For CHOCHO and HCHO,
860   we observed small reductions in column amount due the COVID-19 measures, where these observed effects are
861   slightly larger than the interannual variability as determined using an OMI climatology (2010-2018). The observed
862   reduction of 25% of CHOCHO in this region is of the same order as the typical interannual variability. A stronger
863   reduction of 60% is observed for the city of New Delhi, which is similar to the reduction observed over northern China
864   but occurs later due to the difference in lockdown timing. For HCHO, we also observe a significant 40% decrease
865   over New Delhi in April, while over the whole Indo-Gangetic Plain, a decrease of 20% is observed.

866   For CO, reductions related to COVID-19 measures were much more difficult to identify, although over northern
867   China we see that the reductions in CO correlate with those for HCHO and CHOCHO. We could not find a similar
868   effect for CO over New Delhi. The fact that it is so hard to draw conclusions for CO based on the TROPOMI data
869   alone is due to the high variability in CO driven by meteorological conditions, in combination with the difficulty of
870   distinguishing localized emission changes from the high and variable background values, caused by the long
871   atmospheric lifetime of CO.

872   TROPOMI data have already been used in many publications (Gkatzelis et al., 2021; Bauwens et al., 2020; Liu et
873   al., 2020; Huang et al., 2020) aiming to analyze the impact of COVID-19 lockdown measures on air pollution levels.
874   Predominantly, these studies have been based on the use of TROPOMI NO_2 observations alone. We anticipate that
875   the combined use of multiple trace gases from TROPOMI together with the high spatial resolution of the
876   measurements, has large potential for a significantly improved sector-specific analysis of the impact of the COVID-
877   19 lockdown measures than previously possible. Such a multi-species analysis offers promise for in-depth
878   understanding of changes in air quality, the chemical interplay of pollutants in the atmosphere and their relation to
879   emissions. While keeping in mind the importance of accounting for interannual, seasonal, and meteorologically driven
880   variability (e.g. Miyazaki et al., 2020), it is clear that a detailed analysis cannot be based on TROPOMI observations
881   alone. For more quantitative estimates of the impact of COVID-19 lockdown measures on trace gas concentrations
882   and emissions, we need (inverse) models driven by high-quality meteorological analyses, or at least wind information
883   or statistical relationships to account for weather-driven variability (Goldberg et al., 2020; Miyazaki et al., 2020; Ding
884   et al., 2020).

885   In summary, our analyses using the most recent operational and scientific retrieval techniques have shown that by
886   taking emission sources, atmospheric lifetime as well the seasonal and meteorological variability into account for a
887   variety of trace gases measured by TROPOMI, rapid changes in anthropogenic emissions can be observed as induced
888   by the implementation of regional COVID-19 lockdown measures. It is our hope that this case study will serve as

889 reference for future analyses aimed at characterizing emission changes of not just NO_2, but by utilizing the
890 concomitant observation of the variety of trace gases measured by TROPOMI.
891

892 **Appendix A**

893 **Table A1: Summary of documentation available for TROPOMI operational data products from the Sentinel 5-P Library**
894 **(https://sentinels.copernicus.eu/web/sentinel/technical-guides/sentinel-5p/products-algorithms).**

Title	Document content description and product-specific reference	Document and Data links
Product Readme File (PRF)	Description of changes ~~between~~ in ~~different~~ product versions, recommended qa_values, and overall quality information	https://sentinels.copernicus.eu/web/sentinel/technical-guides/sentinel-5p/products-algorithms
NO₂	Eskes and Eichmann, 2020	qa_value recommendation: > 0.75
CO	Landgraf et al., 2020	qa_value recommendation: > 0.5
HCHO	De Smedt et al., 2020a	qa_value recommendation: > 0.5
Product User Manual (PUM)	Technical description of file formatting for each TROPOMI Level 2 operational data product	https://sentinels.copernicus.eu/web/sentinel/technical-guides/sentinel-5p/products-algorithms
NO₂	Eskes et al., 2020	
CO	Apituley et al., 2018	
HCHO	Romahn et al., 2020	
Algorithm Theoretical Basis Document (ATBD)	Detailed description of methods used for each TROPOMI L2 operational retrieval algorithm	https://sentinels.copernicus.eu/web/sentinel/technical-guides/sentinel-5p/products-algorithms
NO₂	van Geffen et al., 2019; 2021	Note: the 2019 ATBD describes v. 1.3.0 NO₂ data used in this paper.
CO		
HCHO	Landgraf et al., 2018 De Smedt et al., 2020b	
Quarterly Validation Report (ROCVR)	Detailed description of the latest validation available for each TROPOMI L2 operational dataset, product-specific	https://mpc-vdaf.tropomi.eu/
Operational Data Product Specifications	Product-specific overview pages with TROPOMI L2 dataset specifications, including how to access and how to cite each data product.	https://sentinels.copernicus.eu/web/sentinel/data-products

	NO$_2$	
Operational Data Product Citation and Digital Object Identifier (DOI)	Copernicus Sentinel 5-P, 2018a	doi:10.5270/S5P-s4ljg54
	CO Copernicus Sentinel 5-P, 2018b	doi:10.5270/S5P-1hkp7rp
	HCHO Copernicus Sentinel 5-P, 2018c	doi:10.5270/S5P-tjlxfd2

895

896 **Appendix B**

897 Appendix B contains additional information (Table B2) and description supporting the timing of COVID-19 driven

898 emissions changes for global cities evaluated in this study and shown in Figure 2. Fig. 2.

899

900 **Table B2. Details about the lockdown dates for the cities illustrated in Figure 2.Figure 2.**

City	Date (2020)	Comment	Reference
Wuhan	23 January	Lockdown Wuhan and Hubei province	Bloomberg (2020)
	8 April	Lockdown lifted	Bloomberg (2020)
Mumbai and New Delhi	24 March	Closure of schools, public transport and most businesses	BBC (2020a)
	31 May	Nationwide lockdown is extended until end of May	Aljazeera (2020a)
Manila	16 March	Philippines announced strict home quarantine	Calonzo and Jiao (2020)
	1 June	Most businesses allowed to re-open, but bars, restaurants and schools remain closed	Jennings (2020)
Madrid	14 March	Nationwide lockdown	Minder and Peltier (2020)
	9 May	Easing, stores and restaurants allowed to open	Goodman et al. (2020)
Milan	8 March	Locking down of Northern Italy including Milan	Horowitz (2020a)
	4 May	Loosening of strictest lockdown measures	Horowitz (2020b)
Paris	17 March	France imposes nationwide the restriction	Onishi and Méheut (2020)
	11 May	Gradually relaxed lockdown measures, most shops open	Makooi (2020)
Los Angeles	19 March	California enters lockdown	BBC (2020b)
	1 June	Reopening of some shops and restaurants	Patel (2020)

New York	22 March	New York state enters lockdown	BBC (2020b)
	13 June	Stay-at-home orders put in place until further notice	CBS News (2020)
Sydney	24 March	Strict lockdown measures adopted in Australia	Wahlquist (2020)
	15 May	New South Wales eases lockdown restrictions	Sonali (2020)
Auckland	23 March	In New Zealand stay-at-home orders are issued	Menon (2020)
	14 May	All businesses can open in New Zealand	Conforti (2020)
Mexico City	23 March	Most economic sectors stopped in Mexico	Pasley (2020)
	1 June	Gradual reopening of Mexico city	Associated Press (2020)
Lima	16 March	Stringent quarantine enforced by police and army	Collyns (2020)
	30 June	Peru extended nationwide lockdown through end of June	Aljazeera (2020b)
Sao Paulo	24 March	Start of lockdown, but measures were largely ignored	Uchoa (2020)
	31 May	Quarantine extended through May	CGTN (2020)
Buenos Aires	20 March	Argentina under mandatory lockdown	Do Rosario and Gillespie (2020)
	28 June	Lockdown extended	Misculin and Garrison (2020)
Baghdad	22 March	Iraq imposed a total nationwide lockdown	The Star (2020)
	21 April	Relaxed restrictions: shops reopen for limited hours	Saleh (2020)
	20 May	In Baghdad strict lockdown re-imposed for 6 districts	Saleh (2020)
Lagos	30 March	Stay-at-home order, markets open for limited hours	Orjinmo (2020)
	4 May	Easing of restrictions, but schools, bars, and cinemas remain closed	Mbah (2020)
Johannesburg	26 March	Stay-at-home orders issued in South Africa	Winter (2020)
	1 June	Most economic sectors permitted to operate	Aljazeera (2020c)

901

Detailed observations of NO$_2$ reductions in major cities worldwide

Three examples of lockdown-related NO$_2$ column reductions in major cities are shown for Santiago, Paris and New

Delhi in Figure 1 with time windows selected to reflect region-specific lockdown periods. A strong reduction in the

NO$_2$ tropospheric concentration of about 40% is observed over Santiago. In Paris, the NO$_2$ levels for the period 15 March to 15 April 2020 are about a factor of two lower than in March-April 2019 (see also Figure 4). For New Delhi the reduction is even more striking in comparison to April 2019 (about a factor of 3, Figure 2c). Both Paris and New Delhi also show significant reductions in background values around the cities. Background locations are subject to a variety of wind directions and sometimes downwind of city plumes thus influencing background concentrations. Such plumes are typically on the order of 100 km long, and, given the atmospheric residence time of NO$_2$ (2-12 hours), these plumes can fill the small domains around Paris and New Delhi shown in Figure 1.

In Wuhan, the first city to issue quarantines and lockdown measures, the observed NO$_2$ column drastically declined (-60%) between 23 January and 8 April 2020 compared to the same period in 2019 (Figure 2a, Table B2). This decrease is in good agreement with estimated reductions for the period 11 February to 2 March 2020 based on TROPOMI NO$_2$ (-43%, Bauwens et al., 2020) and in situ NO$_2$ observations in Wuhan (-55%, Shi and Brasseur, 2020). However, it should be noted that there was strong day-to-day variability in the NO$_2$ column amount due to meteorological factors, as well as missing data over Wuhan in February 2019 due to clouds. Model calculations by Liu et al. (2020) indicate that meteorological variability could have led to increased NO$_2$ columns in 2020 compared to 2019, suggesting that the observed NO$_2$ reductions underestimate the impact of emission reductions due to COVID-19. The partial lifting of the restrictions on 8 April led to a progressive increase in NO$_2$ levels, yet remained lower than in 2019, likely because the population was still advised to stay at home and schools remained closed. A similar response in NO$_2$ levels was observed in Beijing. The decreases were less pronounced (-40%) and are in excellent agreement with the reported decrease based on in situ NO$_2$ measurements (-40%, Shi and Brasseur, 2020). The weaker response could be due to the less drastic measures adopted in Beijing, because locally sustained COVID-19 cases were lower than in the Hubei province (Leung et al., 2020). Strong NO$_2$ reductions were observed for other Chinese cities, like Nanjing, Qingdao, and Zhengzhou, based on TROPOMI NO$_2$ observations (Bauwens et al., 2020).

India enforced strict restrictions of human activities on 24 March 2020 to tackle the spread of COVID-19. In New Delhi and Mumbai, the onset of the lockdown induced a sharp decline in the observed NO$_2$ columns (by a factor of 2). The columns remained low during the entire lockdown period (-56% and -46%, respectively) (see Table 2 for timing of Indian lockdown phases). This is very much in line with the decreases reported in New Delhi based on NO$_2$ data from monitoring stations, -53% (Mahato et al., 2020) and -48% (Jain and Sharma, 2020).

As compared to other cities, a very strong NO$_2$ decrease was observed in Lima (-63%), where strict regulations to stay indoors were enforced (Collyns, 2020). A drastic drop in NO$_2$ compared to the 2019 levels marked the start of the lockdown, and the levels remained very low throughout the entire lockdown period. The gradual increase of NO$_2$ columns in Lima and other Southern Hemispheric cities from January to May (Figure 2j) reflects the natural seasonal variation when levels peak during the Southern Hemispheric winter, as temperatures decrease and NO$_2$ lifetime increases.

In Buenos Aires, the observed reduction was not as strong compared to Lima for the entire lockdown period (-34%, Table B2), but was particularly marked during the first month of the lockdown (20 March through 20 April 2020), due to a compulsory quarantine period and strict limitation of activities for many sectors. Although partial lifting of measures was issued after 10 April for many provinces in Argentina, the measures in the Buenos Aires agglomeration

were maintained due to the elevated number of cases (Raszewski and Garrison, 2020). More moderate reductions are found for Mexico City (-22%) and Santiago (-23%) during the lockdown in comparison to the same period in 2019, that could be attributed to less strict adherence to and enforcement of lockdown measures (Uchoa, 2020; Pasley, 2020).

Strong reductions were observed over the entire lockdown period in the heavily hit cities in southwest Europe, Los Angeles, and New York, with reductions ranging between -32% and -54% (Bauwens et al., 2020). It should be noted however, that in these regions, the start of the lockdown period is generally less marked partly because the lockdowns were not as strictly enforced in Europe and the U.S. as in China and India. Moreover, the observed TROPOMI data displays a strong variability attributable to meteorology, e.g. over Paris, New York and Los Angeles in 2019.

In Sydney, the reduction was moderate (-14%) and delayed with respect to the onset of the measures (Figure 2g). This could be related to observations of less strict compliance in the early period of lockdown measures (New South Wales Public Health, 2020). A rapid and strong decrease was observed for NO_2 column amount as a result of lockdown measures in Auckland, New Zealand (-55%). Similarly, the lockdown measures in New Zealand were implemented swiftly with high levels of compliance (Matthews, 2020). The end of the lockdown coincided with a strong increase in NO_2 pollution, from 1.8×10^{15} molec cm^{-2} to 3×10^{15} molec cm^{-2} in the last three weeks of May.

In Africa, Nigeria is among the countries most affected by COVID-19 and reported the first confirmed case in sub-Saharan Africa (Odunsi, 2020; Adigun and Anna, 2020). A two-week lockdown period was put in place for Lagos starting 30 March. The NO_2 column amount decreased by 33% during the lockdown with respect to the same period of 2019 and remained lower even after the lifting of restrictions on 4 May (Table B2). An NO_2 column decrease of similar magnitude (-35%) was observed in Johannesburg (Figure 2p), where a national lockdown was issued on 26 March 2020, with a gradual easing of restrictions starting 1 May. In Sub-Saharan Africa, the emission reductions in April were significant for larger populous and industrialized areas, whereas no noticeable drop was found in less developed regions (Masaki et al., 2020).

Finally, the Iraqi capital of Baghdad faced an initial lockdown from 22 March through 21 April. A second partial lockdown was issued starting 20 May in response to a sharp increase in COVID-19 cases due to the temporary relaxation of restrictions to allow the celebration of Ramadan in late April (Table B2). The NO_2 column responded quickly (Figure 2n) as confirmed by the rapid decrease once curfew measures were issues in late-May.

Figure 3 and Figure 4 illustrate the tropospheric column amount of NO_2 over Europe, focusing on Milan, Madrid, Paris and Berlin, extending the analysis up to 1 December. In France, Spain and Italy we detect strong reductions of NO_2, which can be largely attributed to the lockdown measures. In Berlin, the measured differences are smaller, and a more detailed analysis of the meteorological variability is needed to quantify the impact of the lockdown (see Figure 3). The extended time series shows a recovery of the NO_2 pollution levels to pre-COVID-19 values. However, the recovery is not complete, suggesting that remaining restrictions, new stay-at-home life and working practices, together with a downturn in industrial and service-based activities have contributed to a longer lasting impact.

Appendix C

Appendix C contains figures which support the technical understanding of individual retrieval algorithms.

977

978
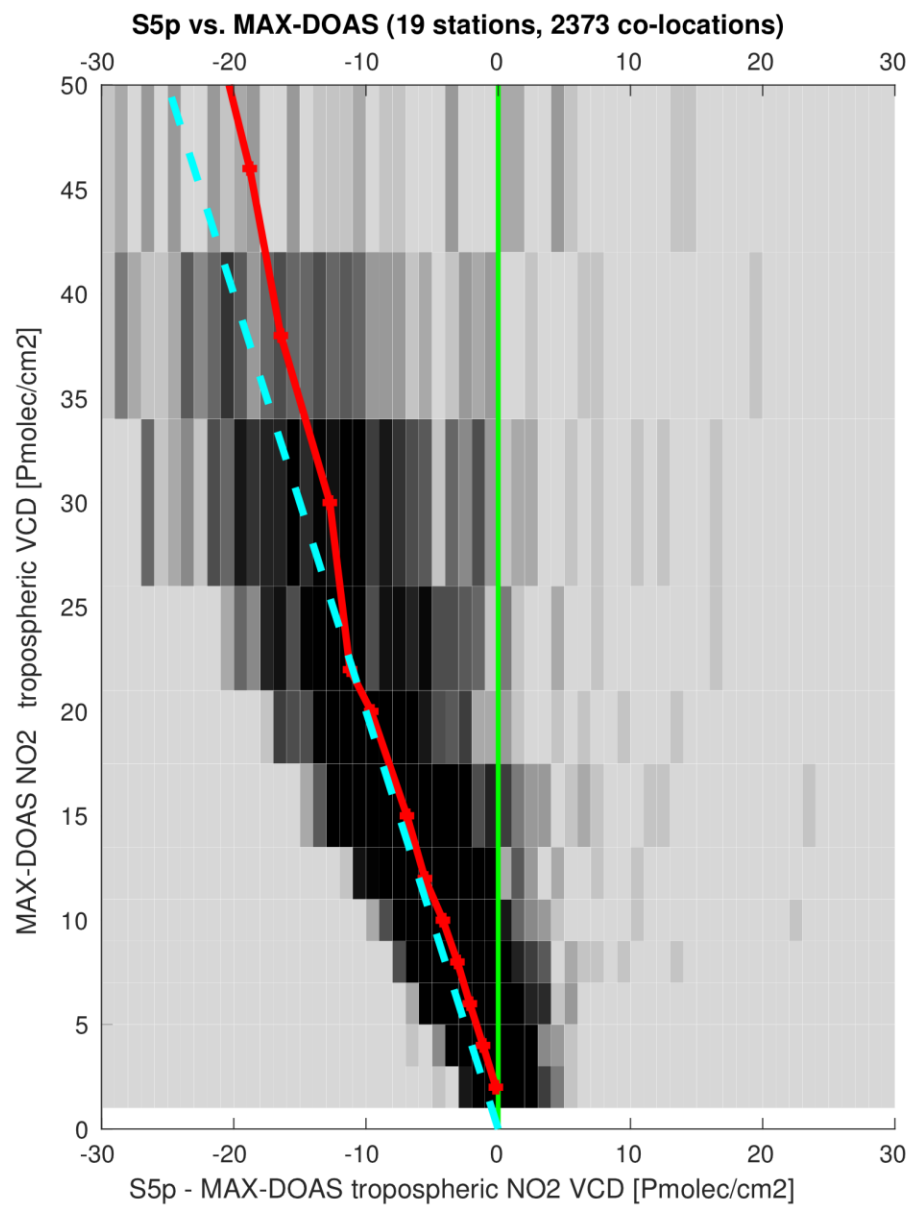
Figure C1: Bias in S5p-TROPOMI tropospheric NO₂ as estimated from comparisons to co-located ground-based MAX-
DOAS measurements, presented as a function of the ground-based VCD measurement. The grey-scale background
represents a 2-D histogram, where the median difference per MAX-DOAS VCD bin is shown as the red curve, and the blue
dashed line shows a multiplicative bias (b) model with b ~ 0.5 x VCD. More details on the ground-based data and co-
location scheme can be found in Verhoelst et al., 2021.

984

985

SO₂ vertical column (DU) - April 2019

986
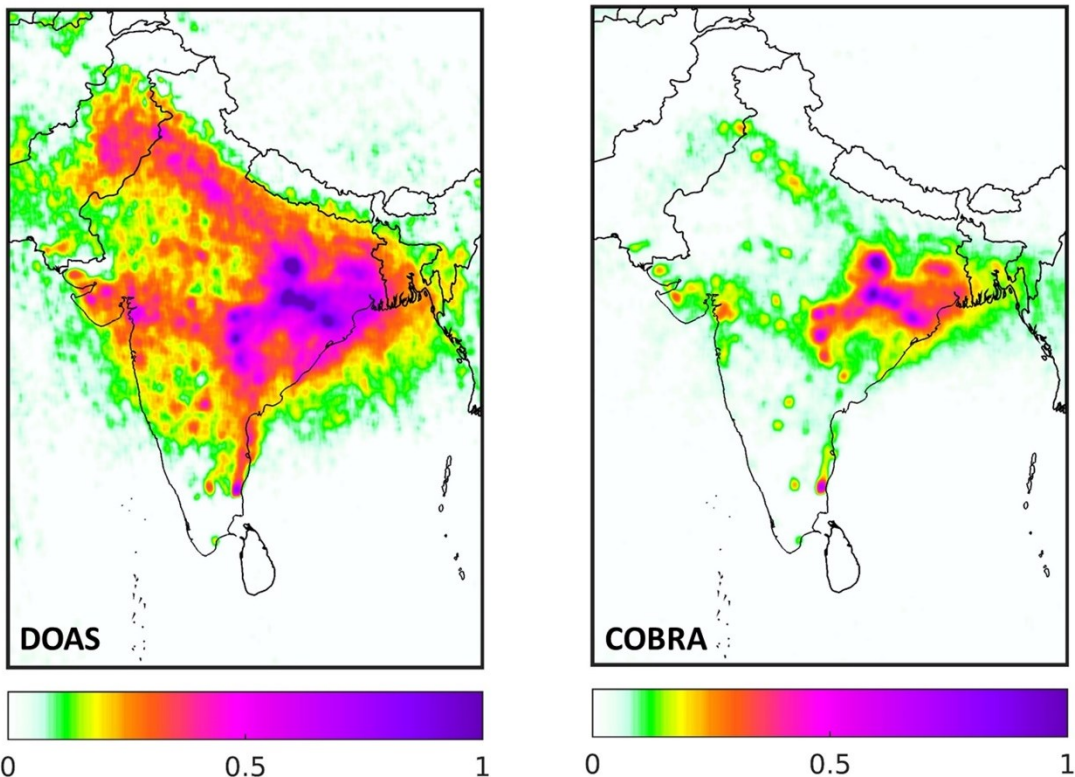
Figure C2: Monthly averaged TROPOMI SO₂ columns over India for April 2019, from (left) DOAS operational product and (right) COBRA scientific product. The ~~reduction in~~ noise and offsets ~~reduction~~as described and illustrated in Theys et al. (2021) can also be seen here where there is more contrast between~~is clear from the maps~~ the background and the~~. The emissions from~~ individual point sources (power plants, darker pink and purple) can be better discerned in the COBRA SO₂ map.

992

993

994
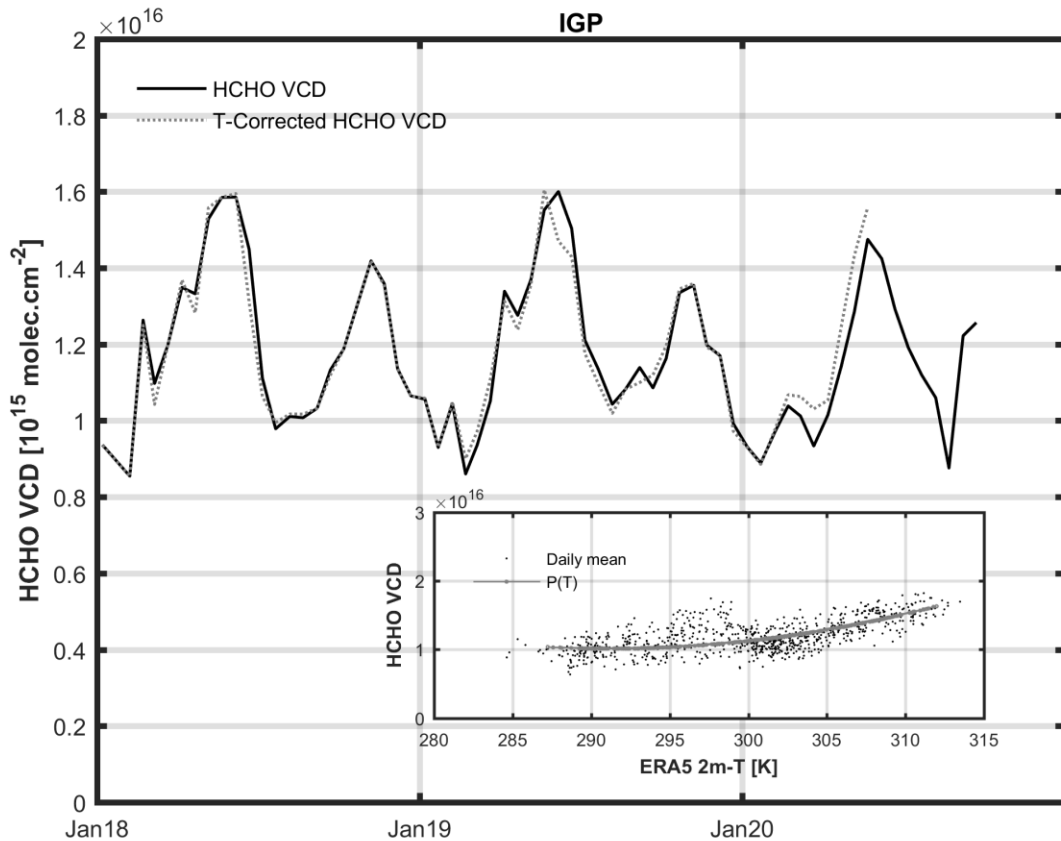
Figure C3: Example of temperature correction of the TROPOMI HCHO tropospheric columns in the Indogangetic Plain region. The dashed line presents the HCHO columns after correction using climatological temperatures. The correlation between the local daily temperatures from ERA5-Land 2m and the HCHO columns is shown inset for the entire period.

Appendix D

Appendix D contains additional figures that support the interpretation timing of observed changes in COVID-19 driven emissions related to power generation (Fig. D1) and meteorological conditions (Fig. D2).
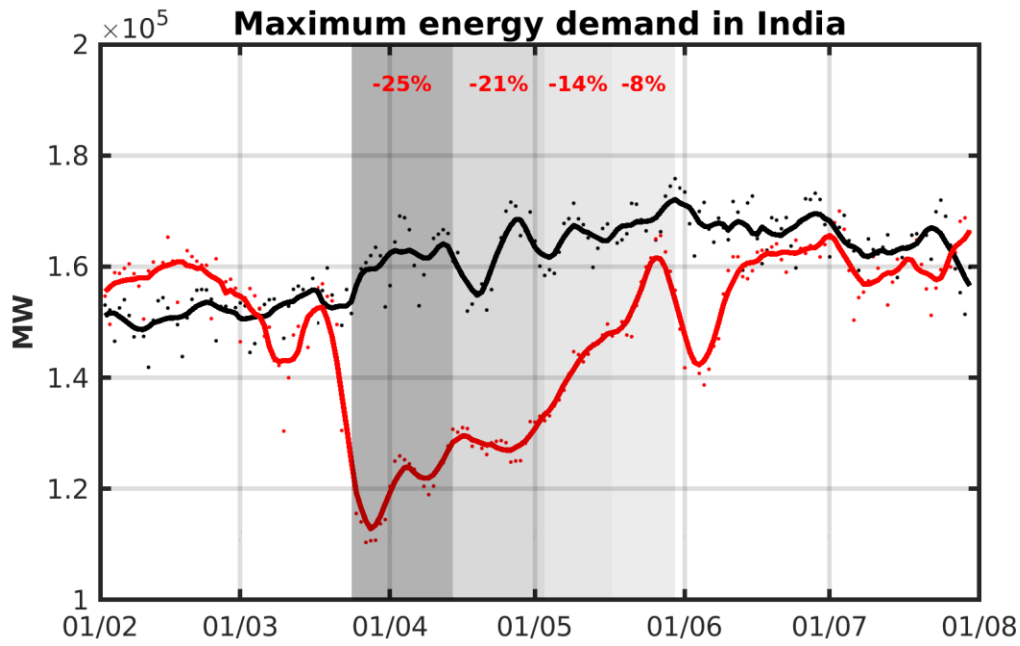
1001

Figure D1: Maximum energy demand over India during the period of the lockdown (red) compared to the same period in 2019 (black), For each of the phases of the lockdown the reductions in maximum energy demand is given relative to the same period in 2019. Data from: www.posoco.in/covid-19.

1005

1006

1007

1015

1016
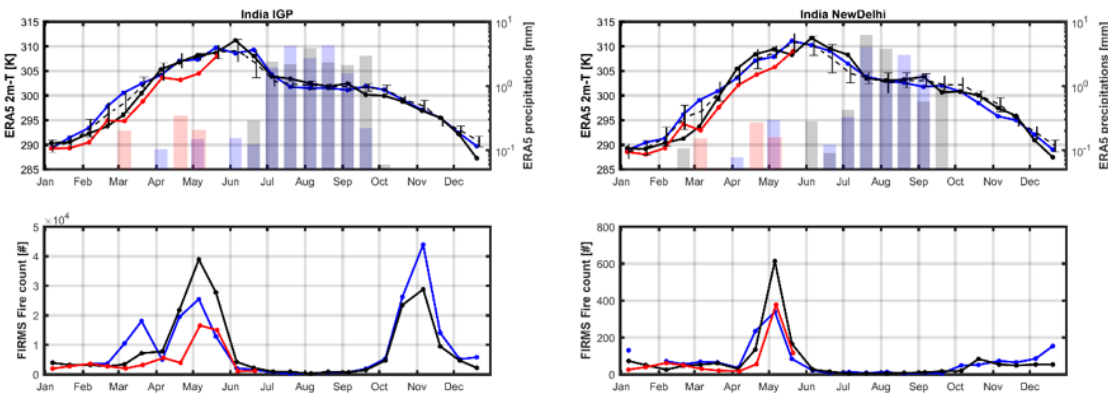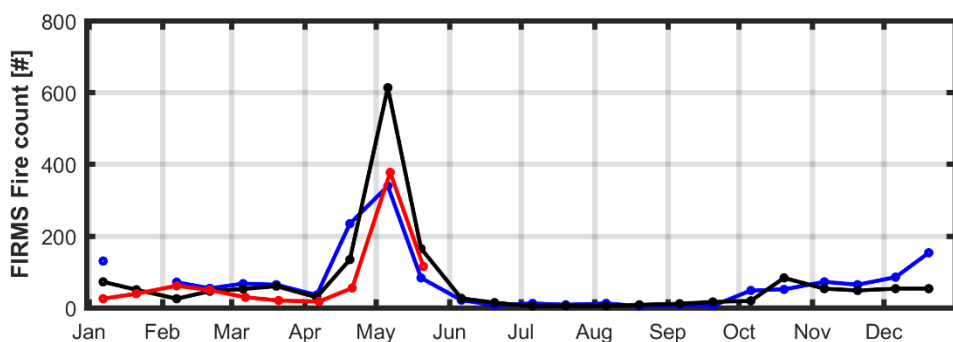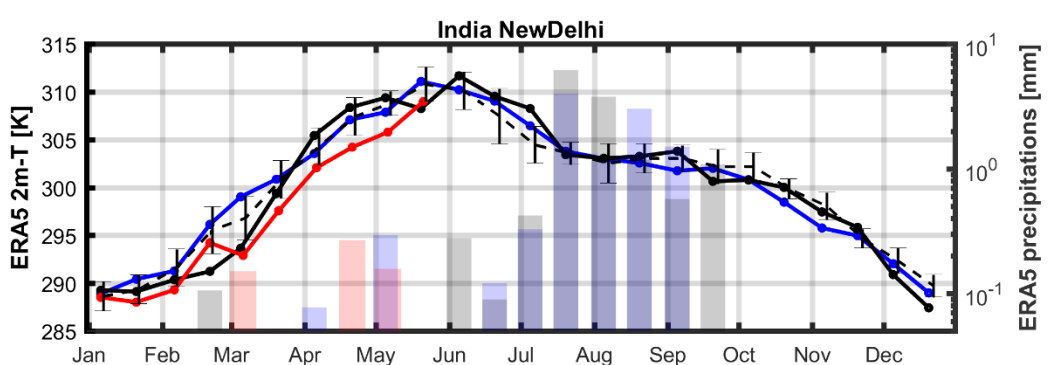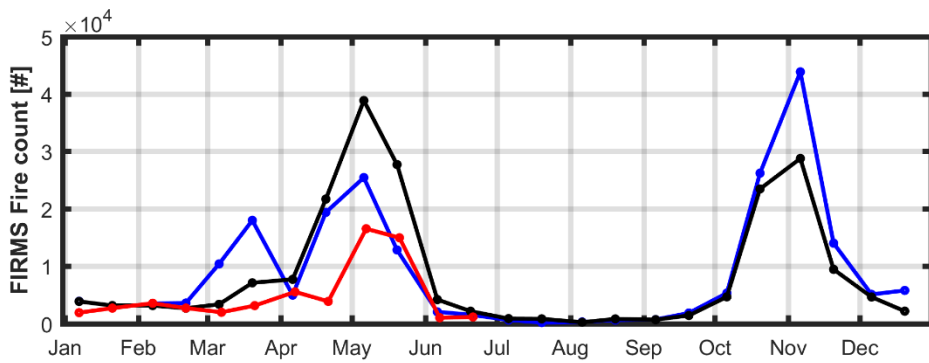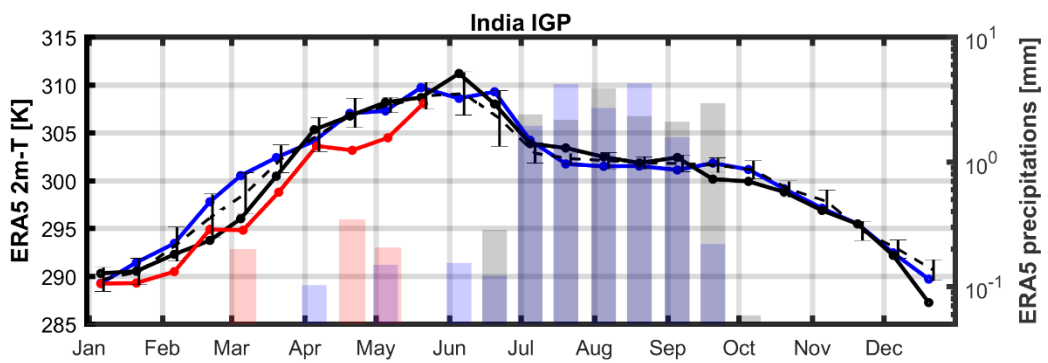
Figure D2: Meteorological and fire count information for the same regions as shown in

Figure 9 (IGP plain upper two panels, and New Delhi lower two panels). Near-surface~~Upper panels: ombrothermic~~ temperature and precipitation ~~diagrams~~ (top panel and second from bottom) ~~for the same regions as shown in Figure 9~~ show~~ing~~ the two-week average temperature at 2m as lines ~~(upper left)~~ and precipitation amounts as bars ~~(upper right,~~ source ERA5, Muñoz Sabater, 2019b). ~~Lower~~ Second from top and bottom panels show ~~:~~ fire counts (source FIRMS, https://earthdata.nasa.gov/firms). The year 2020 is represented in red, 2019 in black, and 2018 is in blue.

Data Availability

Operational versions of all Copernicus Sentinel 5-P Data TROPOMI data are freely available from the European Union/ESA/Copernicus Sentinel-5P Pre-Operations Data Hub (https://s5phub.copernicus.eu; S5P Pre-Ops Data Hub, 2021). The TROPOMI COBRA SO$_2$ dataset is available on request as described in Theys et al., 2021. OMI HCHO and NO$_2$ datasets are openly available on http://www.qa4ecv.eu/ecvs. TROPOMI Glyoxal data is available upon request as a part of the ESA S5p+I GLYRETRO project as detailed on the project website: https://glyretro.aeronomie.be/.

Author Contributions

PFL conceptualized, initiated, and managed this manuscript with contributions from IA, MB, TB, IDS, HE, CL, TS, DSZ, NT, MVR, PV, and TV. Formal analysis was carried out by MB, TB, IDS, HE, CL, and NT. DL and FR provided data curation and software support for TROPOMI HCHO data products. DSZ prepared, edited, and co-managed the manuscript with contributions from IA, MB, TB, IDS, HE, CL, PFL, TS, NT, MVR, PV, and TV.

Competing Interests

The authors declare that they have no conflict of interest.

Acknowledgements

We acknowledge financial support from the following projects: ESA S5P MPC (4000117151/16/I-LG); Netherlands Space Office TROPOMI Science Project; ESA S5p+Innovation GLYRETRO and ICOVAC projects (No. 4000127610/19/I-NS); Belgium Prodex TRACE-S5P (PEA 4000105598), and TROVA-2 (PEA 4000130630); Belgium BRAIN-2.be LEGO-BEL-AQ; EU FP7 QA4ECV project (grant no. 607405). This paper contains modified Copernicus data (2018/2020) processed by KNMI, BIRA-IASB, DLR, and SRON.

References

van der A, R., Mijling, B., Ding, J., Koukouli, M., Liu, F., Li, Q., Mao, H., and Theys, N.: Cleaning up the air: Effectiveness of air quality policy for SO_2 and NO_x emissions in China, Atmos. Chem. Phys., 17, 1775-1789, doi:10.5194/acp-17-1775-2017, 2017.

Adigun, B. and Anna, C.: Nigeria confirms 1st case of new virus in sub-Saharan Africa, AP News, https://apnews.com/article/5de56b2fcaffae583c7c57b82c1a4fff, last access: 30 March 2021, 2020.

Aljazeera: Coronavirus in India: What we know about world's largest lockdown, https://www.aljazeera.com/news/2020/05/india-coronavirus-crisis-200519120521747.html, last access: 17 June 2020, 2020a.

Aljazeera: Peru extends nationwide lockdown until end of June, https://www.aljazeera.com/news/2020/05/peru-extends-nationwide-lockdown-june-200523073017946.html, last access: 17 June 2020, 2020b.

Aljazeera: South Africa coronavirus lockdown to ease from June 1, https://www.aljazeera.com/news/2020/05/ramaphosa-south-africa-coronavirus-lockdown-ease-june-1-200525070634938.html, last access: 17 June 2020, 2020c.

Aloi, A., Alonso, B., Benavente, J., Cordera, R., Echániz, E., González, F., Ladisa, C., Lezama-Romanelli, R., López-Parra, Á., Mazzei, V., Perrucci, L., Prieto-Quintana, D., Rodríguez, A. and Sañudo, R.: Effects of the COVID-19 Lockdown on Urban Mobility: Empirical Evidence from the City of Santander (Spain), Sustainability, 12(9), 3870, doi:10.3390/su12093870, 2020.

Alvarado, L., Richter, A., and Lerot, C.: GLYoxal Retrievals from TROPOMI (GLYRETRO) Validation Report, S5p+Innovation – theme 1 (CHOCHO), 5p+I_CHOCHO_BIRA_VR, 1.1, 35 pp., https://glyretro.aeronomie.be/, 2020.

Apituley, A., Pedergnana, M., Sneep, M., Veefkind, J. P., Loyola, D., Landgraf, J., and Borsdorff, T.: Sentinel-5 precursor/TROPOMI Level 2 Product User Manual Carbon Monoxide, document number: SRON-S5P-LEV2-MA-002, 1.0.0, SRON Netherlands Institute for Space Research, Utrecht, The Netherlands, https://sentinels.copernicus.eu/web/sentinel/technical-guides/sentinel-5p/products-algorithms, 2018.

Associated Press: Mexico City will begin gradually reopening June 1, mayor says, https://www.latimes.com/world-nation/story/2020-05-21/mexico-city-will-begin-gradual-reopening-coronavirus-june-1, last access: 17 June 2020, 2020.

1081 Baldasano, J. M.: COVID-19 lockdown effects on air quality by NO_2 in the cities of Barcelona and Madrid (Spain),

1082 Sci. Total Environ., 741, 140353, doi:10.1016/j.scitotenv.2020.140353, 2020.

1083

1084 Barré, J., Petetin, H., Colette, A., Guevara, M., Peuch, V.-H., Rouil, L., Engelen, R., Inness, A., Flemming, J., Pérez

1085 García-Pando, C., Bowdalo, D., Meleux, F., Geels, C., Christensen, J. H., Gauss, M., Benedictow, A., Tsyro, S., Friese,

1086 E., Struzewska, J., Kaminski, J. W., Douros, J., Timmermans, R., Robertson, L., Adani, M., Jorba, O., Joly, M., and

1087 Kouznetsov, R.: Estimating lockdown-induced European NO_2 changes using satellite and surface observations and air

1088 quality models, Atmos. Chem. Phys., 21, 7373–7394, doi:10.5194/acp-21-7373-2021, 2021.

1089

1090 Bauwens, M., Stavrakou, T., Müller, J.-F., De Smedt, I., Van Roozendael, M., van der Werf, G. R., Wiedinmyer, C.,

1091 Kaiser, J. W., Sindelarova, K. and Guenther, A.: Nine years of global hydrocarbon emissions based on source inversion

1092 of OMI formaldehyde observations, Atmos. Chem. Phys., 16(15), 10133–10158, doi:10.5194/acp-16-10133-2016,

1093 2016.

1094

1095 Bauwens, M. Compernolle, S., Stavrakou, T., Müller, J.-F., van Gent, J., Eskes, H., Levelt, P. F., van der A, R.,

1096 Veefkind, J. P., Vlietinck, J., Yu, H., and Zehner, C.: Impact of coronavirus outbreak on NO_2 pollution assessed using

1097 TROPOMI and OMI observations, Geophys. Res. Lett., 47(11), doi:10.1029/2020GL087978, 2020.

1098

1099 BBC: India extends coronavirus lockdown by two weeks, https://www.bbc.com/news/world-asia-india-52698828, last

1100 access: 17 June 2020, 2020a.

1101

1102 BBC: Earlier coronavirus lockdown 'could have saved 36,000 lives', https://www.bbc.com/news/world-us-canada-

1103 52757150, last access: 17 June 2020, 2020b.

1104

1105 Beirle, S., Borger, C., Dörner, S., Li, A., Hu, Z., Liu, F., Wang, Y., and Wagner, T.: Pinpointing nitrogen oxide

1106 emissions from space, Sci. Adv. 5, doi:10.1126/sciadv.aax9800, 2019.

108 ~~Beirle, S., Borger, C., Dörner, S., Eskes, H., Kumar, V., de Laat, A., and Wagner, T.: Catalog of NOx emissions from~~

109 ~~point sources as derived from the divergence of the NO_2 flux for TROPOMI, Earth Syst. Sci. Data Discuss. [preprint],~~

110 ~~doi:10.5194/essd-2020-280, in review, 2021.~~

111 Beirle, S., Borger, C., Dörner, S., Eskes, H., Kumar, V., de Laat, A., and Wagner, T.: Catalog of NOx emissions from

112 point sources as derived from the divergence of the NO2 flux for TROPOMI, Earth Syst. Sci. Data, 13, 2995–3012,

113 https://doi.org/10.5194/essd-13-2995-2021, 2021.

1114

1115 Bloomberg News: China to lift lockdown over virus epicenter Wuhan on April 8,

1116 https://www.bloomberg.com/news/articles/2020-03-24/china-to-lift-lockdown-over-virus-epicenter-wuhan-on-april-

1117 8, last access: 1 July 2020, 2020.

1118

1119   Boersma, K. F., Eskes, H. J., Richter, A., De Smedt, I., Lorente, A., Beirle, S., van Geffen, J. H. G. M., Zara, M.,

1120   Peters, E., Van Roozendael, M., Wagner, T., Maasakkers, J. D., van der A, R. J., Nightingale, J., De Rudder, A., Irie,

1121   H., Pinardi, G., Lambert, J.-C., and Compernolle, S.: Improving algorithms and uncertainty estimates for satellite NO_2

1122   retrievals: Results from the Quality Assurance for Essential Climate Variables (QA4ECV) project, Atmos. Meas.

1123   Tech., 11, 6651-6678, doi:10.5194/amt-11-6651-2018, 2018.

1124

1125   Borsdorff, T., Hasekamp, O. P., Wassmann, A., and Landgraf, J.: Insights into Tikhonov regularization: Application

1126   to trace gas column retrieval and the efficient calculation of total column averaging kernels, Atmos. Meas. Tech., 7(2),

1127   523–535, 2014.

1128

1129   Borsdorff, T., Tol, P., Williams, J. E., de Laat, J., aan de Brugh, J., Nédélec, P., Aben, I., and Landgraf, J.: Carbon

1130   monoxide total columns from SCIAMACHY 2.3 µm atmospheric reflectance measurements: towards a full-mission

1131   data product (2003–2012), Atmos. Meas. Tech., 9, 227–248, doi:10.5194/amt-9-227-2016, 2016.

1132

1133   Borsdorff, T., aan de Brugh, J., Hu, H., Nédélec, P., Aben, I., and Landgraf, J.: Carbon monoxide column retrieval for

1134   clear-sky and cloudy atmospheres: a full-mission data set from SCIAMACHY 2.3 µm reflectance measurements,

1135   Atmos. Meas. Tech., 10, 1769–1782, doi:10.5194/amt-10-1769-2017, 2017.

1136

1137   Borsdorff, T., aan de Brugh, J., Hu, H., Hasekamp, O., Sussmann, R., Rettinger, M., Hase, F., Gross, J., Schneider,

1138   M., Garcia, O., Stremme, W., Grutter, M., Feist, D. G., Arnold, S. G., De Mazière, M., Kumar Sha, M., Pollard, D.

1139   F., Kiel, M., Roehl, C., Wennberg, P. O., Toon, G. C., and Landgraf, J.: Mapping carbon monoxide pollution from

1140   space down to city scales with daily global coverage, Atmos. Meas. Tech., 11, 5507–5518, doi:10.5194/amt-11-5507-

1141   2018, 2018.

1142

1143   Borsdorff, T., aan de Brugh, J., Pandey, S., Hasekamp, O., Aben, I., Houweling, S., and Landgraf, J.: Carbon monoxide

1144   air pollution on sub-city scales and along arterial roads detected by the Tropospheric Monitoring Instrument, Atmos.

1145   Chem. Phys., 19, 3579–3588, doi:10.5194/acp-19-3579-2019, 2019.

1146

1147   Borsdorff, T., García Reynoso, A., Maldonado, G., Mar-Morales, B., Stremme, W., Grutter, M., and Landgraf, J.:

1148   Monitoring CO emissions of the metropolis Mexico City using TROPOMI CO observations, Atmos. Chem. Phys.,

1149   20, 15761–15774, doi:10.5194/acp-20-15761-2020, 2020.

1150

1151   Bovensmann, H., Burrows, J. P., Buchwitz, M., Frerick, J., Noel, S., Rozanov, V. V., Chance, L.V., and Goede,

1152   A.P.H.: SCIAMACHY: Mission objectives and measurement modes, Atmos. Sci., 56, 127-150, 1999.

1153

Braaten, J.: Monitoring air quality with S5P TROPOMI data, Medium, https://medium.com/google-earth/monitoring-air-quality-with-s5p-tropomi-data-4f6b0aebe1c0, last access: 20 June 2021, 2020.

Broomandi, P., Karaca, F., Nikfal, A., Jahanbakhshi, A., Tamjidi, M., and Kim, J. R.: Impact of COVID-19 Event on the Air Quality in Iran. Aerosol Air Qual. Res., 20, 1793–1804, doi:10.4209/aaqr.2020.05.0205, 2020.

Calonzo, A. and Jiao C.: Duterte expands Philippine lockdown to 60 million people, https://www.bloomberg.com/news/articles/2020-03-16/duterte-widens-lockdown-to-main-philippine-island-to-fight-virus, last access: 17 June 2020, 2020a.

Cao, H., Fu, T.-M., Zhang, L., Henze, D. K., Miller, C. C., Lerot, C., Abad, G. G., De Smedt, I., Zhang, Q., van Roozendael, M., Hendrick, F., Chance, K., Li, J., Zheng, J. and Zhao, Y.: Adjoint inversion of Chinese non-methane volatile organic compound emissions using space-based observations of formaldehyde and glyoxal, Atmos. Chem. Phys., 18(20), 15017–15046, doi:10.5194/acp-18-15017-2018, 2018.

CBS News: Lockdown extended for most of coronavirus-battered New York, https://www.cbsnews.com/news/new-york-stay-at-home-extended-coronavirus-lockdown/, last access: 17 June 2020, 2020.

CGTN: Sao Paulo extends the quarantine through May, https://newsus.cgtn.com/news/2020-05-10/Sao-Paulo-extends-quarantine-through-May-QmDnOJo6bK/index.html, last access: 1 July 2020, 2020.

Chan Miller, C., Jacob, D. J., González Abad, G., and Chance, K.: Hotspot of glyoxal over the Pearl River delta seen from the OMI satellite instrument: implications for emissions of aromatic hydrocarbons, Atmos. Chem. Phys., 16, 4631–4639, doi:10.5194/acp-16-4631-2016, 2016.

Chandra, K. K., and Kumar Bhardwaj, A.: Incidence of forest fire in India and its effect on terrestrial ecosystem dynamics, nutrient and microbial status of soil, International Journal of Agriculture and Forestry, 5(2), 69-78doi:10.5923/j.ijaf.20150502.01, 2015.

Chang, Y., Huang, R.J., Ge, X., Huang, X., Hu, J., Duan, Y., Zou, Z., Liu, X., and Lehmann, M. F.: Puzzling haze events in China during the coronavirus (COVID-19) shutdown. Geophys. Res. Lett., 47, e2020GL088533, doi:10.1029/2020GL088533, 2020.

Clark, H., Bennouna, Y., Tsivlidou, M., Wolff, P., Sauvage, B., Barret, B., Le Flochmoën, E., Blot, R., Boulanger, D., Cousin, J.-M., Nédélec, P., Petzold, A., and Thouret, V.: The effects of the COVID-19 lockdowns on the composition of the troposphere as seen by In-service Aircraft for a Global Observing System (IAGOS) at Frankfurt, Atmos. Chem. Phys., 21, 16237–16256, https://doi.org/10.5194/acp-21-16237-2021, 2021.

1191

1192 Collivignarelli, M. C., Abba, A., Bertanza, G., Pedrazzani, R., Ricciardi, P., and Miino, M. C.: Lockdown for Covid-
1193 2019 in Milan: What are the effects on air quality?, Sci. Total Environ., 732, 139280,
1194 doi:10.1016/j.scitotenv.2020.139280, 2020.

1195

1196 Collyns, D.: Peru's coronavirus response was 'right on time' – so why isn't it working?, The Guardian,
1197 https://www.theguardian.com/global-development/2020/may/20/peru-coronavirus-lockdown-new-cases, last access:
1198 17 June 2020, 2020.

1199

1200 Conforti K.: Alert Level 2 restrictions to begin in New Zealand this week,
1201 https://www.forbes.com/sites/kaeliconforti/2020/05/13/alert-level-2-restrictions-to-begin-in-new-zealand-this-
1202 week/#52517b326497, last access: 17 June 2020, 2020.

1203

1204 Copernicus Sentinel-5P (processed by ESA): TROPOMI Level 2 Nitrogen Dioxide total column products. Version
1205 01. European Space Agency, doi:10.5270/S5P-s4ljg54, 2018a.

1206

1207 Copernicus Sentinel-5P (processed by ESA): TROPOMI Level 2 Carbon Monoxide total column products. Version
1208 01. European Space Agency, doi:10.5270/S5P-1hkp7rp, 2018b.

1209

1210 Copernicus Sentinel-5P (processed by ESA): TROPOMI Level 2 Formaldehyde Total Column products. Version 01.
1211 European Space Agency, doi:10.5270/S5P-tjlxfd2, 2018c.

1212

1213 Dattakiran, J.: Impact of lockdown on India's electricity sector, EnergyA, http://www.energy-a.eu/impact-of-ongoing-
1214 lockdown-on-indias-electricity-sector-an-overview/, last access: 9 June 2020, 2020.

1215

1216 De Smedt, I., Theys, N., Yu, H., Danckaert, T., Lerot, C., Compernolle, S., Van Roozendael, M., Richter, A., Hilboll,
1217 A., Peters, E., Pedergnana, M., Loyola, D., Beirle, S., Wagner, T., Eskes, H., van Geffen, J., Boersma, K. F., and
1218 Veefkind, P.: Algorithm theoretical baseline for formaldehyde retrievals from S5P TROPOMI and from the QA4ECV
1219 project, Atmos. Meas. Tech., 11, 2395–2426, doi:10.5194/amt-11-2395-2018, 2018.

1220

1221 De Smedt, I., Romahn, F., and Eichmann, K.-U.: S5P Mission Performance Centre Formaldehyde [L2__HCHO___]
1222 Readme, document number: S5P-MPC-BIRA-PRF-HCHO, 2.1, BIRA-IASB Royal Belgian Institute for Space
1223 Aeronomy, Brussels, Belgium, https://sentinels.copernicus.eu/web/sentinel/technical-guides/sentinel-5p/products-
1224 algorithms, 2020a.

1225

1226 De Smedt, I., Theys, N., Yu, H., Vlietinck, J., Lerot, C., and Van Roozendael, M.: S5P/TROPOMI HCHO ATBD,
1227 document number: S5P-BIRA-L2-400F-ATBD, 2.2.0, BIRA-IASB Royal Belgian Institute for Space Aeronomy,

1228   Brussels,   Belgium,   https://sentinels.copernicus.eu/web/sentinel/technical-guides/sentinel-5p/products-algorithms,
1229   2020b.

1230

1231   Diamond, M. S. and Wood, R.: Limited regional aerosol and cloud microphysical changes despite unprecedented
1232   decline in nitrogen oxide pollution during the February 2020 COVID-19 shutdown in China, Geophys. Res. Lett., 47,
1233   doi:10.1029/2020GL088913, 2020.

1234

1235   Dimitropoulou, E., Hendrick, F., Pinardi, G., Friedrich, M. M., Merlaud, A., Tack, F., De Longueville, H., Fayt, C.,
1236   Hermans, C., Laffineur, Q., Fierens, F., and Van Roozendael, M.: Validation of TROPOMI tropospheric NO_2 columns
1237   using dual-scan multi-axis differential optical absorption spectroscopy (MAX-DOAS) measurements in Uccle,
1238   Brussels, Atmos. Meas. Tech., 13, 5165–5191, doi:10.5194/amt-13-5165-2020, 2020.

1239

1240   Ding, J., van der A, R. J., Eskes, H. J., Mijling, B., Stavrakou, T., van Geffen, J. H. G. M., and Veefkind, J. P.: NOx
1241   emissions reduction and rebound in China due to the COVID-19 crisis. Geophys. Res. Lett., 46, e2020GL089912,
1242   doi.org:10.1029/2020GL089912, 2020.

1243

1244   Do   Rosario,   J.,   Gillespie   P.:   Argentina   orders   'exceptional'   Lockdown   in   bid   to   stem   virus,
1245   https://www.bloomberg.com/news/articles/2020-03-20/argentina-orders-exceptional-lockdown-in-bid-to-contain-
1246   virus, last access: 17 June 2020, 2020.

1247

1248   Sentinel-5P Pre-Operations Data Hub: https://s5phub.copernicus.eu/, last access: 18 June 2021.

1249

1250   Eskes, H. J. and Boersma, K. F.: Averaging kernels for DOAS total-column satellite retrievals, Atmos. Chem. Phys.,
1251   3, 1285–1291, doi:10.5194/acp-3-1285-2003, 2003.

1252

1253   Eskes, H., van Geffen, J., Boersma, K. F., Eichmann, K.-U., Apituley, A., Pedergnana, M., Sneep, M., Veefkind, J.
1254   P., and Loyola, D.: Sentinel-5 precursor/TROPOMI Level 2 Product User Manual Nitrogendioxide, document
1255   number: S5P-KNMI-L2-0021-MA, 4.0.0, Royal Netherlands Meteorological Institute, De Bilt, The Netherlands,
1256   https://sentinels.copernicus.eu/web/sentinel/technical-guides/sentinel-5p/products-algorithms, 2020.

1257

1258   Eskes, H. J., and Eichmann, K.-U.: S5P Mission Performance Centre Nitrogen Dioxide [L2__NO2___] Readme,
1259   document number: S5P-MPC-KNMI-PRF-NO2, 1.6, Royal Netherlands Meteorological Institute, De Bilt, The
1260   Netherlands, https://sentinels.copernicus.eu/web/sentinel/technical-guides/sentinel-5p/products-algorithms, 2020.

1261

1262   Forster, P. M., Forster, H. I., Evans, M. J., Gidden, M. J., Jones, C. D., Keller, C. A., Lamboll, R. D., Le Quéré, C.,
1263   Rogelj, J., Rosen, D., Schleussner, C.-F., Richardson, T. B., Smith C. J., and Turnock, S. T.: Current and future global
1264   climate impacts resulting from COVID-19, Nat. Clim. Chang., 10, 913–919, doi:10.1038/s41558-020-0883-0, 2020.

1265

1266   Fioletov, V. E., McLinden, C. A., Krotkov, N., Li, C., Joiner, J., Theys, N., Carn, S., and Moran, M. D.: A global

1267   catalogue of large SO_2 sources and emissions derived from the Ozone Monitoring Instrument, Atmos. Chem. Phys.,

1268   16, 11497–11519, doi:10.5194/acp-16-11497-2016, 2016.

1269

1270   Fioletov, V., McLinden, C. A., Griffin, D., Theys, N., Loyola, D. G., Hedelt, P., Krotkov, N. A., and Li, C.:

1271   Anthropogenic and volcanic point source SO_2 emissions derived from TROPOMI on board Sentinel-5 Precursor: first

1272   results, Atmos. Chem. Phys., 20, 5591–5607, doi:10.5194/acp-20-5591-2020, 2020.

1273

1274   Fu, T.-M., Jacob, D. J., Wittrock, F., Burrows, J. P., Vrekoussis, M., and Henze, D. K.: Global budgets of atmospheric

1275   glyoxal and methylglyoxal, and implications for formation of secondary organic aerosols, J. Geophys. Res., 113,

1276   D15303, doi:10.1029/2007JD009505, 2008.

1277

1278   van Geffen, J. H. G. M., Eskes, H. J., Boersma, K. F., Maasakkers, J. D., and Veefkind, J. P.: TROPOMI ATBD of

1279   the total and tropospheric NO_2 data products, document number: S5P-KNMI-L2-0005-RP, 1.4.0, Royal Netherlands

1280   Meteorological Institute, De Bilt, The Netherlands, ~~https://sentinels.copernicus.eu/web/sentinel/technical-~~

1281   ~~guides/sentinel-5p/products-algorithms,~~ 2019.

1282

1283   van Geffen, J., Boersma, K. F., Eskes, H., Sneep, M., ter Linden, M., Zara, M., and Veefkind, J. P.: S5P TROPOMI

1284 NO_2 slant column retrieval: method, stability, uncertainties and comparisons with OMI, Atmos. Meas. Tech., 13,

1285   1315–1335, doi:10.5194/amt-13-1315-2020, 2020.

1286

1287   van Geffen, J. H. G. M., Eskes, H. J., Boersma, K. F., and Veefkind, J. P.: TROPOMI ATBD of the total and

1288   tropospheric NO_2 data products, document number: S5P-KNMI-L2-0005-RP, 2.2.0, Royal Netherlands

1289   Meteorological Institute, De Bilt, The Netherlands, https://sentinels.copernicus.eu/web/sentinel/technical-

1290   guides/sentinel-5p/products-algorithms, 2021.

1291

1292   Gkatzelis, G. I., Gilman, J. B., Brown, S. S., Eskes, H., Gomes, A. R., Lange, A. C., McDonald, B. C., Peischl, J.,

1293   Petzold, A., Thompson, C. R., and Kiendler-Scharr, A.: The Global Impacts of COVID-19 Lockdowns on Urban Air

1294   Quality: A Critical Review and Recommendations, Elem. Sci. Anth., 9, doi:10.1525/elementa.2021.00176, 2021.

1295

1296   Goldberg, D. L., Lu, Z., Streets, D. G., de Foy, B., Griffin, D., McLinden, C. A., Lamsal, L. N., Nickolay A. Krotkov,

1297   N. A., and Eskes, H.: Enhanced Capabilities of TROPOMI NO_2: Estimating NOx from North American Cities and

1298   Power Plants, Environ. Sci. Technol., 53(21), 12594-12601, doi:10.1021/acs.est9b04488, 2019.

1299

Goldberg, D. L., Anenberg, S. C., Griffin, D., McLinden, C. A., Lu, Z., and Streets, D. G.: Disentangling the impact of the COVID-19 lockdowns on urban NO_2 from natural variability, Geophys. Res. Lett., 47, e2020GL089269, doi:10.1029/2020GL089269, 2020.

Goodman, A.: De Moura H., and Rebaza C. After 7 weeks of lockdown, Spaniards can finally exercise outdoors -- as death toll passes 25,000, https://edition.cnn.com/2020/05/02/europe/spain-lockdown-coronavirus-exercise-intl/index.html, last access: 17 June 2020, 2020.

Granier, C., Darras, S., Denier van der Gon, H., Doubalova, J., Elguindi, N., Galle, B., Gauss, M., Guevara, M., Jalkanen, J.-P., Kuenen, J., Liousse, C., Quack, B., Simpson, D., and Sindelarova, K.: The Copernicus Atmosphere Monitoring Service global and regional emissions (April 2019 version), Copernicus Atmosphere Monitoring Service (CAMS) Report, Laboratoire d'Aérologie, Toulouse, France, 54pp., doi:10.24380/d0bn-kx16, 2019.

Guevara, M., Jorba, O., Soret, A., Petetin, H., Bowdalo, D., Serradell, K., Tena, C., Denier van der Gon, H., Kuenen, J., Peuch, V.-H., and Pérez García-Pando, C.: Time-resolved emission reductions for atmospheric chemistry modelling in Europe during the COVID-19 lockdowns, Atmos. Chem. Phys., 21, 773–797, https://doi.org/10.5194/acp-21-773-2021, 2021.

Holloway, T., Levy, H., and Kasibhatla, P.: Global distribution of carbon monoxide, J. Geophys. Res., 105, D10, 12123-12147, doi:10.1029/1999JD901173, 2000.

Horowitz, J.: Italy Locks Down Much of the Country's North Over the Coronavirus, https://www.nytimes.com/2020/03/07/world/europe/coronavirus-italy.html, last access: 17 June 2020, 2020a.

Horowitz, J.: Hope and Worry Mingle as Countries Relax Coronavirus Lockdowns, https://www.nytimes.com/2020/05/04/world/europe/coronavirus-restrictions.html, last access: 17 June 2020, 2020b.

Huang, G. and Sun, K.: Non-negligible impacts of clean air regulations on the reduction of tropospheric NO_2 over East China during the COVID-19 pandemic observed by OMI and TROPOMI, Sci. Total Environ., 745, 141023, doi:10.1016/j.scitotenv.2020.141023, 2020.

Ialongo, I., Virta, H., Eskes, H., Hovila, J., and Douros, J.: Comparison of TROPOMI/Sentinel-5 Precursor NO_2 observations with ground-based measurements in Helsinki, Atmos. Meas. Tech., 13, 205–218, doi:10.5194/amt-13-205-2020, 2020.

Jain, S. and Sharma, T.: Social and travel lockdown impact considering Coronavirus disease (COVID-19) on air quality in megacities of India: present benefits, future challenges and way forward, Aerosol Air Qual. Res., 20, 1222–1236, doi:10.4209/aaqr.2020.04.0171, 2020.

Janssens-Maenhout, G., Crippa, M., Guizzardi, D., Dentener, F., Muntean, M., Pouliot, G., Keating, T., Zhang, Q., Kurokawa, J., Wankmüller, R., Denier van der Gon, H., Kuenen, J. J. P., Klimont, Z., Frost, G., Darras, S., Koffi, B., and Li, M.: HTAP_v2.2: a mosaic of regional and global emission grid maps for 2008 and 2010 to study hemispheric transport of air pollution, Atmos. Chem. Phys., 15, 11411–11432, https://doi.org/10.5194/acp-15-11411-2015, 2015.

Jennings, R., Philippines allows soft post-lockdown reopening to avert dire economic fall, https://www.voanews.com/east-asia-pacific/philippines-allows-soft-post-lockdown-reopening-avert-dire-economic-fall, last access: 17 June 2020, 2020.

Judd, L. M., Al-Saadi, J. A., Szykman, J. J., Valin, L. C., Janz, S. J., Kowalewski, M. G., Eskes, H. J., Veefkind, J. P., Cede, A., Mueller, M., Gebetsberger, M., Swap, R., Pierce, R. B., Nowlan, C. R., Abad, G. G., Nehrir, A., and Williams, D.: Evaluating Sentinel-5P TROPOMI tropospheric NO$_2$ column densities with airborne and Pandora spectrometers near New York City and Long Island Sound, Atmos. Meas. Tech., 13, 6113–6140, doi:10.5194/amt-13-6113-2020, 2020.

Kharol, S. K., Fioletov, V., McLinden, C. A., Shephard, M. W., Sioris, C. E., Li, C., and Krotkov, N.A.: Ceramic industry at Morbi as a large source of SO$_2$ emissions in India, Atmos. Environ., 223, doi:10.1016/j.atmosenv.2019.117243, 2019.

Koukouli, M. E., Skoulidou, I., Karavias, A., Parcharidis, I., Balis, D., Manders, A., Segers, A., Eskes, H. and Van Geffen, J.: Sudden changes in nitrogen dioxide emissions over Greece due to lockdown after the outbreak of COVID-19, Atmos. Chem. Phys., 21(3), 1759–1774, doi:10.5194/acp-21-1759-2021, 2021.s

Krol, M., Houweling, S., Bregman, B., van den Broek, M., Segers,A., van Velthoven, P., Peters, W., Dentener, F., and Bergamaschi, P.: The two-way nested global chemistry-transport zoom model TM5: algorithm and applications, Atmos. Chem. Phys., 5, 417–432, doi:10.5194/acp-5-417-2005, 2005.

Kroll, J. H., Heald, C. L., Cappa, C. D., Farmer, D. K., Fry, J. L., Murphy, J. G., and Steiner, A. L.: The complex chemical effects of COVID-19 shutdowns on air quality, Nat. Chem., 12, 777-779, doi:10.1038/s41557-020-0535-z, 2020.

Kumari, P., and Toshniwal, D.: Impact of lockdown measures during COVID-19 on air quality–a case study of India. Int. J. Environ. Heal. R., 1-8, doi:10.1080/09603123.2020.1778646, 2020.

1372

1373 Lambert, J.-C., S. Compernolle, K.-U. Eichmann, M. de Graaf, D. Hubert, A. Keppens, Q. Kleipool, B. Langerock,

1374 M.K. Sha, T. Verhoelst, T. Wagner, C. Ahn, A. Argyrouli, D. Balis, K.L. Chan, I. De Smedt, H. Eskes, A.M. Fjæraa,

1375 K. Garane, J.F. Gleason, F. Goutail, J. Granville, P. Hedelt, K.-P. Heue, G. Jaross, ML. Koukouli, J. Landgraf, R.

1376 Lutz, S. Nanda, S. Niemeijer, A. Pazmiño, G. Pinardi, J.-P. Pommereau, A. Richter, N. Rozemeijer, M. Sneep, D.

1377 Stein Zweers, N. Theys, G. Tilstra, O. Torres, P. Valks, J. van Geffen, C. Vigouroux, P. Wang, and M. Weber. S5P

1378 MPC Routine Operations Consolidated Validation Report series, Issue #09, document number: S5P-MPC-IASB-

1379 ROCVR-09.01.01-20201221, 9.01.01, Royal Belgian Institute for Space Aeronomy, Brussels, Belgium, http://mpc-

1380 vdaf.tropomi.eu/index.php?option=com_vdaf&view=showReport&format=rawhtml&id=45

1381 2020.

1382

1383 Landgraf, J., aan de Brugh, J., Scheepmaker, R., Borsdorff, T., Hu, H., Houweling, S., Butz, A., Aben, I., and

1384 Hasekamp, O.: Carbon monoxide total column retrievals from TROPOMI shortwave infrared measurements, Atmos.

1385 Meas. Tech., 9, 4955–4975, doi:10.5194/amt-9-4955-2016, 2016.

1386

1387 Landgraf, J., aan de Brugh, J., Scheepmaker, R. A., Borsdorff, T., Houweling, S., and Hasekamp, O. P.: Algorithm

1388 Theoretical Baseline Document for Sentinel-5 Precursor: Carbon Monoxide Total Column Retrieval, document

1389 number: SRON-S5P-LEV2-RP-002, 1.10, SRON Netherlands Institute for Space Research, Utrecht, The Netherlands,

1390 https://sentinels.copernicus.eu/web/sentinel/technical-guides/sentinel-5p/products-algorithms, 2018.

1391

1392 Landgraf, J., Borsdorff, T., Langerock, B., and Keppens, A.: S5P Mission Performance Centre Carbon Monoxide

1393 [L2__CO____] Readme, document number: S5P-MPC-SRON-PRF-CO, 1.5, SRON Netherlands Institute for Space

1394 Research, Utrecht, The Netherlands, https://sentinels.copernicus.eu/web/sentinel/technical-guides/sentinel-

1395 5p/products-algorithms, 2020.

1396

1397 Lee, C., Martin, R. V., van Donkelaar, A., Lee, H., Dickerson, R. R., Hains, J. C., Krotkov, N., Richter, A., Vinnikov,

1398 K., and Schwab, J. J.: SO_2 emissions and lifetimes: Estimates from inverse modeling using in situ and global, space-

1399 based (SCIAMACHY and OMI) observations, J. Geophys. Res., 116, D06304, doi:10.1029/2010JD014758, 2011.

1400

1401 Lee, J. D., Drysdale, W. S., Finch, D. P., Wilde, S. E., and Palmer, P. I.: UK surface NO_2 levels dropped by 42%

1402 during the COVID-19 lockdown: impact on surface O_3, Atmos. Chem. Phys., doi:10.5194/acp-2020-838, 2020.

1403

1404 Le Quéré, C., Jackson, R. B., Jones, M. W., Smith, A. J. P., Abernethy, S., Andrew, R. M., De-Gol, A. J., Willis, D.

1405 R., Shan, Y., Canadell, J. G., Friedlingstein, P., Creutzig F., and Peters, G. P.: Temporary reduction in daily global

1406 CO_2 emisisons during the COVID-19 forced confinement, Nat. Clim. Chang., 10, 647-653, doi:10.1038/s41558-020-

1407 0797-x, 2020.

1408

1409 Lerot, C., Stavrakou, T., De Smedt, I., Müller, J.-F., and Van Roozendael, M.: Glyoxal vertical 576 columns from
1410 GOME-2 backscattered light measurements and comparisons with a global 577 model. Atmos. Chem. Phys. 10,
1411 12059-12072, 2010.

1413 Lerot, C., Stavrakou, T., Van Roozendael, M., Alvarado, L. M. A., and Richter, A.: GLYoxal Retrievals from
1414 TROPOMI (GLYRETRO) ATBD, S5p+Innovation – theme 1 (CHOCHO), 5p+I_CHOCHO_BIRA_ATBD, issue
1415 2.1, 16 November 2020, https://glyretro.aeronomie.be/, 2020.

1417 Leung, K., Wu, J. Liu, D., and Leung, G. M.: First-wave COVID-19 transmissibility and severity in China outside
1418 Hubei after control measures, and second-wave scenario planning: a modelling impact assessment, The Lancet, 395
1419 (10233), 1382-1393, doi:10.1016/S0140-6736(20)30746-7, 2020.

1421 Li, C., McLinden, C., Fioletov, V., Krotkov, N., Carn, S., Joiner, J., Streets, D., He, H., Ren, X., Zhanqing Li, Z., and
1422 Dickerson, R. R.: India Is Overtaking China as the World's Largest Emitter of Anthropogenic Sulfur Dioxide, Sci.
1423 Rep., 7, 14304, doi:10.1038/s41598-017-14639-8, 2017.

1425 Liu, F., Page, A., Strode, S. A., Yoshida, Y., Choi, S., Zheng, B., Lamsal, L. N., Li, C., Krotkov, N. A., Eskes, H.,
1426 van der A, R., Veefkind, P., Levelt, P. F., Hauser, O. P., and Joiner, J.: Abrupt decline in tropospheric nitrogen dioxide
1427 over China after the outbreak of COVID-19, Sci. Adv., 6, 28, eabc2992, doi:10.1126/sciadv.abc2992, 2020.

1429 Lorente, A., Boersma, K. F., Eskes, H. J., Veefkind, J. P., van Geffen, J. H. G. M., de Zeeuw, M. B., Denier van der
1430 Gon, H. A. C., Beirle, S., and Krol, M. C.: Quantification of nitrogen oxides emissions from build-up of pollution over
1431 Paris with TROPOMI, Sci. Rep., 9, 20033, doi:10.1038/s41598-019-56428-5, 2019.

1433 Loyola, D. G., Gimeno García, S., Lutz, R., Argyrouli, A., Romahn, F., Spurr, R. J. D., Pedergnana, M., Doicu, A.,
1434 Molina García, V., and Schüssler, O.: The operational cloud retrieval algorithms from TROPOMI on board Sentinel-
1435 5 Precursor, Atmos. Meas. Tech., 11, 409–427, doi:10.5194/amt-11-409-2018, 2018.

1437 Ludewig, A., Kleipool, Q., Bartstra, R., Landzaat, R., Leloux, J., Loots, E., Meijering, P., van der Plas, E., Rozemeijer,
1438 N., Vonk, F., and Veefkind, P.: In-flight calibration results of the TROPOMI payload on board the Sentinel-5
1439 Precursor satellite, Atmos. Meas. Tech., 13, 3561–3580, doi:10.5194/amt-13-3561-2020, 2020.

1441 Mahato, S., Pal, S., and Ghosh, K. G., Effect of lockdown amid COVID-19 pandemic on air quality of the megacity
1442 Delhi, India, Sci. Total Environ., 730, 139086, doi:10.1016/j.scitotenv.2020.139086, 2020.

1444   Makooi, B.:   Key points of France's strategy for lifting its nationwide Covid-19 lockdown.
1445   https://www.france24.com/en/20200429-key-points-of-france-s-strategy-for-lifting-its-nationwide-covid-19-
1446   lockdown, last access: 17 June 2020, 2020.

1448   Masaki, T., Nakamura, S., Newhouse, D.: How is the COVID-19 crisis affecting nitrogen dioxide emissions in Sub-
1449   Saharan Africa? Poverty and Equity Notes, No. 21. World Bank, Washington, DC, World Bank.
1450   https://openknowledge.worldbank.org/handle/10986/33801, License: CC BY 3.0 IGO, 2020.

1452   Matthews, A.: Coronavirus: 5 things New Zealand got right, Deutsche Welle, https://p.dw.com/p/3dSVh, last access:
1453   2 July 2020, 2020.

1455   Mbah,   F.:   Businesses   reopen   as   Nigeria   eases   coronavirus   lockdown.   Available   from
1456   https://www.aljazeera.com/news/2020/05/businesses-reopen-nigeria-eases-coronavirus-lockdown-
1457   200504094440082.html, last access: 17 June 2020, 2020.

1459   Menon, P.:   'Stay at home' New Zealand PM urges ahead of coronavirus lockdown. Available from
1460   https://www.reuters.com/article/us-health-coronavirus-newzealand/stay-at-home-new-zealand-pm-urges-ahead-of-
1461   coronavirus-lockdown-idUSKBN21A3RN, last access: 17 June 2020, 2020.

1463   Millet, D. B., Jacob, D. J., Boersma, K. F., Fu, T. M., Kurosu, T. P., Chance, K., Heald, C. L., and Guenther, A.:
1464   Spatial distribution of isoprene emissions from North America derived from formaldehyde column measurements by
1465   the OMI satellite sensor, J. Geophys. Res., 113, D02307, doi:10.1029/2007jd008950, 2008.

1467   Minder, R. and Peltier, E.: Spain imposes nationwide lockdown to fight coronavirus. Available from
1468   https://www.nytimes.com/2020/03/14/world/europe/spain-coronavirus.html, last access: 17 June 2020, 2020.

1470   Misculin N., and Garrison C.: Argentina extends lockdown in Buenos Aires as coronavirus cases surpass 20,000.
1471   Available from https://www.thejakartapost.com/news/2020/06/05/argentina-extends-lockdown-in-buenos-aires-as-
1472   coronavirus-cases-surpass-20000.html, last access: 17 June 2020, 2020.

1474   Miyazaki, K., Bowman, K., Sekiya, T., Jiang, Z., Chen, X., Eskes, H., Ru, M., Zhang, Y., and Shindell, D.: Air
1475   quality response in China linked to the 2019 novel coronavirus (COVID-19) lockdown, Geophys. Res. Lett., 47,
1476   e2020GL089252, doi:10.1029/2020GL089252, 2020.

1478   Müller, J.-F., Stavrakou, T., Bauwens, M., Compernolle, S., and Peeters, J.: Chemistry and deposition in the Model
1479   of Atmospheric composition at Global and Regional scales using Inversion Techniques for Trace gas Emissions
1480   (MAGRITTE v1.0). Part B. Dry deposition, Geosci. Model Dev. Discuss., 1–49, doi:10.5194/gmd-2018-317, 2018.

1481

1482 Müller, J.-F., Stavrakou, T., and Peeters, J.: Chemistry and deposition in the Model of Atmospheric composition at

1483 Global and Regional scales using Inversion Techniques for Trace gas Emissions (MAGRITTE v1.1) – Part 1:

1484 Chemical mechanism, Geosci. Model Dev., 12, 2307–2356, doi:10.5194/gmd-12-2307-2019, 2019.

1485

1486 Muñoz Sabater, J.: ERA5-Land monthly averaged data from 1981 to present, Copernicus Climate Change Service

1487 (C3S) Climate Data Store (CDS) [data set], last access: 09 June 2021, doi:10.24381/cds.68d2bb30, 2019a.

1488

1489 Muñoz Sabater, J.: ERA5-Land hourly averaged data from 1981 to present, Copernicus Climate Change Service (C3S)

1490 Climate Data Store (CDS) [data set], last access: 09 June 2021, doi:10.24381/cds.e2161bac, 2019b.

1491

1492 New South Wales Public Health: Public Health (COVID-19 Restrictions on Gathering and Movement) Order 2020,

1493 https://www.legislation.nsw.gov.au, last access: 2 July 2020, 2020.

1494

1495 Odunsi, P.: Africa: COVID-19 deaths hits 37,000, Nigeria on top 5, Daily Post Nigeria,

1496 https://dailypost.ng/2020/10/06/africa-covid-19-deaths-hits-37000-nigeria-on-top-5/, last access: 30 March 2021,

1497 2020.

1498

1499 Onishi, N. and Méheut, C.: Paris, a magnet for the world, becomes a ghost city after a lockdown takes effect. Available

1500 from https://www.nytimes.com/2020/03/17/world/europe/paris-coronavirus-lockdown.html, last access: 17 June

1501 2020, 2020.

1502

1503 Orjinmo, N.: Coronavirus lockdown: Nigerians cautious as restrictions eased in Lagos and Abuja. Available from

1504 https://www.bbc.com/news/world-52526923, last access: 17 June 2020, 2020.

1505

1506 Palmer, P. I., Jacob, D. J., Chance, K., Martin, R. V., Spurr, R. J. D., Kurosu, T. P., Bey, I., Yantosca, R., Fiore, A.,

1507 and Li, Q.: Air mass factor formulation for spectroscopic measurements from satellites: Application to formaldehyde

1508 retrievals from the Global Ozone Monitoring Experiment, J. Geophys. Res. Atmos., 106, D13, 14539–14550,

1509 doi:10.1029/2000JD900772, 2001.

1510

1511 Pasley, J.: Mexico has moved to 'Phase 3' — its most serious level of coronavirus alert — and faces a looming

1512 outbreak. Here's how it got to this point, https://www.insider.com/photo-mexico-coronavirus-move-to-phase-three-

1513 2020-4, last access: 17 June 2020, 2020.

1514

1515 Patel S.: When Is California Reopening? The New York Times. Available from

1516 https://www.nytimes.com/article/coronavirus-california-reopening-phases.html, last access: 17 June 2020, 2020.

1517

1518 POSOCO, Power System Operation Corporation Limited, National Load Despatch Centre: https://posoco.in/covid-
1519 19/, last access: 30 March 2021.

1521 Prabhjote, G.: The most congested cities in India low lie vacant midst the nationwide lockdown, Business Insider
1522 India, https://www.businessinsider.in/india/news/most-congested-cities-in-india-low-lie-vacant-midst-the-
1523 nationwide-lockdown/articleshow/75243376.cms, last access: 30 March 2021, 2020.

1525 Qu, Z., Jacob, D. J., Silvern, R. F., Shah, V., Campbell, P. C., Valin, L. C. and Murray, L. T.: US COVID-19 shutdown
1526 demonstrates importance of background NO2 in inferring NOx emissions from satellite NO2 observations, Geophys.
1527 Res. Lett., 48(10), doi:10.1029/2021GL092783, 2021.

1529 Raszewski, E., and Garrison, C.: Buenos Aires lockdown extended until June 7 after rise in coronavirus cases, Reuters,
1530 https://www.reuters.com/article/us-health-coronavirus-argentina/buenos-aires-lockdown-extended-until-june-7-
1531 after-rise-in-coronavirus-cases-idUSKBN22Z0YB?il=0, last access: 17 June 2020, 2020.

1533 Romahn, F., Pedergnana, M., Loyola, D., Apituley, A., Sneep, M., Veefkind, J. P., De Smedt, I., and Chan, K. L.:
1534 Sentinel-5 precursor/TROPOMI Level 2 Product User Manual Formaldehyde HCHO, document number: S5P-L2-
1535 DLR-PUM-400F, 2.01.00, DLR, German Aerospace Center, Oberpfaffenhofen, Germany,
1536 https://sentinels.copernicus.eu/web/sentinel/technical-guides/sentinel-5p/products-algorithms, 2020.

1538 Saleh, I.: Iraq locks down 6 districts in Baghdad to stem virus. Available from https://www.aa.com.tr/en/latest-on-
1539 coronavirus-outbreak/iraq-locks-down-6-districts-in-baghdad-to-stem-virus/1845104, last access: 17 June 2020,
1540 2020.

1542 Sekiya, T., Miyazaki, K., Eskes, H., Sudo, K., Takigawa, M., and Kanaya, Y.: A comparison of the impact of
1543 TROPOMI and OMI tropospheric NO2 on global chemical data assimilation, Atmos. Meas. Tech. Discuss. [preprint],
1544 https://doi.org/10.5194/amt-2021-400, in review, 2021.

1546 Shi, X. and Brasseur, G. P.: The response in air quality to the reduction of Chinese economic activities during the
1547 COVID-19 outbreak, Geophys. Res. Lett., 47, e2020GL088070, doi:10.1029/2020GL088070, 2020.

1549 Singh, K. D., Goel, V., Kumar, H., and Gettleman, J.: India, Day 1: World's Largest Coronavirus Lockdown Begins,
1550 The New York Times, https://www.nytimes.com/2020/03/25/world/asia/india-lockdown-coronavirus.html, last
1551 access: 30 March 2021, 2020.

Sonali P.: Australia's biggest state to ease coronavirus lockdown from May 15, https://www.reuters.com/article/us-health-coronavirus-australia/australias-biggest-state-to-ease-coronavirus-lockdown-from-may-15-idUSKBN22M01U, last access: 17 June 2020, 2020.

Spurr R., and Christi M.: The LIDORT and VLIDORT Linearized Scalar and Vector Discrete Ordinate Radiative Transfer Models: Updates in the Last 10 Years. In: Kokhanovsky A. (eds) Springer Series in Light Scattering. Springer Series in Light Scattering. Springer, Cham., doi:10.1007/978-3-030-03445-0_1, 2019.

Srikanta, S., Pilla, F., Basu, B., Sarkar Basu, A., Sarkar, K., Chakraborti, S., Kumar Joshi, P., Zhang, Q., Wang, Y., Bhatt, S., Bhatt, A., Jha, S., Keesstra, S., and Roy, P. S.: Examining the effects of forest fire on terrestrial carbon emission and ecosystem production in India using remote sensing approaches, Sci. Tot. Environ., 725, doi:10.1016/j.scitotenv.2020.138331, 2020.

Stavrakou, T., Müller, J.-F., De Smedt, I., Van Roozendael, M., Kanakidou, M., Vrekoussis, M., Wittrock, F., Richter, A., and Burrows, J. P.: The continental source of glyoxal estimated by the synergistic use of spaceborne measurements and inverse modelling, Atmos. Chem. Phys., 9, 8431–8446, doi:10.5194/acp-9-8431-2009, 2009.

Stavrakou, T., Müller, J.-F., Bauwens, M., De Smedt, I., Van Roozendael, M., and Guenther, A. B.: Impact of short-term climate variability on volatile organic compounds emissions assessed using OMI satellite formaldehyde observations. Geophys. Res. Lett., 45, 8681–8689, doi:10.1029/2018GL078676, 2018.

Stavrakou, T., Müller, J.-F., Bauwens, M., Doumbia, T., Elguindi, N., Darras, S., Granier, C., DeSmedt, I., Lerot, C., Van Roozendael, M., Franco, B., Clarisse, L., Clerbaux, C., Coheur, P.-F., Liu, Y., Wang, T., Shi, X., Gaubert, B., Tilmes, S., and Brasseur, G.: Atmospheric Impacts of COVID-19 on NO_x and VOC Levels over China Based on TROPOMI and IASI Satellite Data and Modeling, Atmosphere, 12(8):946, https://doi.org/10.3390/atmos12080946, 2021.

Sun, W., Zhu, L., De Smedt, I., Bai, B., Pu, D., Chen, Y., Shu, L., Wang, D., Fu, T.-M., Wang, X., and Yang, X.: Global significant changes in formaldehyde (HCHO) columns observed from space at the early stage of the COVID-19 pandemic, Geophys. Res. Lett., 48, e2020GL091265, doi:10.1029/2020GL091265, 2021.

Tack, F., Merlaud, A., Iordache, M.-D., Pinardi, G., Dimitropoulou, E., Eskes, H., Bomans, B., Veefkind, P., and Van Roozendael, M.: Assessment of the TROPOMI tropospheric NO_2 product based on airborne APEX observations, Atmos. Meas. Tech., 14, 615–646, doi:10.5194/amt-14-615-2021, 2021.

Tan, P. H., Chou, C., Liang, J. Y., Chou, C. C. K., and Shiu, C. J.: Air pollution "holiday effect" resulting from the Chinese New Year, Atmos. Environ., 43(13), 2114–2124, doi:10.1016/j.atmosenv.2009.01.037, 2009.

The Star: Iraq on total lockdown until March 28 over virus fears, https://www.thestar.com.my/news/regional/2020/03/22/iraq-on-total-lockdown-until-march-28-over-virus-fears, last access: 17 June 2020, 2020.

~~Theys, N., Fioletov, V., Li, C., De Smedt, I., Lerot, C., McLinden, C., Krotkov, N., Griffin, D., Clarisse, L., Hedelt, P., Loyola, D., Wagner, T., Kumar, V., Innes, A., Ribas, R., Hendrick, F., Vlietinck, J., Brenot, H., and Van Roozendael, M.: A Sulfur Dioxide Covariance Based Retrieval Algorithm (COBRA): application to TROPOMI reveals new emission sources, Atmos. Chem. Phys. Discuss. [preprint], doi:10.5194/acp-2021-294, in review, 2021.~~ Theys, N., Fioletov, V., Li, C., De Smedt, I., Lerot, C., McLinden, C., Krotkov, N., Griffin, D., Clarisse, L., Hedelt, P., Loyola, D., Wagner, T., Kumar, V., Innes, A., Ribas, R., Hendrick, F., Vlietinck, J., Brenot, H., and Van Roozendael, M.: A sulfur dioxide Covariance-Based Retrieval Algorithm (COBRA): application to TROPOMI reveals new emission sources, Atmos. Chem. Phys., 21, 16727–16744, https://doi.org/10.5194/acp-21-16727-2021, 2021.

Uchoa, P.: Brazil coronavirus: 'Our biggest problem is fake news', BBC, https://www.bbc.com/news/world-latin-america-52739734, last access: 17 June 2020, 2020.

Veefkind, J. P., Aben, I., McMullan, K., Forster, H., de Vries, J., Otter, G., Claas, J., Eskes, H. J., de Haan, J. F., Kleipool, Q., van Weele, M., Hasekamp, O., Hoogeveen, R., Landgraf, J., Snel, R., Tol, P., Ingmann, P., Voors., R., Kruizinge, B., Vink, R., Visser, H., and Levelt, P. F.: TROPOMI on the ESA Sentinel-5 Precursor: A GMES mission for global observations of the atmospheric composition for climate, air quality and ozone layer applications, Remote Sens. Environ., 120, 70-83, 2012.

Verhoelst, T., Compernolle, S., Pinardi, G., Lambert, J.-C., Eskes, H. J., Eichmann, K.-U., Fjæraa, A. M., Granville, J., Niemeijer, S., Cede, A., Tiefengraber, M., Hendrick, F., Pazmiño, A., Bais, A., Bazureau, A., Boersma, K. F., Bognar, K., Dehn, A., Donner, S., Elokhov, A., Gebetsberger, M., Goutail, F., Grutter de la Mora, M., Gruzdev, A., Gratsea, M., Hansen, G. H., Irie, H., Jepsen, N., Kanaya, Y., Karagkiozidis, D., Kivi, R., Kreher, K., Levelt, P. F., Liu, C., Müller, M., Navarro Comas, M., Piters, A. J. M., Pommereau, J.-P., Portafaix, T., Prados-Roman, C., Puentedura, O., Querel, R., Remmers, J., Richter, A., Rimmer, J., Rivera Cárdenas, C., Saavedra de Miguel, L., Sinyakov, V. P., Stremme, W., Strong, K., Van Roozendael, M., Veefkind, J. P., Wagner, T., Wittrock, F., Yela González, M., and Zehner, C.: Ground-based validation of the Copernicus Sentinel-5P TROPOMI NO_2 measurements with the NDACC ZSL-DOAS, MAX-DOAS and Pandonia global networks, Atmos. Meas. Tech., 14, 481–510, doi:10.5194/amt-14-481-2021, 2021.

Vigouroux, C., Langerock, B., Bauer Aquino, C. A., Blumenstock, T., Cheng, Z., De Mazière, M., De Smedt, I., Grutter, M., Hannigan, J. W., Jones, N., Kivi, R., Loyola, D., Lutsch, E., Mahieu, E., Makarova, M., Metzger, J.-M., Morino, I., Murata, I., Nagahama, T., Notholt, J., Ortega, I., Palm, M., Pinardi, G., Röhling, A., Smale, D., Stremme,

W., Strong, K., Sussmann, R., Té, Y., van Roozendael, M., Wang, P., and Winkler, H.: TROPOMI–Sentinel-5 Precursor formaldehyde validation using an extensive network of ground-based Fourier-transform infrared stations, Atmos. Meas. Tech., 13, 3751–3767, doi:10.5194/amt-13-3751-2020, 2020.

Wahlquist, C.: Australia's coronavirus lockdown – the first 50 days, https://www.theguardian.com/world/2020/may/02/australias-coronavirus-lockdown-the-first-50-days, last access: 17 June 2020, 2020.

Wang, Y., Yuan, Y., Wang, Q., Liu, C. G., Zhi, Q., and Cao, J.: Changes in air quality related to the control of coronavirus in China: Implications for traffic and industrial emissions, Sci. Total Environ., 731, 139133, doi:10.1016/j.scitotenv.2020.139133, 2020.

Wang, Z., Zheng, F., Zhang, W., and Wang, S.: Analysis of SO_2 Pollution Changes of Beijing-Tianjin-Hebei Region over China Based on OMI Observations from 2006 to 2017, Adv. Meteorol., 2018, doi:10.1155/2018/8746068, 2018.

Williams, J. E., Boersma, K. F., Le Sager, P., and Verstraeten, W. W.: The high-resolution version of TM5-MP for optimized satellite retrievals: description and validation, Geosci. Model Dev., 10, 721–750, doi:10.5194/gmd-10-721-2017, 2017.

Winter, S.: Ramaphosa announces 21 day coronavirus lockdown for South Africa, https://businesstech.co.za/news/government/383927/ramaphosa-announces-21-day-coronavirus-lockdown-for-south-africa/, last access: 17 June 2020, 2020.

Zhang, R., Zhang, Y., Lin, H., Feng, X., Fu, T.-M., and Wang, Y.: NOx Emission Reduction and Recovery during COVID-19 in East China, Atmosphere (Basel)., 11(4), 433, doi:10.3390/atmos11040433, 2020.

Zhang, Z., Arshad, A., Zhang, C., Hussain, S. and Li, W.: Unprecedented Temporary Reduction in Global Air Pollution Associated with COVID-19 Forced Confinement: A Continental and City Scale Analysis, Remote Sens., 12(15), 2420, doi:10.3390/rs12152420, 2020.

Zhao, N., G. Wang, G. Li, J. Lang and H. Zhang: Air pollution episodes during the COVID-19 outbreak in the Beijing–Tianjin–Hebei region of China: An insight into the transport pathways and source distribution. Environmental Pollution 267, 115617, https://doi.org/10.1016/j.envpol.2020.115617, 2020.

Zhao, Y., Zhang, K., Xu, X., Shen, H., Zhu, X., Zhang, Y., Hu, Y. and Shen, G.: Substantial Changes in Nitrogen Dioxide and Ozone after Excluding Meteorological Impacts during the COVID-19 Outbreak in Mainland China, Environ. Sci. Technol. Lett., 7(6), 402–408, doi:10.1021/acs.estlett.0c00304, 2020.

1663 Zheng, B., Tong, D., Li, M., Liu, F., Hong, C., Geng, G., Li, H., Li, X., Peng, L., Qi, J., Yan, L., Zhang, Y., Zhao, H.,

1664 Zheng, Y., He, K., and Zhang, Q.: Trends in China's anthropogenic emissions since 2010 as the consequence of clean

1665 air actions, Atmos. Chem. Phys., 18(19), 14095–14111, doi:10.5194/acp-18-14095-2018, 2018a.

1666

1667 Zheng, B., Chevallier, F., Ciais, P., Yin, Y., Deeter, M. N., Worden, H. M., Wang, Y., Zhang, Q., and He, K.: Rapid

1668 decline in carbon monoxide emissions and export from East Asia between years 2005 and 2016, Environ. Res. Lett.,

1669 13(4), doi:10.1088/1748-9326/aab2b3, 2018b.

1670

1671 Zhu, L., Mickley, L. J., Jacob, D. J., Marais, E. A., Sheng, J., Hu, L., Abad, G. G., and Chance, K.: Long-term (2005–

1672 2014) trends in formaldehyde (HCHO) columns across North Americas seen by the OMI satellite instrument:

1673 Evidence of changing emissions of volatile organic compounds, Geophys. Res. Lett., 44, 7079–7086,

1674 doi:10.1002/2017GL073859, 2017.